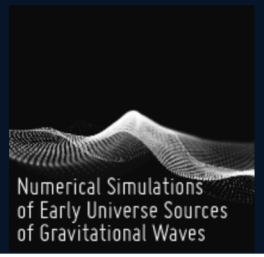


Numerical Simulations of Early Universe Sources of Gravitational Waves

# WHAT DO WE LEARN FROM PULSAR TIMING ARRAYS DATA

Tina Kahniashvili

Carnegie Mellon University, USA and Ilia State University, Georgia
and Abastumani Astrophysical Observatory, Georgia

NORDITA
Aug. 7, 2025

# OUTLINE

- **Introduction:** Why Gravitational Waves - Why New Physics?
- **Fundamental Physics**: Massive Gravity
- **Pulsar Timing Arrays:** Stochastic Gravitational Waves Background and Early Universe Sources Overview
- **Anisotropic Phases in the Early Universe:** Bubbles, Sound Waves, Hydro- and MHD Turbulence; Magnetic Fields…

# COLLABORATION

- **Seniors and Juniors:** Axel Brandenburg, Grigol Gogoberidze, Arthur Kosowsky, Sayan Mandal, Alberto Roper. Pol
- **Students**: Chris Choi, Emma Clarke, Murman Gurgenidze Ved Kenjale, Jacob Magallanes, Nakul Shenoy, Jonathan Stepp

# WHY GRAVITATIONAL WAVES

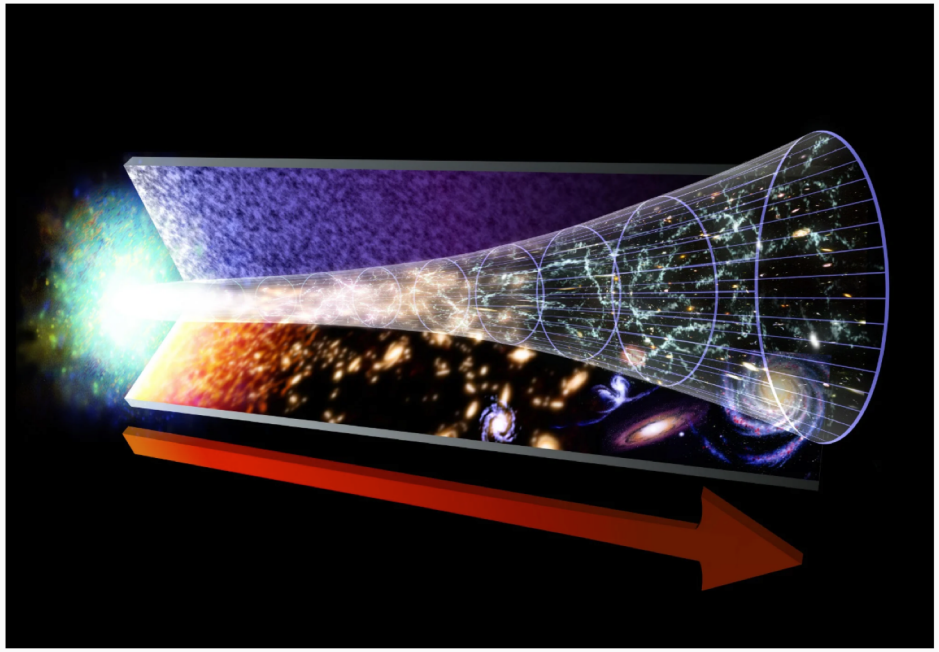

Artist's impression of the "Arrow of Time". Source: NASA/GSFC

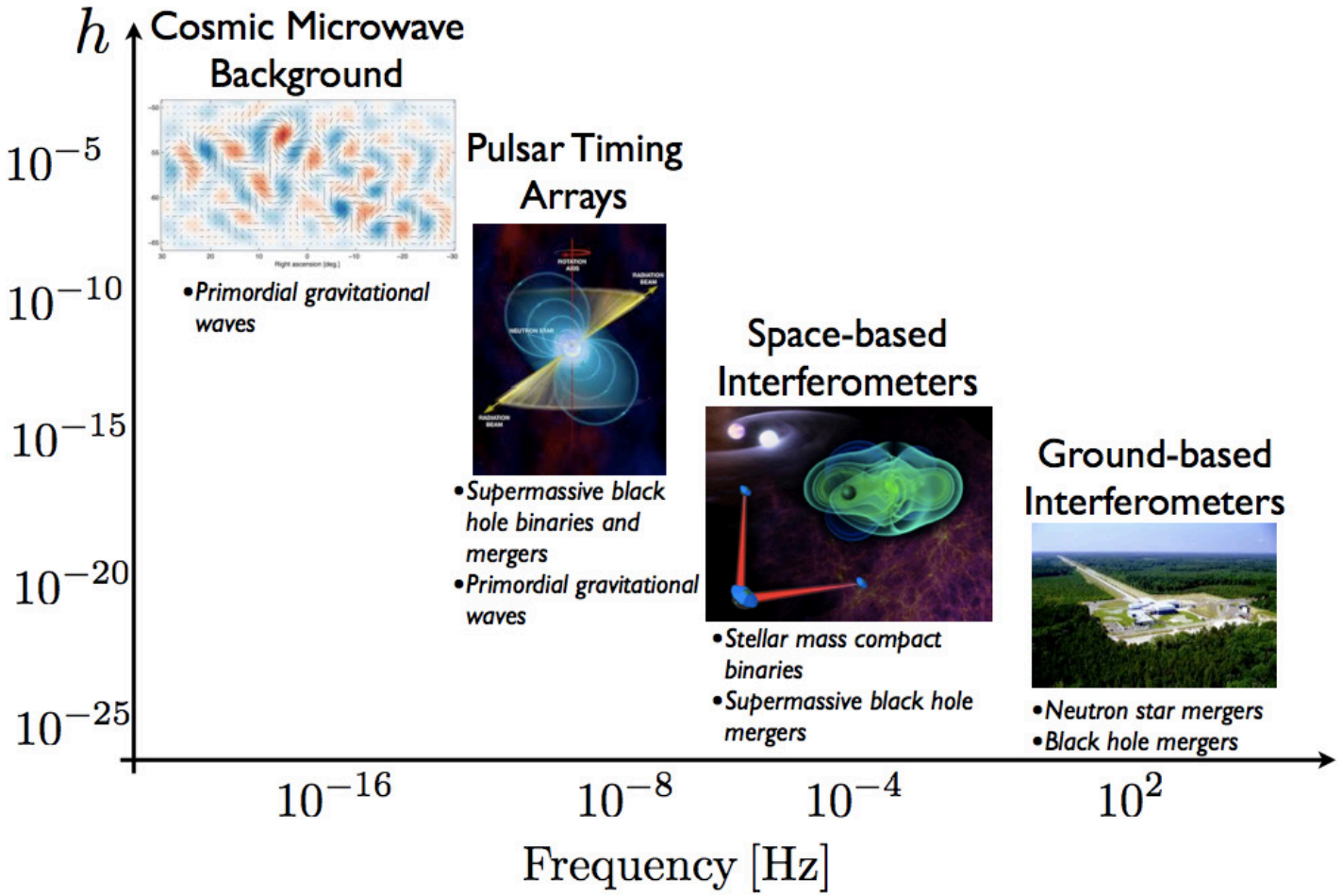

# WHAT IS NEXT?

Garcia Bellido et al. 2020

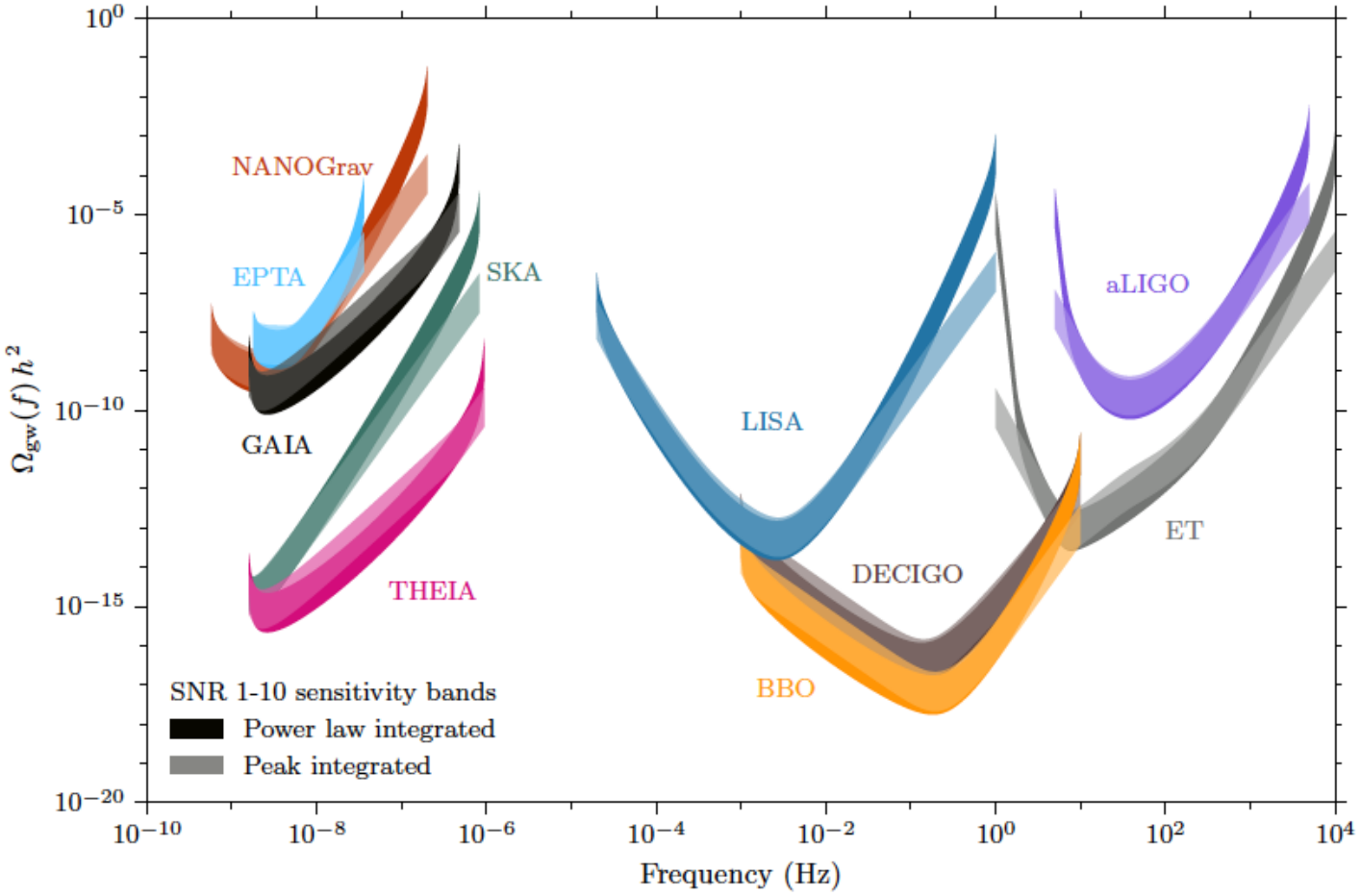


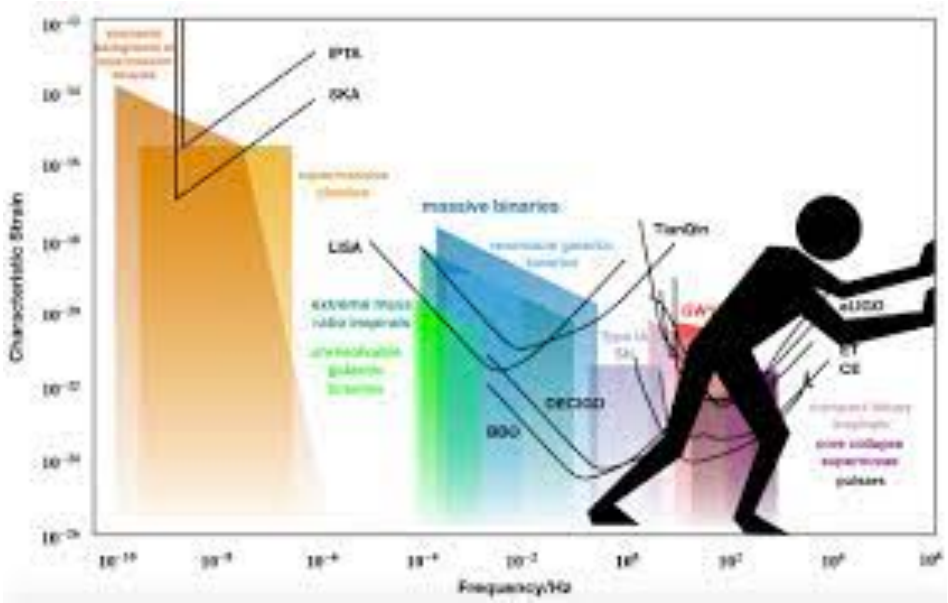


Credit CERN

*Connection with High Energy Particle Physics – the best laboratory to test the energy scales EVEN near the Planck scale*

# LASER VS ATOMIC INTERFEROMETRY

Atom Interferometry
for
Detection of Gravitational Waves

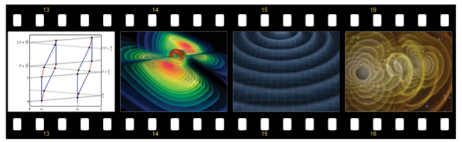

NIAC Phase I Final Report

BABAK N. SAIF • JASON HOGAN • MARK A KASEVICH

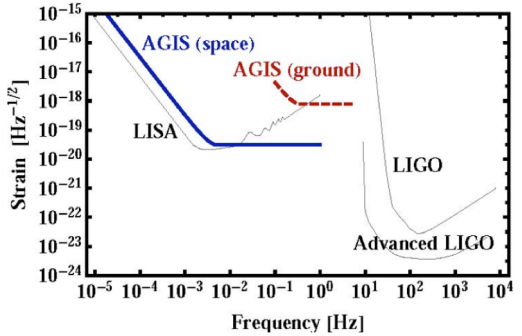


**Figure 1-2:** Example strain sensitivity curves for proposed terrestrial (red dashed) and satellite (blue solid) atom GW detectors. Terrestrial parameters: $L = 4$ km, $1000\hbar k$ atom optics and $T = 1.4$ s; Satellite parameters: $L = 10^3$ km, $100\hbar k$ atom optics (recently demonstrated[8]) and $T = 100$ s. Both assume $10^8$ atoms/s shot-noise limited phase detection. LIGO and LISA sensitivity curves (gray thin) are shown for reference.

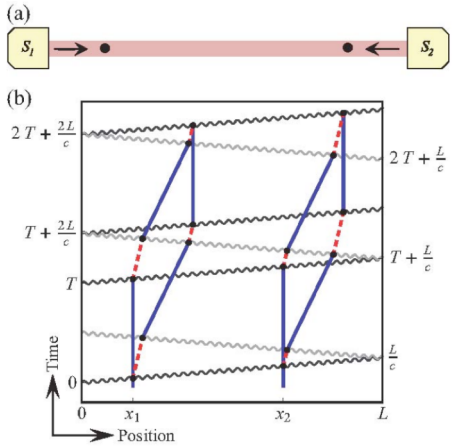


**Figure 1-1:** Gravitational wave detection using atoms. **(a)** Dilute clouds of atoms (black circles) at either end of a long baseline act as inertial test masses. Laser light (red) propagates between the atoms from sources $S_1$ and $S_2$. **(b)** Space-time diagram of the trajectories of both atom interferometers, showing the ground (blue) and excited (red dashed) atomic states. Short laser pulses (wavy lines) traveling from alternating sides of the baseline are used to divide, redirect, and recombine the atom de Broglie waves, yielding atom interference patterns that are highly sensitive to any modulation of the light travel time caused by gravitational radiation. The spatial extent of the atom interferometers relative to the baseline has been exaggerated..

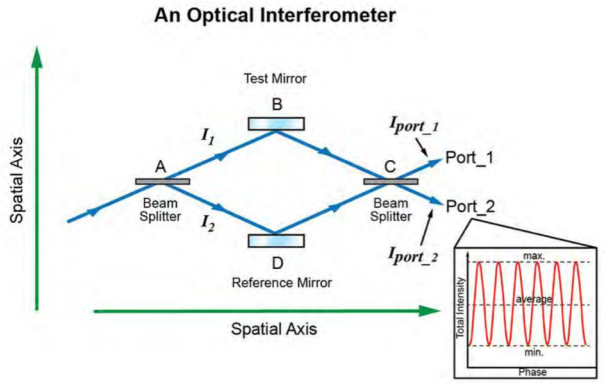


**Figure A.1. An Optical Interferometer**

Optical interferometers are used to measure surfaces, displacements, and absolute lengths. In this case, the desired information is the surface or position of object(s). The desired information about the object is encoded in the reflected light and the interference of the two coherent light beams results in a change of intensity as a function of the controlled phase $\varphi$. This intensity variation is referred to as an interference fringe pattern or "fringes." Fringes are analyzed and $OPD$ are measured.

Figure A.2 represents a three-pulsed Raman atom interferometer Space-Time diagram. Pulses in this interferometer consist of two counter propagating lasers.

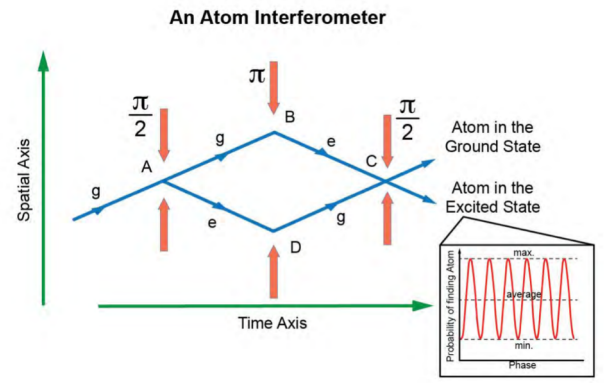


**Figure A.2. A Three-Pulsed Raman Atom Interferometer**

The proposed atom-based GW antenna (see Fig. 1.1(a)) is similar to well-established atom interferometric gravity gradiometers. Dilute clouds of ultracold atoms at either end of the baseline act as inertial test masses, and laser light propagates between the atoms. To implement atom interferometry, the lasers from sources S1 and S2 are briefly pulsed a number of times during each measurement cycle. The paths of these light pulses appear as wavy lines in Fig. 1.1(b). The two diamond-shaped loops represent the atom interferometers. Interaction with a light pulse transfers momentum to the atom and toggles the atomic state between the ground and the excited states. As a result, the light pulses act as beam-splitters and mirrors for the atom de Broglie waves, dividing them into a quantum superposition of two paths and eventually recombining them. Similar to an atomic clock, the phase shift recorded by each atom interferometer depends on the time spent in the excited state, which here is directly tied to the light travel time (L/c) across the baseline. GWs can be detected because they modulate the light travel time

# WHY NEW PHYSICS

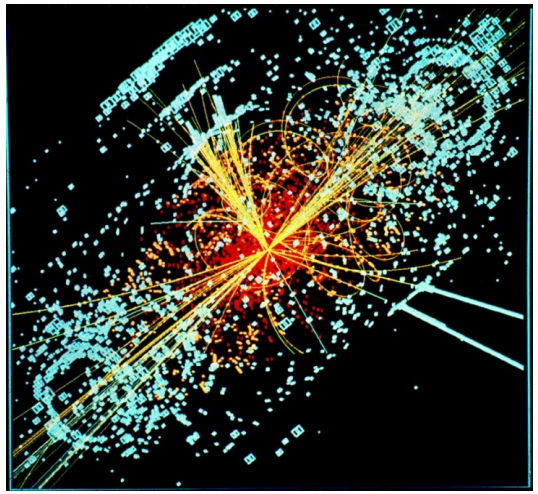


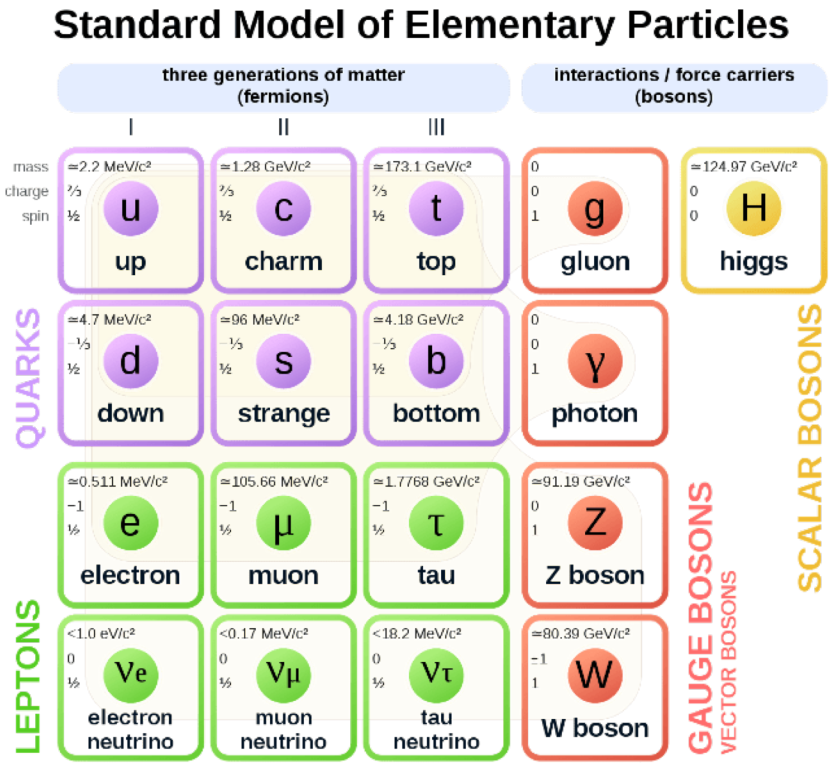


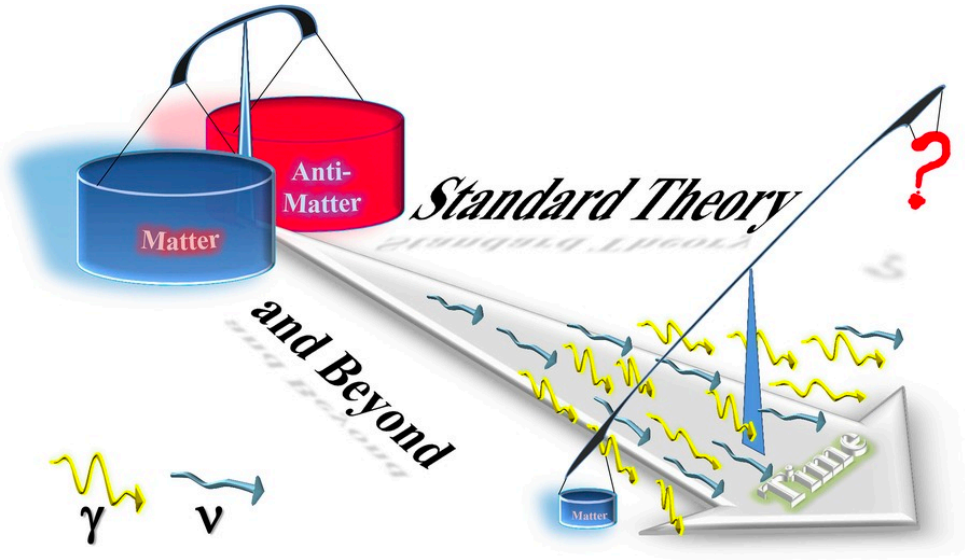

# WHY NEW PHYSICS?

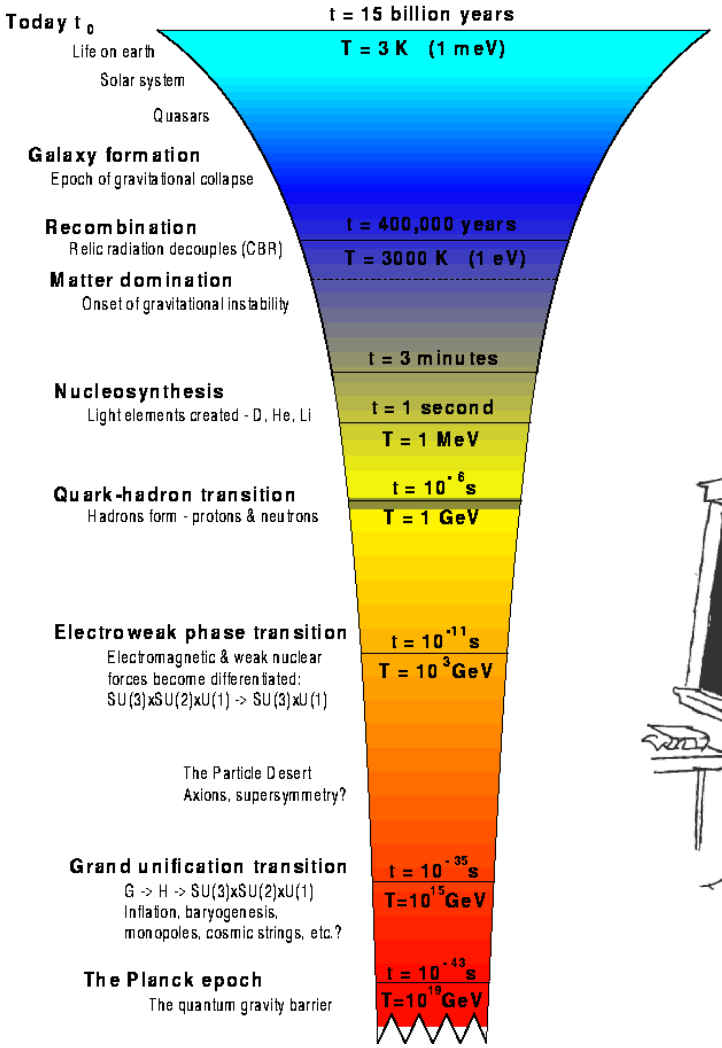


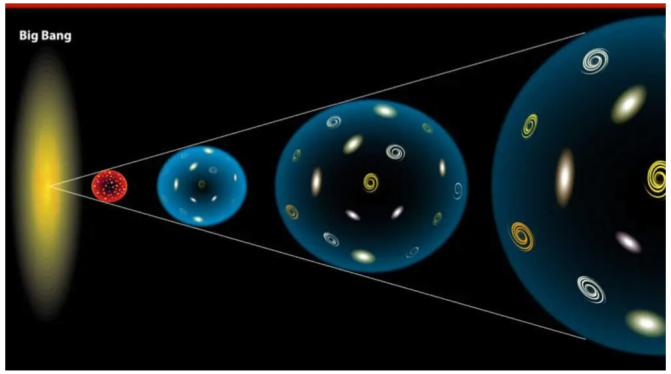


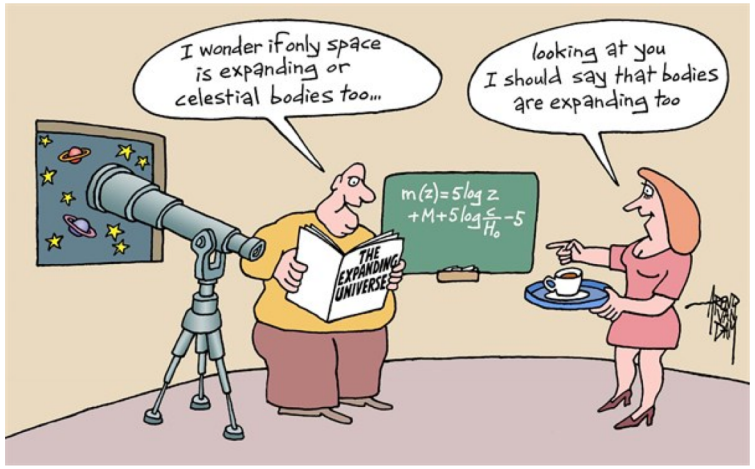


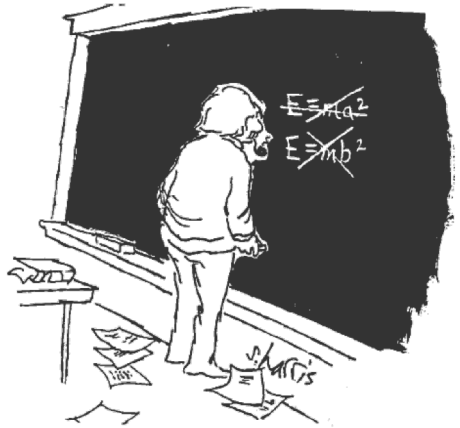


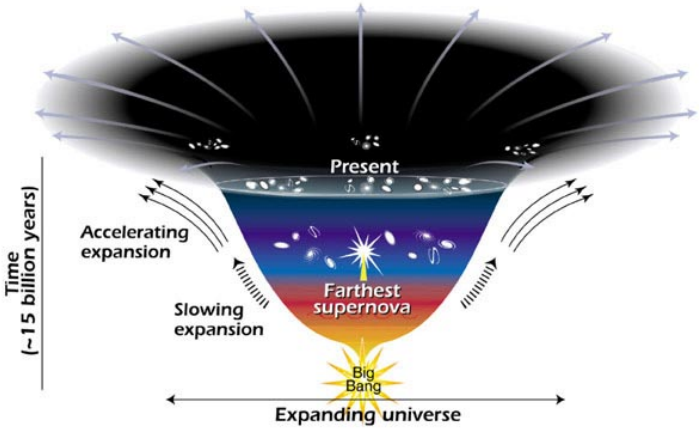

# WHY NEW PHYSICS?


"I've either discovered dark matter, or I've left the lens cap on."

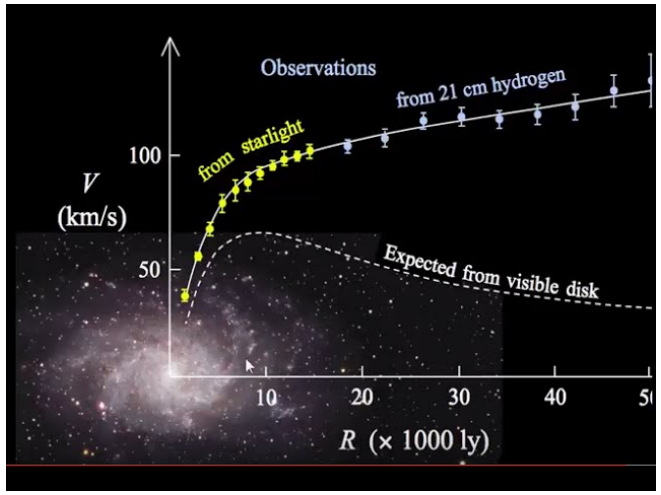


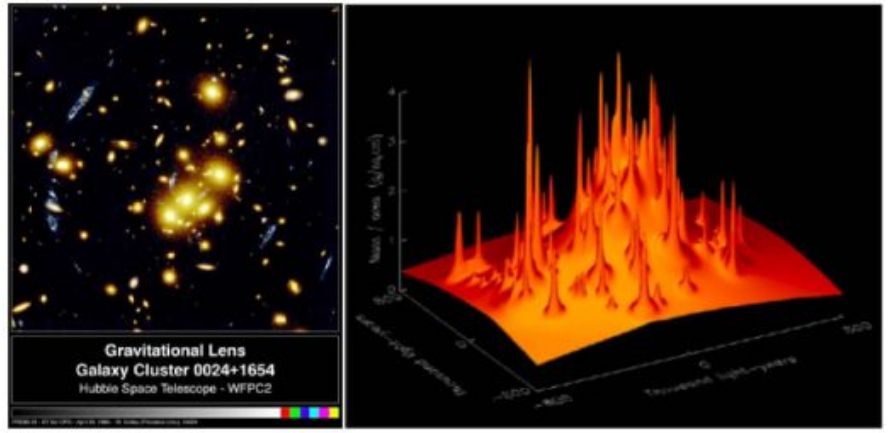


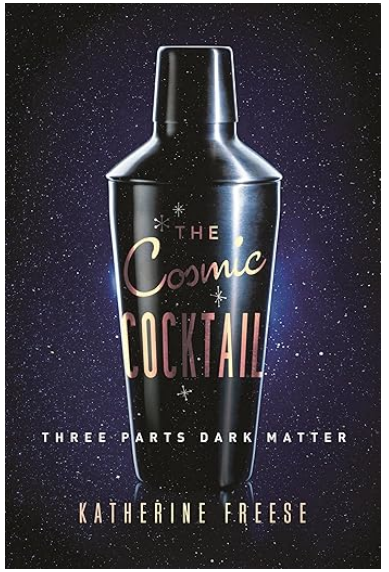

# WHY NEW PHYSICS?

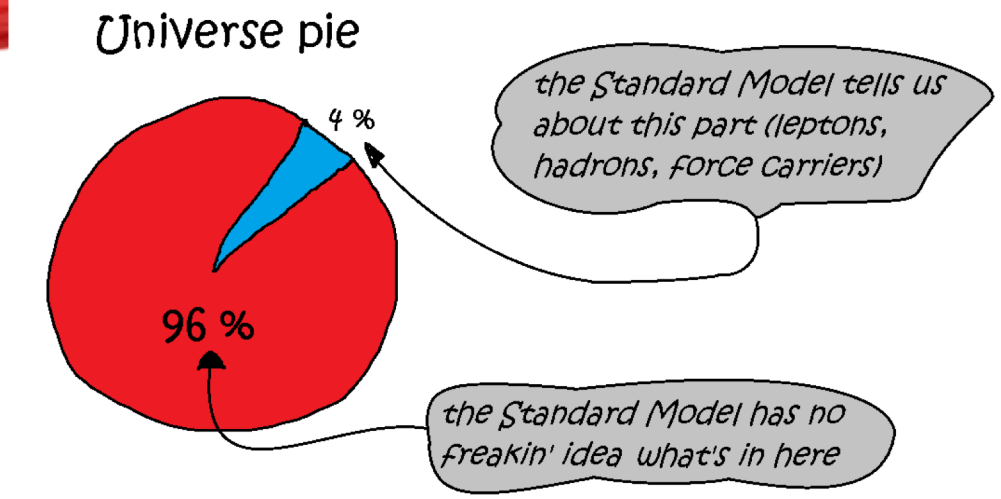


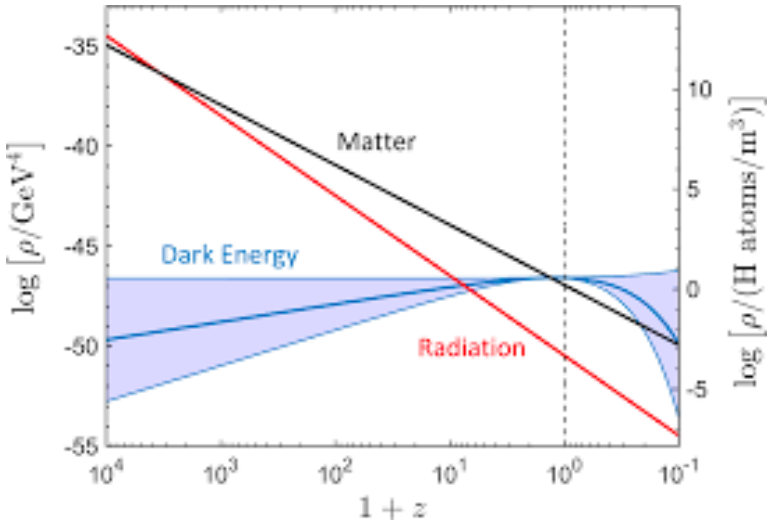


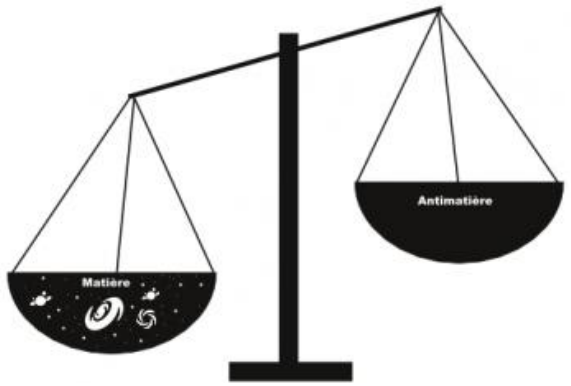


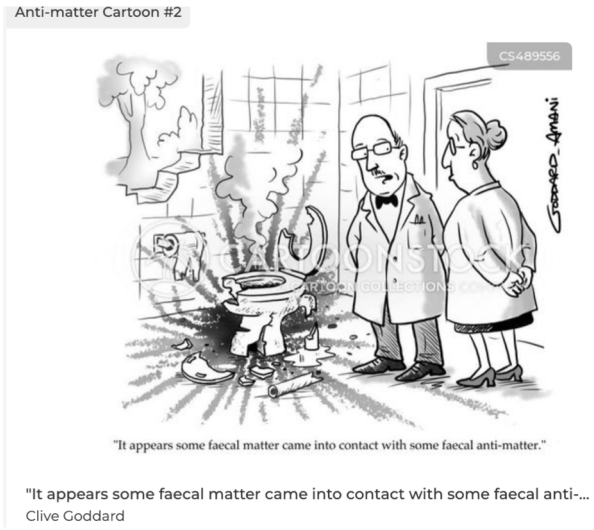


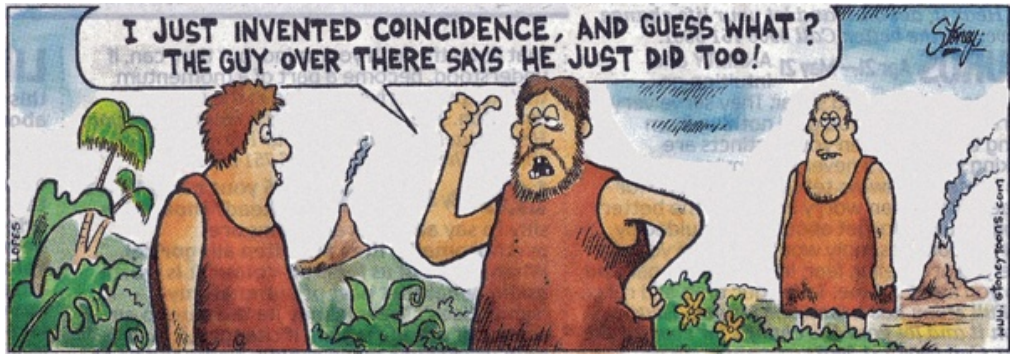

# HUBBLE TENSION

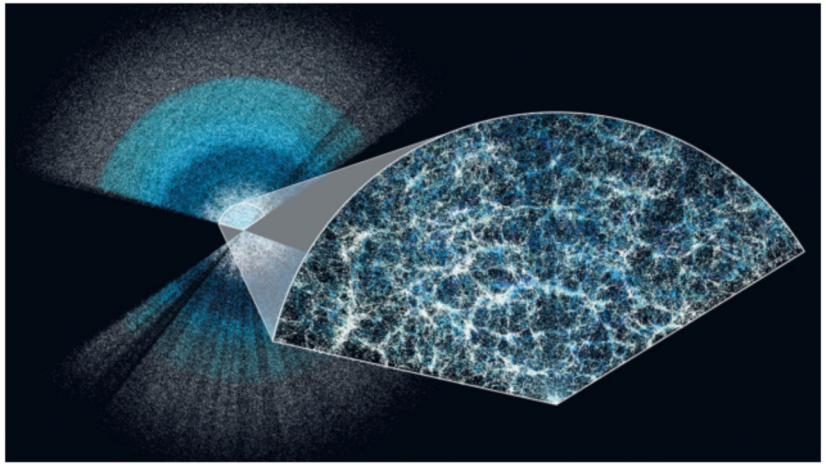

**Wide open** DESI's map of the universe is the largest to date, showing delicate bubble-like structures in the distribution of galaxies (inset) that contain clues to the expansion history of the universe. Credit: C Lamman/DESI/cmastro

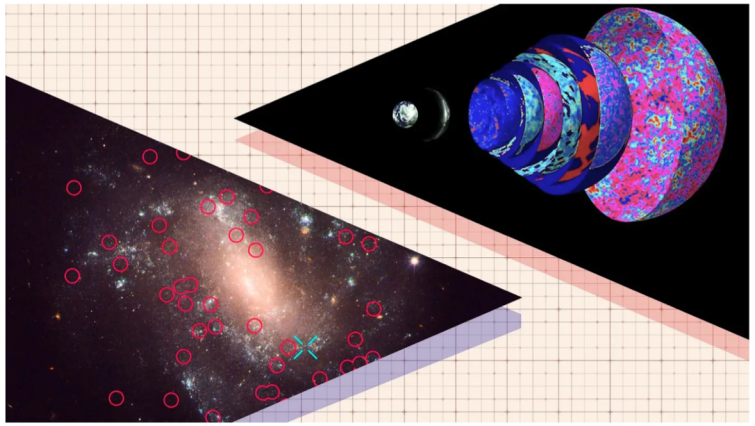

If you measure the expansion rate of the Universe using an early relic method, like the light from the CMB (top right), you get a value of around 67 km/s/Mpc. If you measure it by constructing a distance ladder (below left), such as with Cepheids and type Ia supernovae, you get a value more like 73 km/s/Mpc. This discrepancy is at the root of the Hubble tension. (Credit: Annelisa Leinbach / NASA, Adobe Stock)

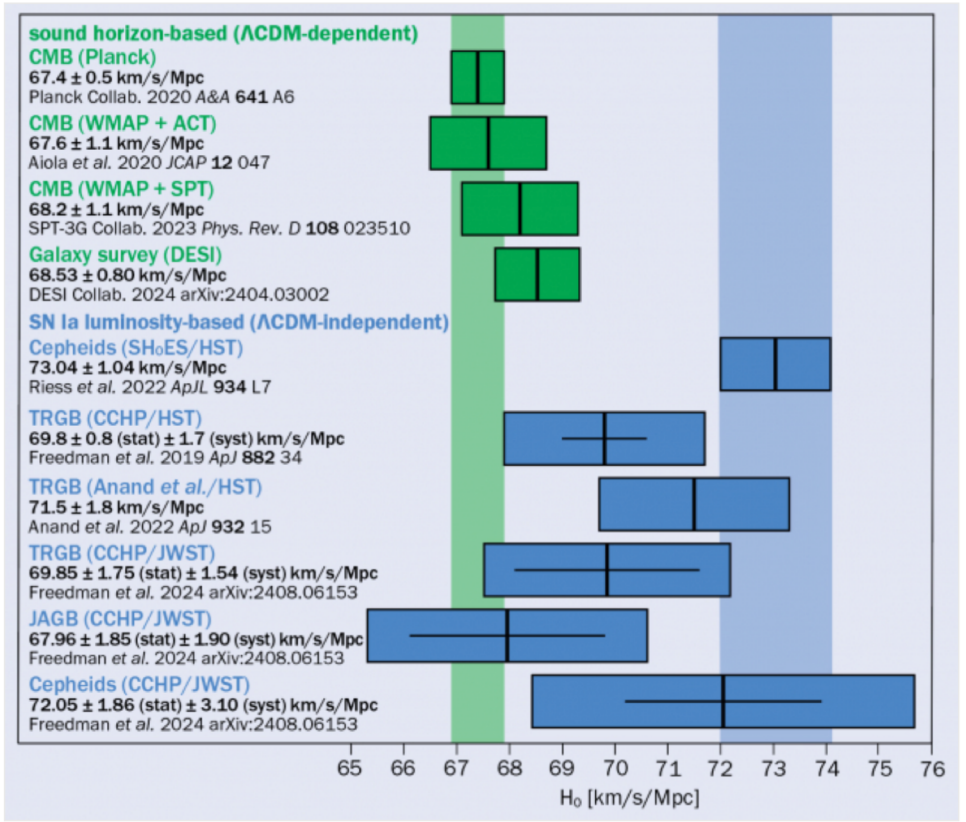


**The Hubble tension** The measurements of the Hubble constant described in this article. ΛCDM predictions (green) are labelled by the method of measuring the scale of baryon acoustic oscillations and the instrument(s) used. Direct measurements are labelled by the means of calibrating the distance to SN Ia, the analysis team and the instrument used for the calibration. Credit: V Poulin

Wiley Online Library
Large-Angle Anomalies in the CMB - Copi ...

# CMB ANOMALIES

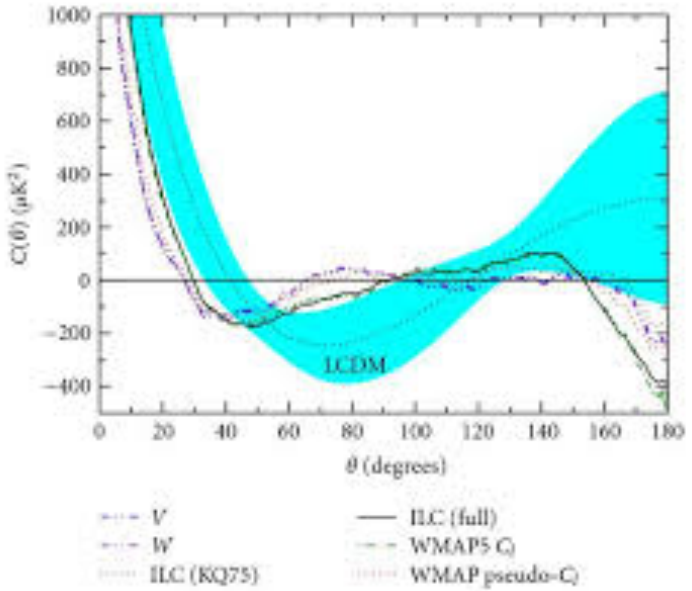


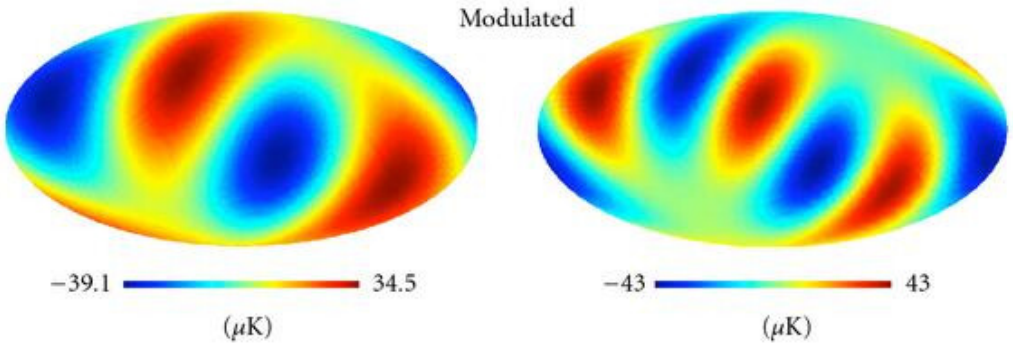


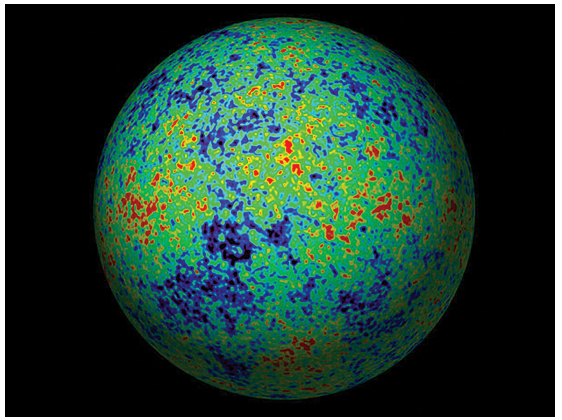

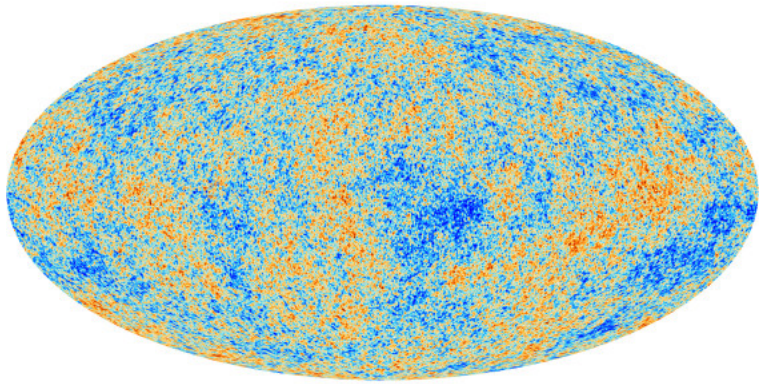

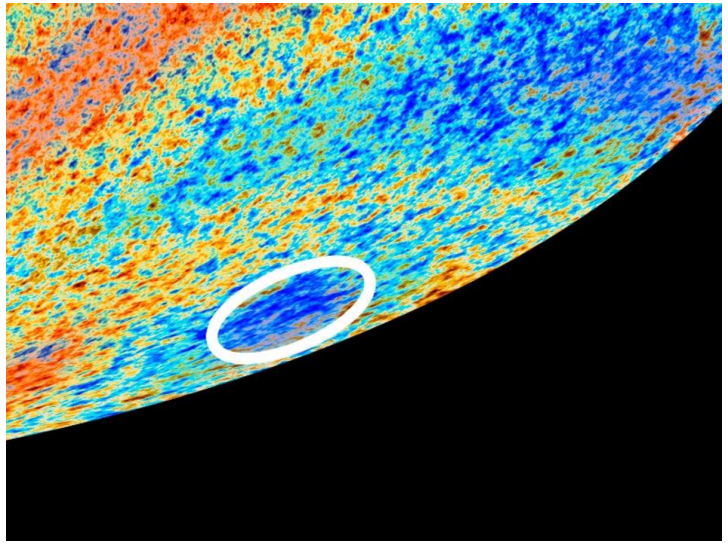

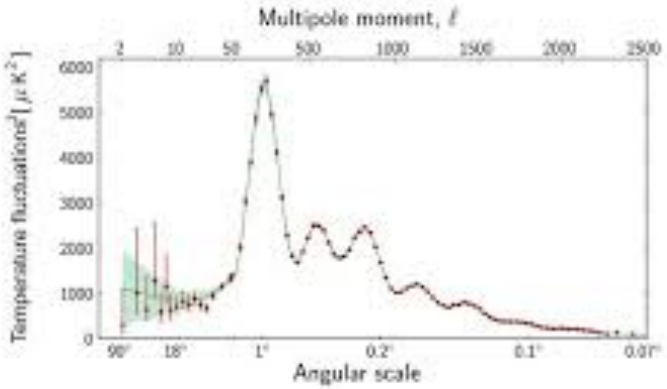

# MODIFICATIONS OF GENERAL RELATIVITY

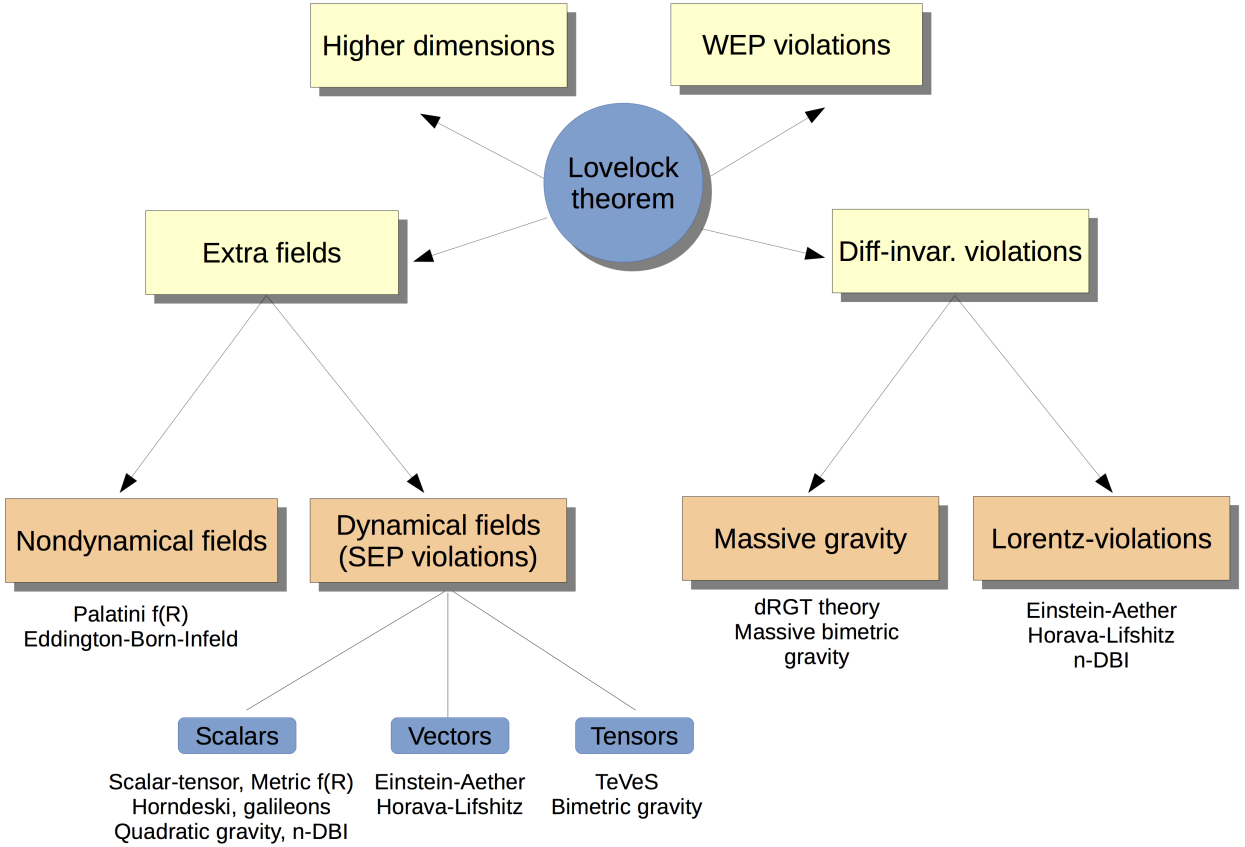


Berti et al.

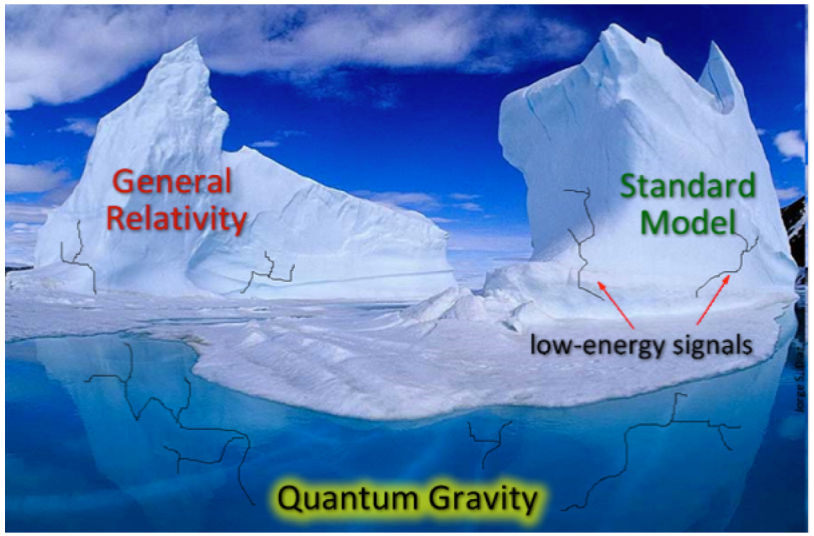


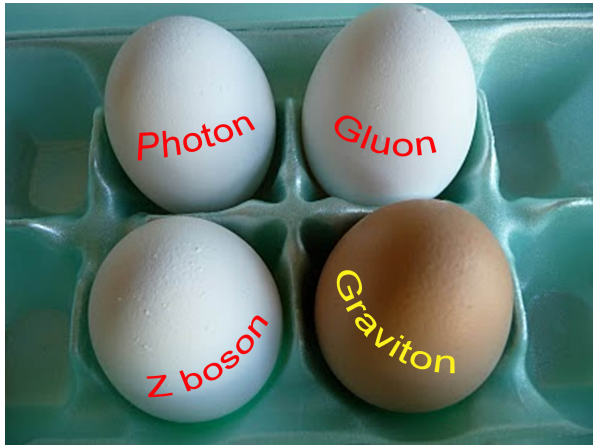

# PULSAR TIMING ARRAYS

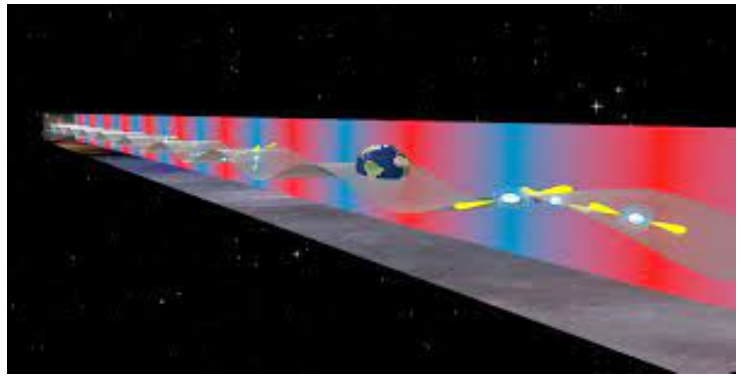

The proposal to use pulsars as GW detectors was originally made by **Sazhin (1978)** and **Detweiler (1979)** iThe idea is to treat the solar system barycenter and a galactic pulsar as opposite ends of an imaginary arm in space.

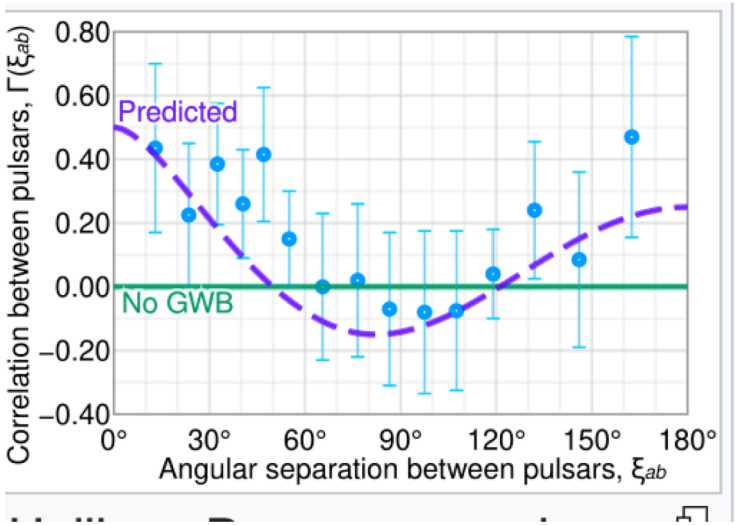


$$\Gamma_{ab} = \frac{1}{2}\delta_{ab} + \frac{1}{2} - \frac{x_{ab}}{4} + \frac{3}{2}x_{ab}\ln x_{ab}$$

$$x_{ab} = (1 - \cos\zeta_{ab})/2$$

**overlap reduction function**

Credit: NANOGrav

In 1983, **Hellings** and **Downs**[1] extended this idea to an array of pulsars and found that a stochastic background of GWs would produce a distinctive GW signature: a quadrupolar spatial correlation between arrival times of pulses emitted by different millisecond pulsar pairings that depends only on the pairing's angular separation in the sky as viewed from Earth (actually the solar system barycenter). The key property of a pulsar timing array is that the signal from a stochastic GW background will be correlated across the sightlines of pulsar pairs, while that from the other noise processes will not.

**Assumptions**: Isotropic GW that obeys Einstein's general relativity. It is valid for "long-arm" detectors like pulsar timing arrays, where the wavelengths of typical GWs are much shorter than the "long-arm" distance between Earth and typical pulsars

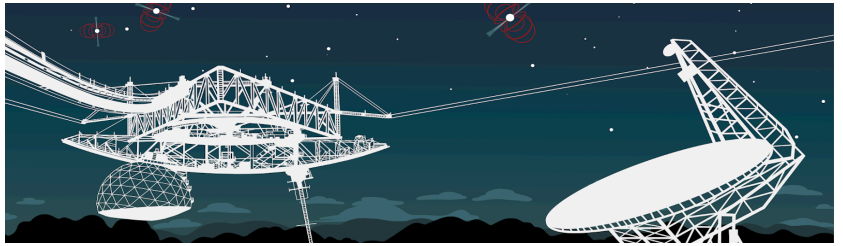

# STOCHASTIC GRAVITATIONAL WAVES DETECTION

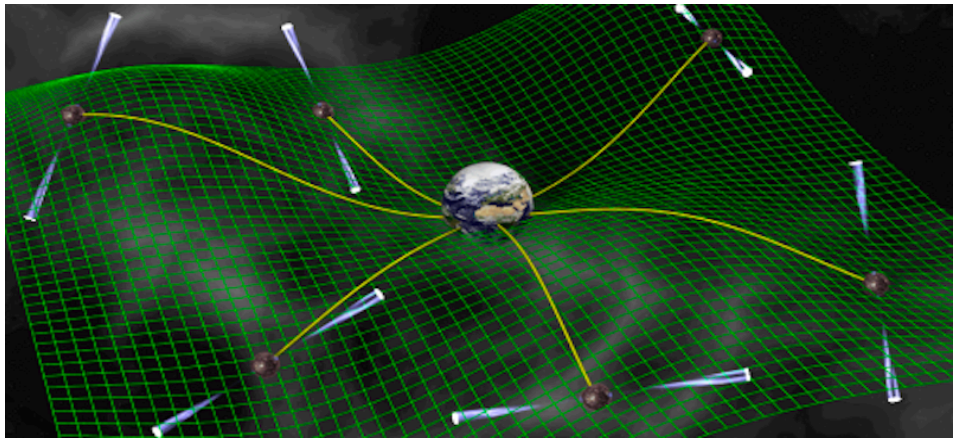

The pulsar acts as the reference clock at one end of the arm sending out regular signals which are monitored by an observer on Earth. The effect of a passing long-wavelength GW would be to perturb the galactic spacetime and cause a small change in the observed time of arrival of the pulses.

Credit: NANOGrav

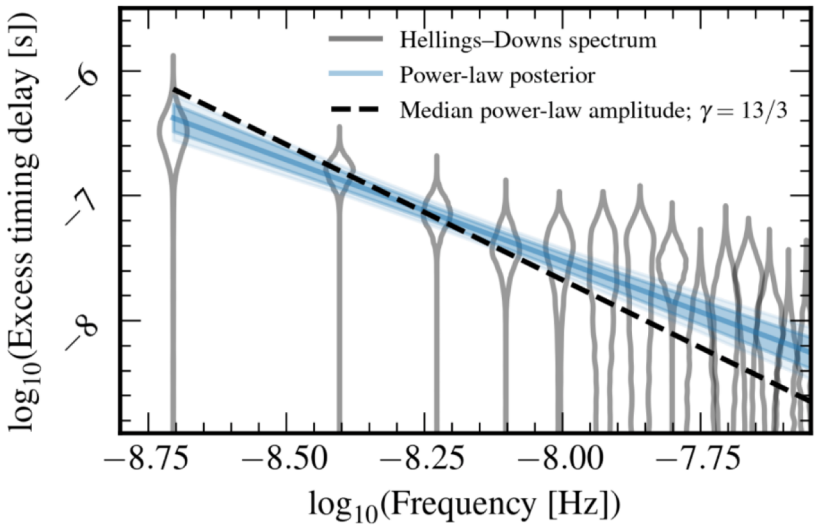


Detection residuals in the time delay in the pulsar signals

$$R(t) \equiv \int_0^t dt' \left( \frac{\nu_0 - \nu(t')}{\nu_0} \right)$$

$$\frac{1}{T_{\rm obs}} < f < \frac{1}{\delta t}$$

$$h_c(f) = A_{\rm CP} \left( \frac{f}{f_{\rm yr}} \right)^{\alpha_{\rm CP}},$$

$$\Omega_{\rm GW}(f) = \frac{2\pi^2}{3H_0^2} f^2 h_c^2(f) = \Omega_{\rm GW}^{\rm yr} \left( \frac{f}{f_{\rm yr}} \right)^{5-\gamma_{\rm CP}}$$

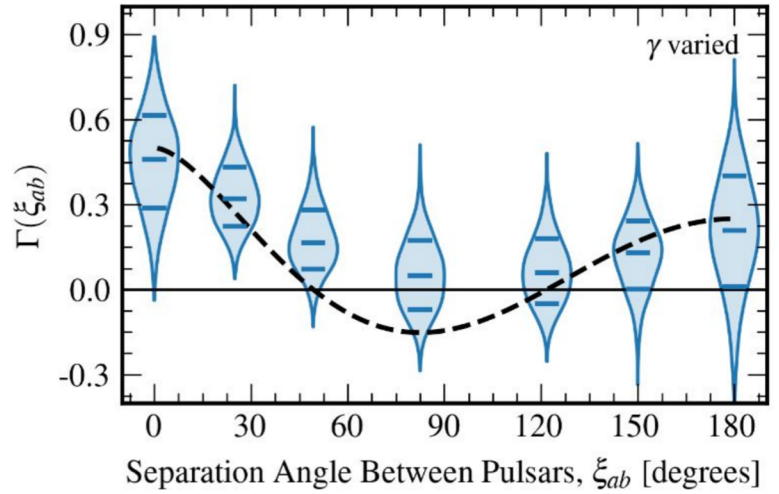

# STOCHASTIC GRAVITATIONAL WAVES DETECTION

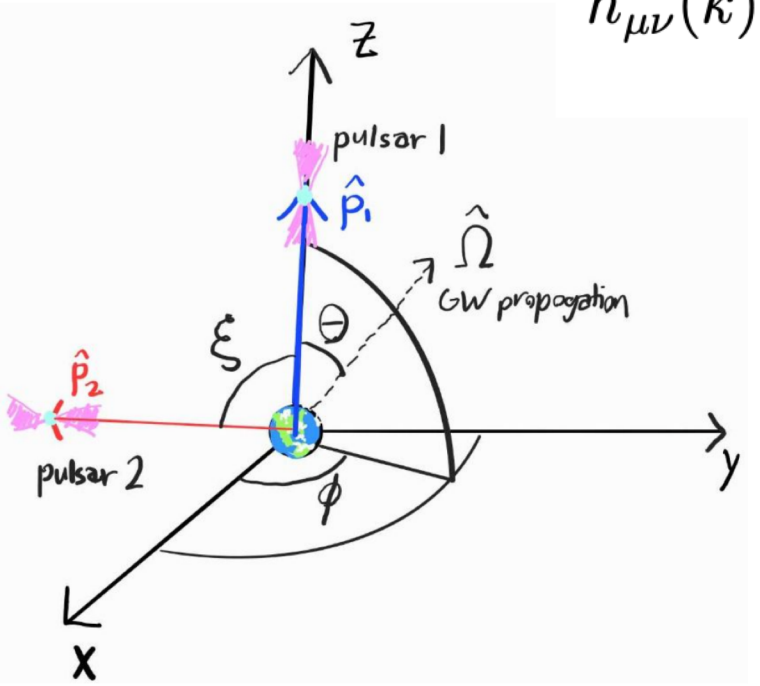


Credit Chris, Choi

$$h_{\mu\nu}(k) = \sum_i h^{(i)}(k)\, \epsilon^{(i)}_{\mu\nu}\ , \qquad \epsilon^{i}_{\mu\nu} \text{ polarization tensor}$$

$$\left\langle h^{(i)*}(f,\hat{\Omega}) h^{(i')}\left(f',\hat{\Omega}'\right)\right\rangle = \frac{3H_0^2}{32\pi^3}\delta^2\left(\hat{\Omega},\hat{\Omega}'\right)\delta_{ii'}\delta\left(f-f'\right)\times|f|^{-3}\Omega_{\rm gw}(|f|)\ .$$

In the barycenter reference frame of the solar system, the frequency shift is characterized by the redshift $z(t) = \frac{\nu_0 - \nu(t)}{\nu_0}$ and averaged redshift: $\tilde{z}(f) \equiv \int d^2\hat{\Omega}\, z(f,\Omega)$

$$\langle \tilde{z}(f)\tilde{z}(f')\rangle = \frac{3H_0^2\delta^2\left(\hat{\Omega},\hat{\Omega}'\right)\delta_{ii'}\delta(f-f')}{32\beta\pi^3|f|^3}\Omega_{\rm gw}(|f|)\Gamma(|f|)$$

$\beta$ is the normalization factor introduced so that $\Gamma(|f|) = 1/2$ for coaligned coincident pulsars to match the conventions of the Hellings-Downs (HD) correlation

$$\Gamma_I(|f|) = \sum_{i\in I}\int_{S^2} d^2\hat{\Omega}\mathcal{E}_1(-f,\hat{\Omega})\mathcal{E}_2(f,\hat{\Omega})F_1^{(i)}(\hat{\Omega})F_2^{(i)}(\hat{\Omega})\ ,$$

# MASSIVE GRAVITY

De Rham 2017

Shankaranarayanan & Johnson

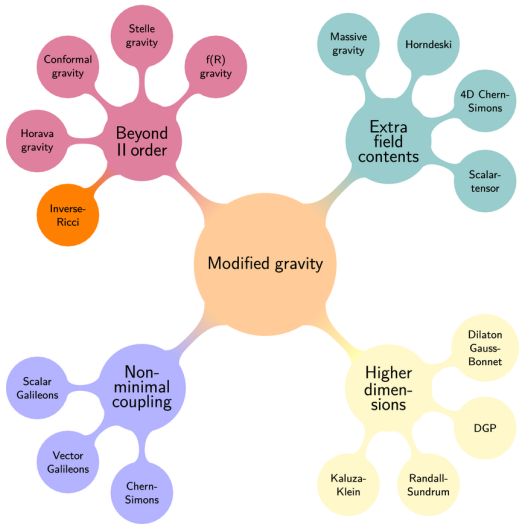


**Yukawa**

| $m_g$ (eV) | $\lambda_g$ (km) | Eq. | |
|---|---|---|---|
| $\mathbf{7.2 \times 10^{-23}}$ | $\mathbf{2.8 \times 10^{12}}$ | (49) | A $2\sigma$ bound from the precession of Mercury (Talmadge *et al.*, 1988; Will, 1998). |
| $6 \times 10^{-32}$ | $3 \times 10^{21}$ | (53) | A $1\sigma$ bound from weak lensing of a cluster at $z = 1.2$ (Choudhury *et al.*, 2004). Sensitive to the dark matter distribution and cosmological model. |
| $10^{-29}$ | $10^{19}$ | (52) | From observations of gravitationally bound clusters of 0.5 Mpc (Goldhaber and Nieto, 1974; Hare, 1973). Sensitive to the dark matter distribution. |

**Dispersion Relation**

| $m_g$ (eV) | $\lambda_g$ (km) | Eq. | |
|---|---|---|---|
| $\mathbf{1.2 \times 10^{-22}}$ | $\mathbf{1.7 \times 10^{12}}$ | (58) | A 90% confidence bound two 30 $M_\odot$ bh-bh merger (GW150916) (Abbott *et al.*, 2016d; Will, 1998). |
| $7.6 \times 10^{-20}$ | $2.6 \times 10^{9}$ | (65) | From pulsar timing of PSR B1913+16 and PSR B1534+12 (Finn and Sutton, 2002). |
| $10^{-30}$ | $10^{20}$ | (63) | Observations of power in B–mode polarization in CMB at low $\ell$ (Dubovsky *et al.*, 2010; Gumrukcuoglu *et al.*, 2012; Raveri *et al.*, 2015). |
| $10^{-26}$ | $10^{16}$ | (59) | A $10^4$ to $10^7$ $M_\odot$ merger by eLISA type experiment (Will, 1998). |
| $10^{-24}$ | $10^{14}$ | (60) | A dual messenger observation of IBWD by eLISA type experiment (Cooray and Seto, 2004; Cutler *et al.*, 2003; Larson and Hiscock, 2000). |
| $10^{-23}$ | $10^{13}$ | (66) | Pulsar timing array of 100ns accuracy with 10 year observation (Lee *et al.*, 2010). |
| $10^{-20}$ | $10^{10}$ | (61) | Dual messenger observation of SNe gamma ray burst and gravitational waves (Nishizawa and Nakamura, 2014). |

**Fifth Force**

| $m_g$ (eV) | $\lambda_g$ (km) | Eq. | |
|---|---|---|---|
| $10^{-32}$ | $10^{22}$ | (77) | From earth-moon precession for cubic Galileon theories (Dvali *et al.*, 2003). |
| $10^{-32}$ | $10^{22}$ | (84) | From precession in full 5D DGP in the Solar System (Gruzinov, 2005; Lue and Starkman, 2003). |
| $10^{-30}$ | $10^{20}$ | (81) | From earth-moon precession for quartic Galileon theories (dRGT-like) (de Rham, 2014). |
| $10^{-27}$ | $10^{17}$ | (86) | From PSR B1913+16 pulsar in cubic Galileon theories (DGP) (de Rham *et al.*, 2013d). |
| $10^{-33}$ | $10^{23}$ | (89) | A prospective $4\sigma$ bound from weak lensing on next-gen surveys (Park and Wyman, 2015; Wyman, 2011). Sensitive to alternative DM halo profiles. |
| $10^{-32}$ | $10^{22}$ | (90) | Observations of altered structure formation from fifth force (Khoury and Wyman, 2009; Park and Wyman, 2015; Wyman, 2011; Zu *et al.*, 2014). Sensitive to the particular theory of massive gravity. |

**Figure 1.** A modified gravity architecture, which gives a representation of some possible ways of modifying GR through breaking the Lovelock's theorem along with some examples. Theories are classified in order to avoid Lovelock's restrictions. In the green region we have theories as de Rham-Gabadadze-Tolley (dRGT) massive gravity theories, and cases with $m_g > 0$. In the red region we have theories with additional field as scalar (Horndeski) which includes cases as Galileon, Quintessence, Brans–Dicke and $f(R)$. Moreover, Vector theories such as Proca and Tensor–Vector–Scalar (TeVes) are presented and, finally, bigravity theories. In the olive region we have an example of theories that are constructed in the break assumption formalism as non-local ones, extra dimensions and Lorentz violating. The main gravitational wave (GW) test of each theory is framed at the top, where the following was considered: GW speed (blue color) and dispersion (red color) refers to constraints from late time GW sources. GW oscillations (yellow color) refer to these oscillations during the propagation introducing a modulation of the GW amplitude. GW damping (green color) refers to probing the damping of GWs using standard sirens from $d_L^{\rm GW}$ (luminosity distance of GWs) and $d_L^{\rm EM}$ (electro-magnetic luminosity distance). Theories that are constrained by these GW observables are enclosed by a dashed square of each GW color, respectively. This figure was designed based on the ideas and discussions behind the construction of theoretically sensible modified gravity theories [10,11,12]. Classification of parameterised post-Newtonian (PPN) tests was based on approximations to obtain the PPN parameters at 1, 2, 4 PN level [13,14,15]. Moreover, a PPN extension for a five-dimensional metric was included [16]. Notice that theories that are in agreement with this PNN test are filled in their respective colors: 2PN level (solid green color), unconstrained (solid red color) and 4PN level/PNN extra-dimensional (olive color).

Escamilla-Rivera and Fabris 2021

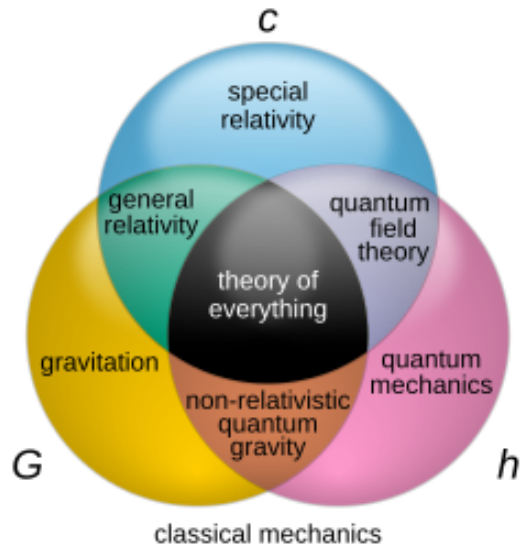


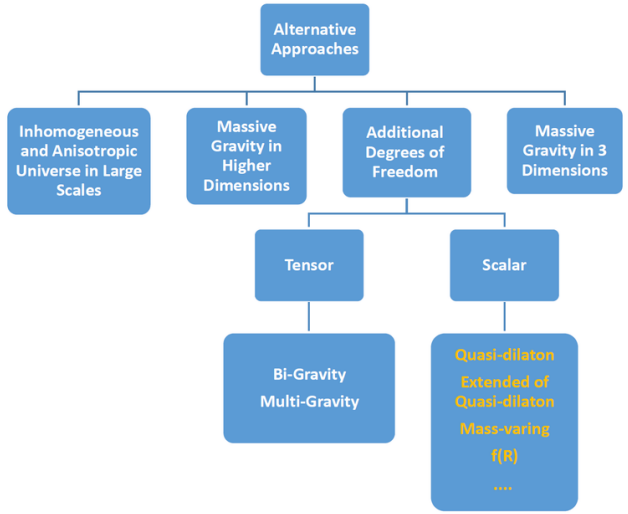


Sobhan Kazempour

# TESTS OF MASSIVE GRAVITY

Fiertz-Pauli

$$S = \int d^4x \left[\frac{1}{2}\partial_\lambda h_{\mu\nu}\partial^\lambda h^{\mu\nu} - \partial_\mu h_{\nu\lambda}\partial^\nu h^{\mu\lambda} + \partial_\mu h^{\mu\nu}\partial_\nu h - \frac{1}{2}\partial_\lambda h \partial^\lambda h + \frac{1}{2}m^2\left(h_{\mu\nu}h^{\mu\nu} - h^2\right)\right]$$

**Yukawa-like exponential suppression** is expected when the force carrier possesses a nonzero mass. In the case of MG, suppression of the gravitational potential is of the form

$$\Phi \propto \exp\left[-m_g R/R\right]$$

There is also a suppression of GWs at wavelengths larger than the Compton length scale of the graviton $R_g \sim (m_g)^{-1}$

**Modification of the dispersion relation** gains a massive term, implying a difference between the GW propagation speed $c_g$ and the speed of light $c$, which can be used to constrain $m_g$.

**Additional degrees of polarization** are characterized by the additional helicity ±1 and 0 modes. Certain theories of MG, such as the minimal theory of MG, only have two tensor modes, as in GR, but a general theory of MG that assumes Lorentz invariance will have five in total, De Rham-Gabadadze-Tolley model

**Figure 5**

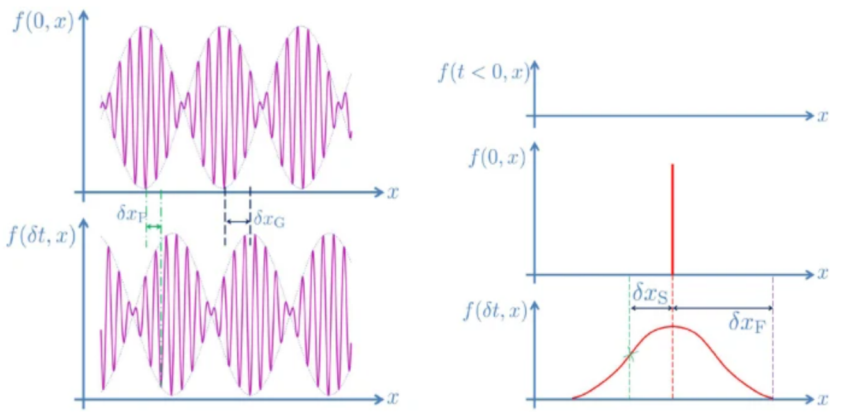


Difference between phase, group, signal and front velocities. At $t = \delta t$, the phase and group velocities are represented on the left and given respectively by $v$ phase = $\delta x_P/\delta t$ and $v_{\text{group}} = \delta x_G/\delta t$ (in the limit $\delta t \to 0$.) The signal and front velocity represented on the right are given by $v_{\text{signal}} = \delta x_S/\delta t$ (where $\delta x_S$ is the point where at least half the intensity of the original signal is reached.) The front velocity is given by $v_{\text{front}} = \delta x_F/\delta t$.

De Rham 2014, Living Review

# PULSAR TIMING ARRAYS DATA AND ADDITIONAL POLARIZATIONS

The Astrophysical Journal Letters, 923:L22 (18pp), 2021 December 20 https://doi.org/10.3847/2041-8213/ac401c


## The NANOGrav 12.5-year Data Set: Search for Non-Einsteinian Polarization Modes in the Gravitational-wave Background

Zaven Arzoumanian[1], Paul T. Baker[2], Harsha Blumer[3,4], Bence Bécsy[5], Adam Brazier[6,7], Paul R. Brook[3,4], Sarah Burke-Spolaor[3,4,8], Maria Charisi[9], Shami Chatterjee[6], Siyuan Chen[10,11,12], James M. Cordes[6], Neil J. Cornish[5], Fronefield Crawford[13], H. Thankful Cromartie[6], Megan E. DeCesar[14,15,48], Dallas M. DeGan[16], Paul B. Demorest[17], Timothy Dolch[18,19], Brendan Drachler[20,21], Justin A. Ellis[22], Elizabeth C. Ferrara[23,24,25], William Fiore[3,4], Emmanuel Fonseca[26], Nathan Garver-Daniels[3,4], Peter A. Gentile[3,4], Deborah C. Good[27], Jeffrey S. Hazboun[28,48], A. Miguel Holgado[29,30], Kristina Islo[31], Ross J. Jennings[6], Megan L. Jones[31], Andrew R. Kaiser[3,4], David L. Kaplan[31], Luke Zoltan Kelley[32], Joey Shapiro Key[28], Nima Laal[16], Michael T. Lam[20,21], T. Joseph W. Lazio[33], Duncan R. Lorimer[3,4], Tingting Liu[31], Jing Luo[34], Ryan S. Lynch[35], Dustin R. Madison[3,4,48], Alexander McEwen[31], Maura A. McLaughlin[3,4], Chiara M. F. Mingarelli[36,37], Cherry Ng[38], David J. Nice[14], Ken D. Olum[39], Timothy T. Pennucci[40,41,48], Nihan S. Pol[3,4,9], Scott M. Ransom[40], Paul S. Ray[42], Joseph D. Romano[43], Shashwat C. Sardesai[31], Brent J. Shapiro-Albert[3,4], Xavier Siemens[16,31], Joseph Simon[33,44], Magdalena S. Siwek[45], Renée Spiewak[46], Ingrid H. Stairs[27], Daniel R. Stinebring[47], Kevin Stovall[17], Jerry P. Sun[16], Joseph K. Swiggum[14,48], Stephen R. Taylor[9], Jacob E. Turner[3,4], Michele Vallisneri[33], Sarah J. Vigeland[31], Haley M. Wahl[3,4], and Caitlin A. Witt[3,4]
The NANOGrav Collaboration

The Astrophysical Journal Letters, 923:L22 (18pp), 2021 December 20

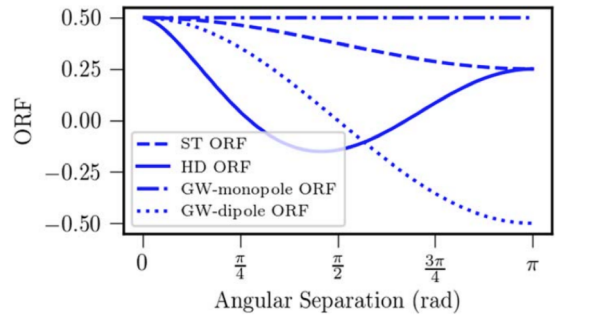


**Figure 4.** The solid line is the HD correlation curve, the dashed line is the ST ORF, the dashed–dotted line is the GW-monopole ORF, and the dotted line is the GW-dipole ORF. These four ORFs can be hard to distinguish if the uncertainties in the timing residual cross-correlations are sufficiently large.

The Astrophysical Journal Letters, 964:L14 (10pp), 2024 March 20 https://doi.org/10.3847/2041-8213/ad2a51


## The NANOGrav 15 yr Data Set: Search for Transverse Polarization Modes in the Gravitational-wave Background

Gabriella Agazie[1], Akash Anumarlapudi[1], Anne M. Archibald[2], Zaven Arzoumanian[3], Jeremy Baier[4], Paul T. Baker[5], Bence Bécsy[4], Laura Blecha[6], Adam Brazier[7,8], Paul R. Brook[9], Sarah Burke-Spolaor[10,11], Rand Burnette[4], Robin Case[4], J. Andrew Casey-Clyde[12], Maria Charisi[13], Shami Chatterjee[7], Tyler Cohen[14], James M. Cordes[7], Neil J. Cornish[15], Fronefield Crawford[16], H. Thankful Cromartie[7,64], Kathryn Crowter[17], Megan E. DeCesar[18], Dallas DeGan[4], Paul B. Demorest[19], Timothy Dolch[20,21], Brendan Drachler[22,23], Elizabeth C. Ferrara[24,25,26], William Fiore[10,11], Emmanuel Fonseca[10,11], Gabriel E. Freedman[1], Nate Garver-Daniels[10,11], Peter A. Gentile[10,11], Joseph Glaser[10,11], Deborah C. Good[12,27], Kayhan Gültekin[28], Jeffrey S. Hazboun[4], Ross J. Jennings[10,11,65], Aaron D. Johnson[1,29], Megan L. Jones[1], Andrew R. Kaiser[10,11], David L. Kaplan[1], Luke Zoltan Kelley[30], Matthew Kerr[31], Joey S. Key[32], Nima Laal[4], Michael T. Lam[22,23], William G. Lamb[13], T. Joseph W. Lazio[33], Natalia Lewandowska[34], Tingting Liu[10,11], Duncan R. Lorimer[10,11], Jing Luo[35,66], Ryan S. Lynch[36], Chung-Pei Ma[30,37], Dustin R. Madison[38], Alexander McEwen[1], James W. McKee[39,40], Maura A. McLaughlin[10,11], Natasha McMann[13], Bradley W. Meyers[17,41], Chiara M. F. Mingarelli[12,27,42], Andrea Mitridate[43], Priyamvada Natarajan[44,45], Cherry Ng[46], David J. Nice[47], Stella Koch Ocker[7], Ken D. Olum[48], Timothy T. Pennucci[49], Benetge B. P. Perera[50], Nihan S. Pol[13], Henri A. Radovan[51], Scott M. Ransom[52], Paul S. Ray[31], Joseph D. Romano[53], Alexander Saffer[10,11], Shashwat C. Sardesai[1], Ann Schmiedekamp[54], Carl Schmiedekamp[54], Kai Schmitz[55], Brent J. Shapiro-Albert[10,11,56], Xavier Siemens[1,4], Joseph Simon[57,67], Magdalena S. Siwek[58], Ingrid H. Stairs[17], Daniel R. Stinebring[59], Kevin Stovall[19], Jerry P. Sun[4], Abhimanyu Susobhanan[1], Joseph K. Swiggum[47,65], Jacob A. Taylor[4], Stephen R. Taylor[13], Jacob E. Turner[10,11], Caner Unal[60,61], Michele Vallisneri[29,33], Sarah J. Vigeland[1], Haley M. Wahl[10,11], Caitlin A. Witt[62,63], Olivia Young[22,23], and
The NANOGrav Collaboration

The analyses in this Letter, as well as those in Bernardo & Ng (2023c) and Chen et al. (2023), do not rule out the possibility of ST correlations in our data. However, our analysis also shows no statistical need for an additional stochastic process with ST correlations.

# ADDITIONAL POLARIZATIONS MODES AND MASSIVE GRAVITY

## ORFs in massive gravity

Liang & Trodden, 2021[2108.05344]

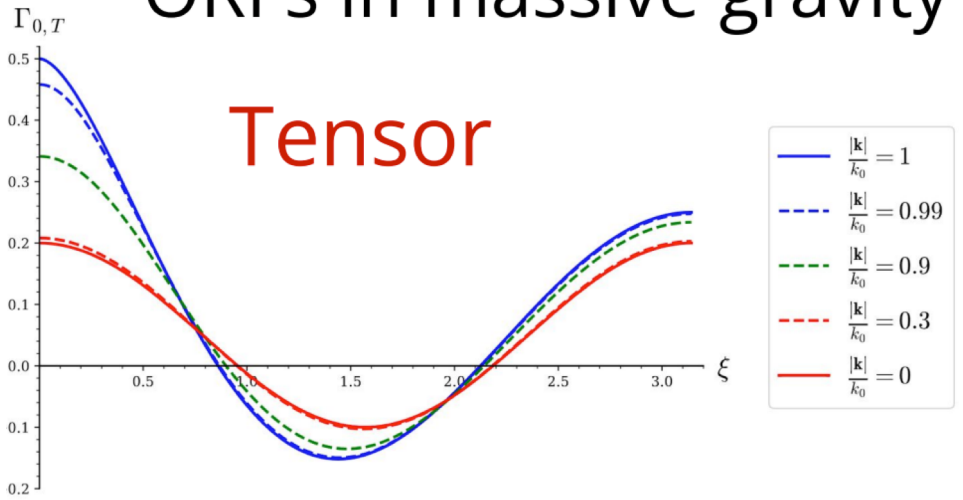


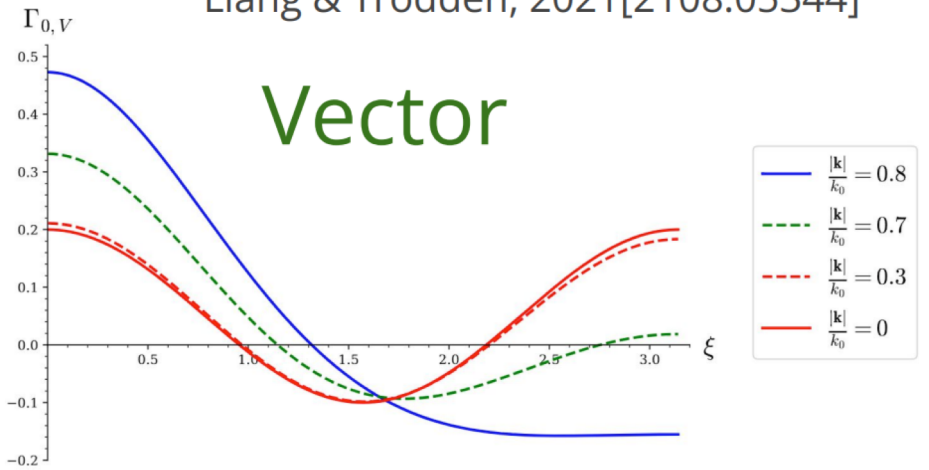


*fL >> 1* limit

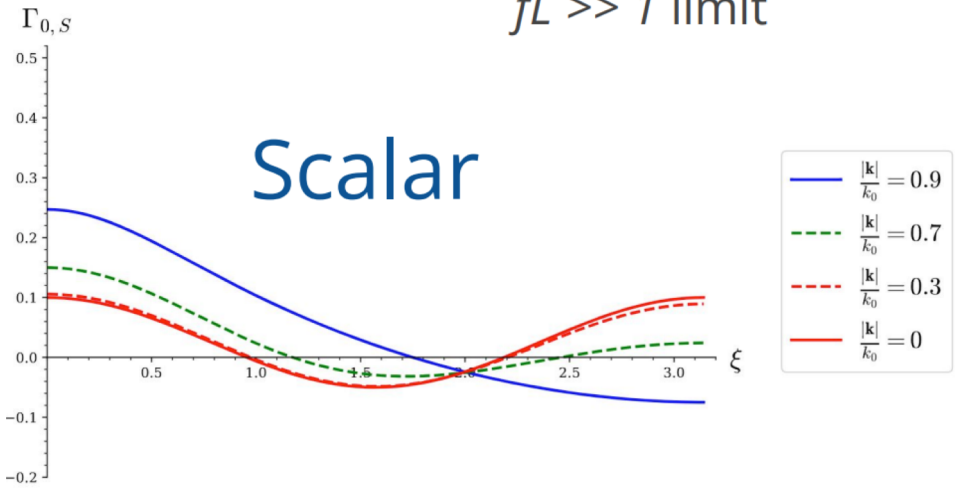


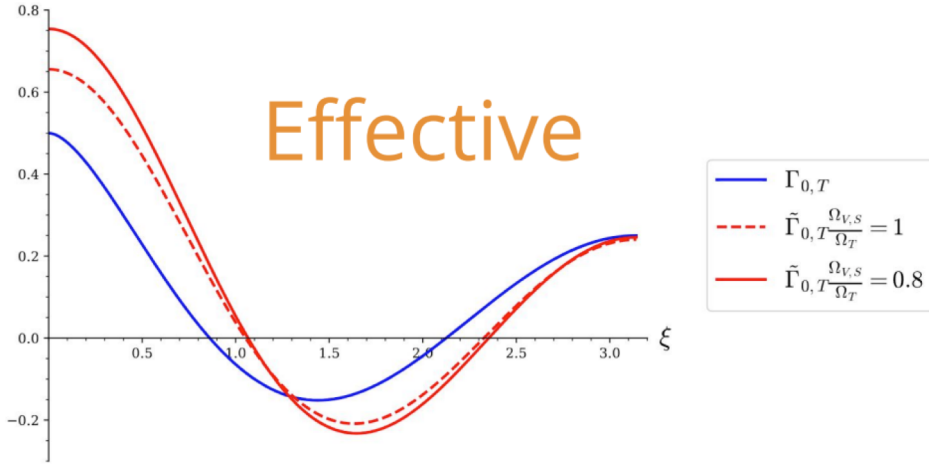


**Results does not depend if the source is astrophysical or cosmological**

Credit Chris Choi

# PULSAR TIMING ARRAYS AND MASSIVE GRAVITY

$$h_{\mu\nu}(x) = \frac{1}{(2\pi)^4}\int d\boldsymbol{k}\; h_{\mu\nu}(k)e^{ikx}\ .$$

$$d\boldsymbol{k} \equiv d^4k\;\delta(|\boldsymbol{k}|^2 - |k_\omega|^2)/|\boldsymbol{k}|,\;\; k_\omega \equiv |\boldsymbol{k}(\omega)|$$

$$\omega \equiv k_0 = 2\pi f\colon \quad \omega^2 = |\boldsymbol{k}|^2 + m_g^2$$

**Do Pulsar Timing Datasets Favor Massive Gravity?**


Chris Choi [1,*] and Tina Kahniashvili [1,2,3,†]

[1] *McWilliams Center for Cosmology and Astrophysics and Department of Physics, Carnegie Mellon University, Pittsburgh, Pennsylvania 15213, USA*
[2] *School of Natural Sciences and Medicine, Ilia State University, 0194 Tbilisi, Georgia*
[3] *Department of Theoretical Astrophysics and Cosmology, Georgian National Astrophysical Observatory, Tbilisi, 47/57 M. Kostava St., GE-0179, Georgia*



(Dated: August 4, 2025)



Several observational phenomena suggest that the standard model of cosmology and particle physics requires revision. To address this, we consider the extension of general relativity known as massive gravity (MG). In this Letter, we explore the imprints of MG on the propagation of gravitational waves (GWs): their modified dispersion relation and their additional (two vector and one scalar) polarization modes on the stochastic GW background (SGWB) detected by pulsar timing arrays (PTAs). We analyze the effects of massive GWs on the Hellings-Downs curve induced by modification of the overlap reduction function. Our study consists of analyzing observational data from the NANOGrav 15-year dataset and the Chinese PTA Data Release I, and is independent of the origin of the SGWB (astrophysical or cosmological). By considering the bound on the graviton mass imposed through the dispersion relation, we scrutinize the possibility of detecting traces of MG in the PTA observational data. We find that massive GWs predict better fits for the observed pulsar correlations. Future PTA missions with more precise data will hopefully be able to detect the GW additional polarization modes and might be effectively used to constrain the graviton mass.


$$\frac{1}{T_{\rm obs}} < f < \frac{1}{\delta t}\ ,$$

- The ORF is defined for each propagating degree of freedom

$$\Gamma(|f|) = \beta\sum_i \int_{S^2} d^2\hat{\boldsymbol{\Omega}} \underbrace{\left(e^{i2\pi f L_1\left(1+\frac{|\boldsymbol{k}|}{k_0}\hat{\boldsymbol{\Omega}}\cdot\hat{\boldsymbol{p}}_1\right)} - 1\right) \times \left(e^{-i2\pi f L_2\left(1+\frac{|\boldsymbol{k}|}{k_0}\hat{\boldsymbol{\Omega}}\cdot\hat{\boldsymbol{p}}_2\right)} - 1\right)}_{\text{exponential factors}} \underbrace{F_1^{(i)}(\hat{\boldsymbol{\Omega}})F_2^{(i)}(\hat{\boldsymbol{\Omega}})}_{\text{Receiving functions}}$$

- Exponential factors reduce to 1 if $fL >> 1$
  - $f \sim 10^{-9}$ Hz ~ 0.1 / year
  - $L$ ~ 100 light years
  - $fL \sim 10$
- Receiving functions describe the dependence on metric perturbation

$$F^{(i)}(\hat{\boldsymbol{\Omega}}) \equiv -\frac{\hat{p}^\mu\hat{p}^\nu}{2\left(1+\frac{|\boldsymbol{k}|}{k_0}\hat{\boldsymbol{\Omega}}\cdot\hat{\boldsymbol{p}}\right)}\epsilon^{(i)}_{\mu\nu} + \frac{\hat{p}^\mu}{2}\epsilon^{(i)}_{0\mu}$$

# OVERALL REDUCTION FUNCTION

Final result, ignoring exponential terms

$$\Gamma_I(|f|) = \sum_{i \in I} \int_{S^2} d^2\hat{\Omega} \mathcal{E}_1(-f,\hat{\Omega}) \mathcal{E}_2(f,\hat{\Omega}) F_1^{(i)}(\hat{\Omega}) F_2^{(i)}(\hat{\Omega}) \,,$$

$$F_j^{(i)}(\hat{\Omega}) = \frac{\hat{p}_j^\mu}{2} \left( - \frac{\hat{p}_j^\nu}{1 + \frac{|\boldsymbol{k}|}{k_0} \hat{\boldsymbol{\Omega}} \cdot \hat{\boldsymbol{p}}_j} \epsilon_{\mu\nu}^{(i)} + \epsilon_{0\mu}^{(i)} \right) ;$$

$$\mathcal{E}_j(f,\hat{\Omega}) = e^{-i2\pi f L_j \left(1 + \frac{|\boldsymbol{k}|}{k_0} \hat{\boldsymbol{\Omega}} \cdot \hat{\boldsymbol{p}}_j\right)} - 1 \,.$$

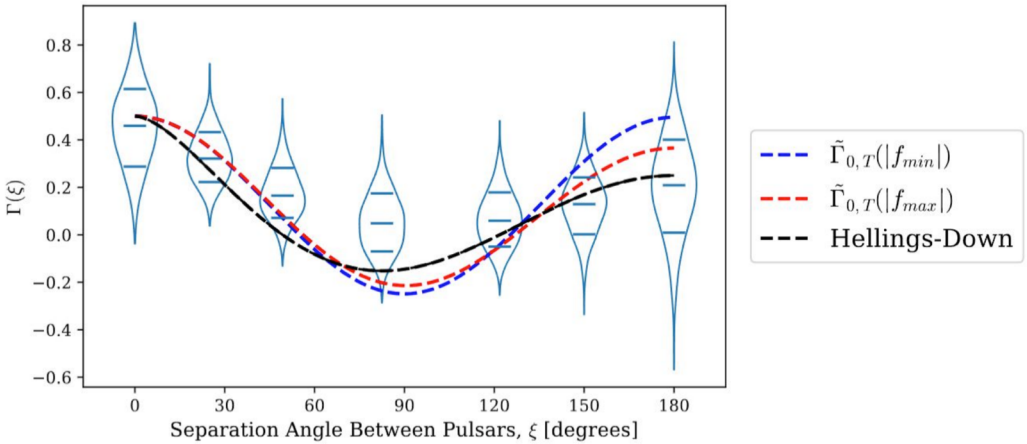


Choi and Kahniashvili 2025

$$\tilde{\Gamma}_T = \beta \left( \Gamma_T + \Gamma_V \frac{\Omega_V}{\Omega_T} + \Gamma_S \frac{\Omega_S}{\Omega_T} \right) \,,$$

*fL* ~ 1, cannot ignore the exponential terms in ORF

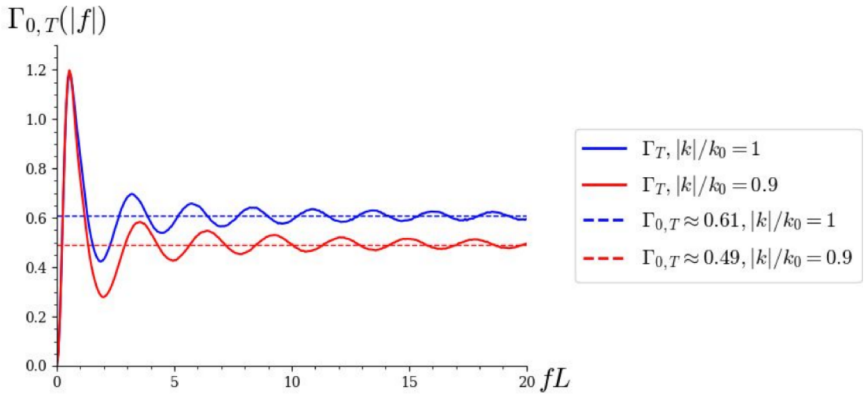


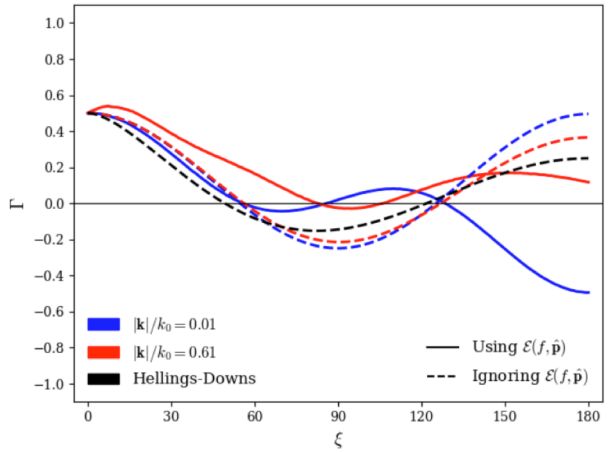


FIG. 1: The ORFs plotted as a function of angular separation $\xi$. The solid lines use the full expression of the ORFs, including $\mathcal{E}$. The dotted lines assume $\mathcal{E}_1(-f)\mathcal{E}_2(f) = 1$.

# MORE DATA – MORE QUESTIONS

## Frequency dependent ORF?

- Chinese Pulsar Timing Array data: frequency dependent!

From a presentation by Qiuyue Liang

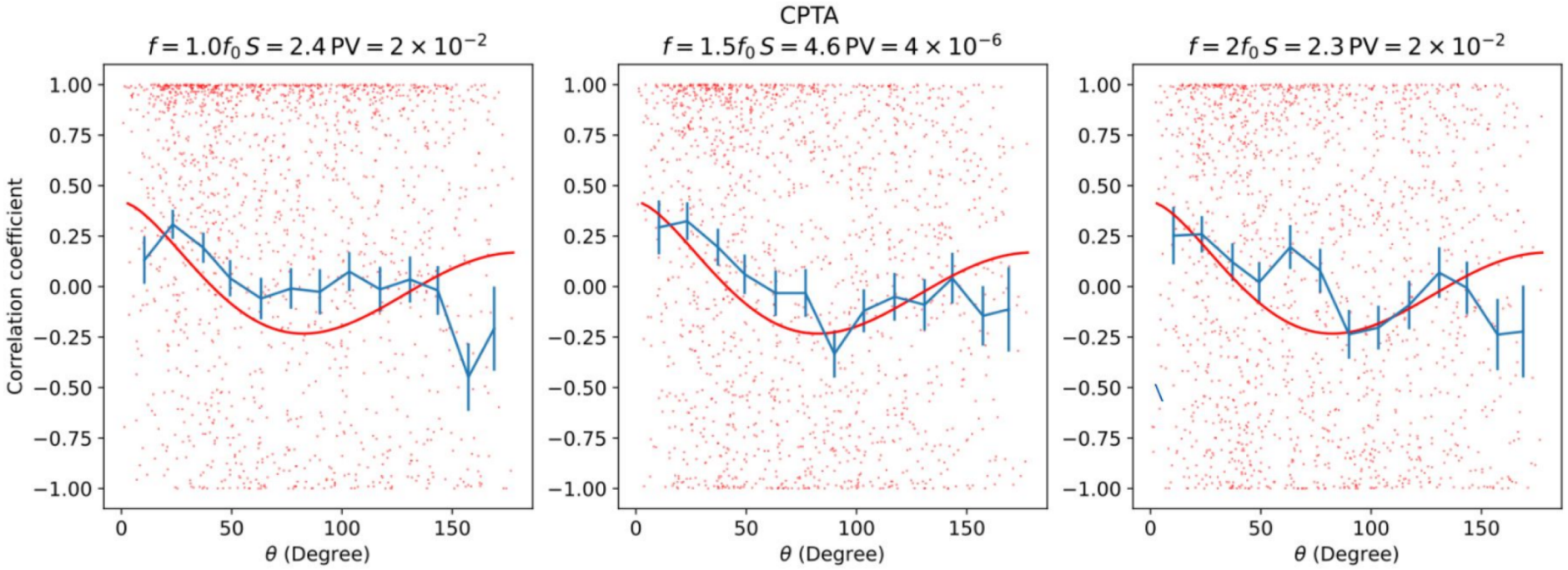

# PULSAR TIMING ARRAYS DATA

Choi and Kahniashvili 2025

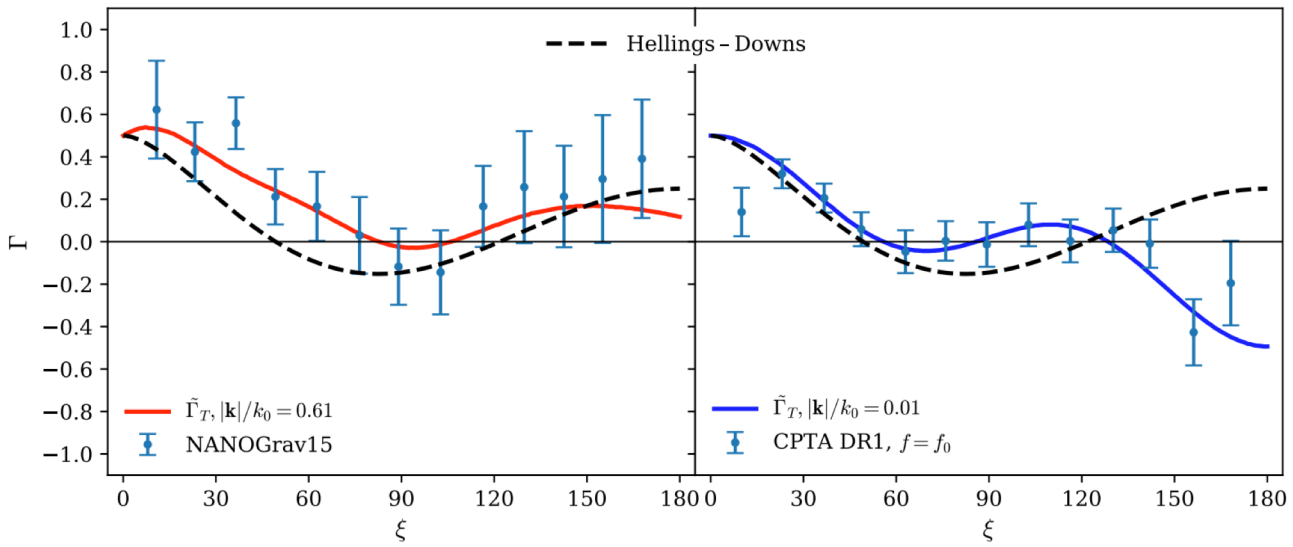


FIG. 2: The effective ORF plotted as a function of the angular separation $\xi$ between a pair of pulsars, for $|\boldsymbol{k}|/k_0 = 0.61$ in red and $|\boldsymbol{k}|/k_0 = 0.01$ in blue. NANOGrav15 is plotted with error bars in the left panel, and CPTA DR1 in the right panel, for $f = 1/T_{\rm CPTA}$. For both panels, we depict the HD correlation as a reference.

| Data | Fit type | Best fit $\frac{k}{k_0}$ | $\chi^2$ | $\chi^2$/d.o.f. |
|---|---|---|---|---|
| NANOGrav15 | HD | – | 22.20 | 1.71 |
| | MG | 0.61 | 6.59 | 0.55 |
| CPTA DR1 | HD | – | 38.95 | 3.00 |
| | MG | 0.01 | 16.58 | 1.35 |

TABLE I: The $\chi^2$ and $\chi^2$/d.o.f. values for different fit functions for the two datasets used in this analysis. We have 13 degrees of freedom for the HD correlation and 12 for the MG model (one fit parameter, $|\boldsymbol{k}|/k_0$).

A rigorous fitting to NANOGrav15 without considering E has been done in Arjona et al. 2024, which found that the best-fit ratio to the frequentist-optimal statistic of NANOGrav15 is $|\mathbf{k}|/k_0 \sim 0.73$. It is set $\Omega_V = \Omega_S$ and had $\Omega_T$ as the second fit parameter, obtaining a best-fit value of 0.46 and a $\chi^2$ of 6.91, slightly worse than our 6.59. ***While we do observe tension between the PTA datasets and the HD interpretation, opening the door for beyond-GR theories such as MG to provide a better fit, it may be addressed by more data from higher precision measurements and extended observing campaigns, as well as improved modeling techniques***.

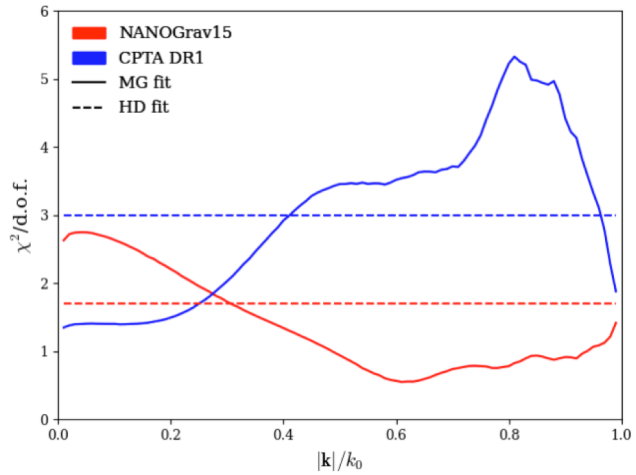


FIG. 3: The $\chi^2$/d.o.f. fitting plotted as a function of the ratio $|\boldsymbol{k}|/k_0$. The values for the horizontal dashed lines, representing the fit for the HD, can be found in Table I.

# DISPERSION RELATION

$\omega \equiv k_0 = 2\pi f$: $\omega^2 = |\boldsymbol{k}|^2 + m_g^2$

$m_g < 8.2 \times 10^{-24}\,\mathrm{eV/c^2}.$

$$\frac{1}{T_{\mathrm{obs}}} < f < \frac{1}{\delta t}$$

$T_{obs}$ – dutation of pulsar observations
$\delta t$ – time between observations

Wu et al. 2023

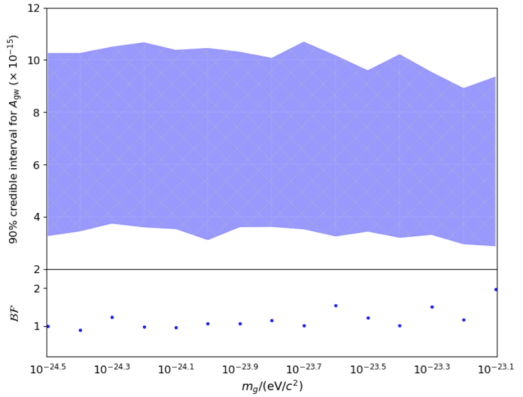


**Figure 1.** Top panel: the 90% credible interval of the power spectrum amplitude $A_{\mathrm{gw}}$ as a function of the graviton mass $m_g$, from NANOGrav 15-year data set. Bottom panel: the corresponding Bayes factor, $\mathcal{BF}$, as a function of the graviton mass $m_g$.

Best case scenario: $3.17 \times 10^{-10}\,Hz < f < 8.27 \times 10^{-7} Hz$

$\rightarrow m \sim 1.e31 \times 10^{-24} eV$

LIGO/VIRGO – propagation speed: 1-2 magnitudes weaker limits!

Still too weaker to influence cosmology (dRGGT – model)  Cosmology needs $10^{-31}$ eV

**Results does not depend if the source is astrophysical or cosmological**

# SIGNAL FROM EARLY UNIVERSE?

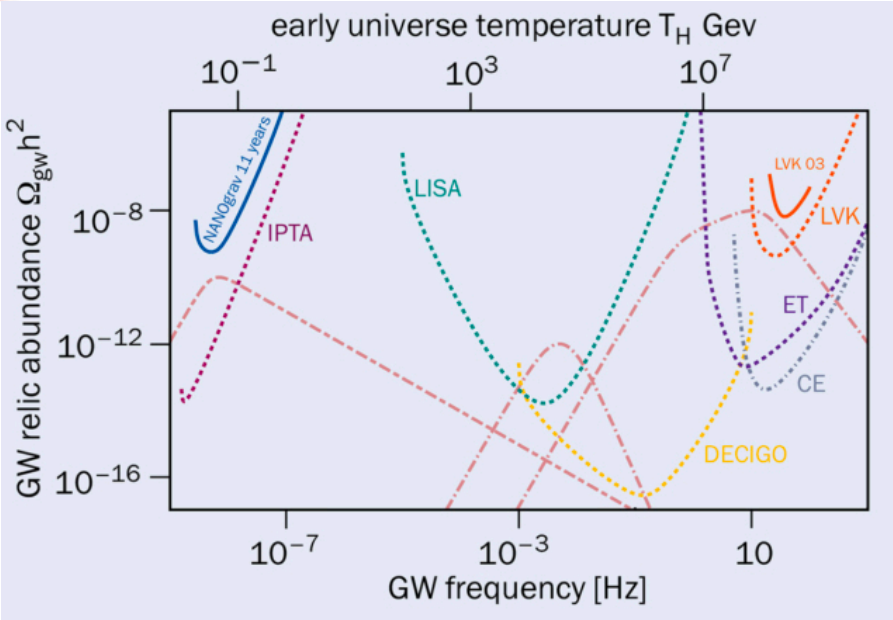


Credit: CERN Courier, 2021

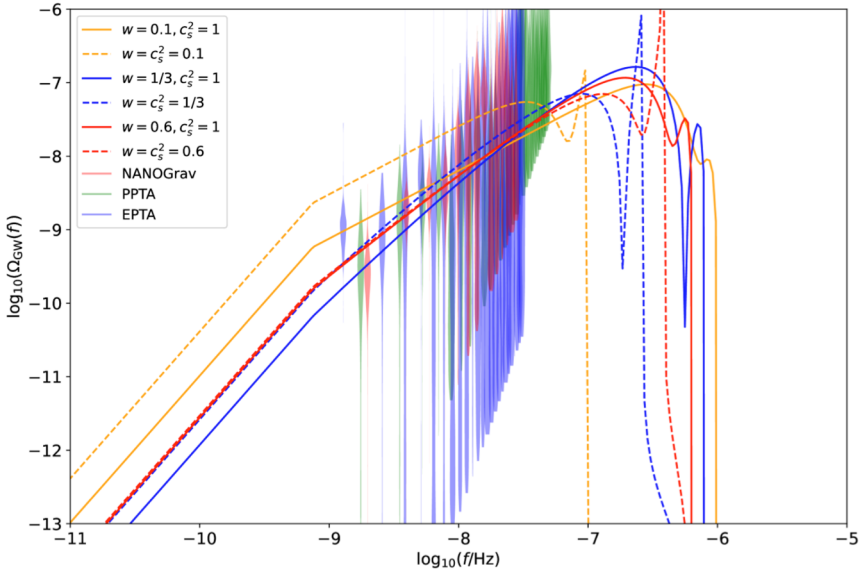


Credit: Liu, Wu, Chen

**Figure 1**: The energy density spectrum of SIGW with different EoS parameter $w$ and sound speed $c_s$ as a function of GW frequency.

Sensitivity of current (solid) and future (dashed) gravitational-wave (GW) observatories to stochastic GW backgrounds (expressed in terms of the energy density fraction in the universe today). On the upper x-axis, the temperature in the early universe is given, which is obtained when the peak frequency of a GW signal is equal to the inverse of the expansion rate when GWs are emitted. Some example possible GW spectra from the early universe are also shown (pink, dashed). F. Rompineve/ arXiv:2101.12130/arXiv:2002.0461

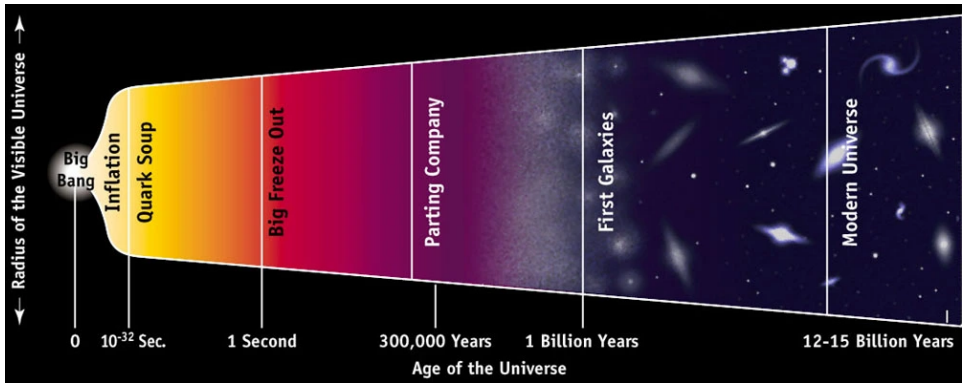

# EARLY UNIVERSE GRAVITATIONAL WAVES: PARAMETRIC RESONANCE

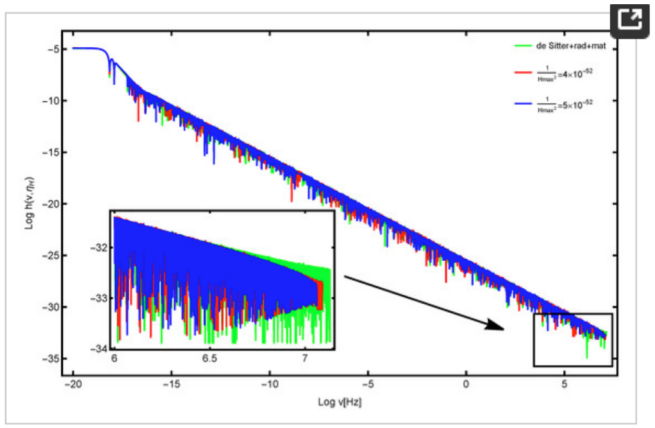


Ho et al. 2025

$$\mu'' + \mu\left[n^2 - \frac{a''}{a}\right] = 0,$$

$$a(\eta) = l_o|\eta|^{1+\beta},$$

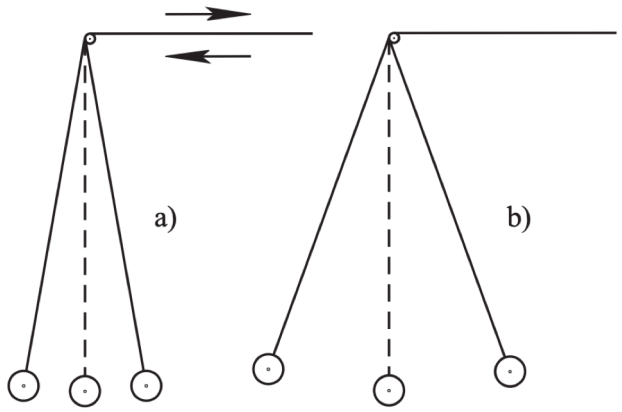


Fig. 1. Parametric amplification. a) variation of the length of the pendulum, b) increased amplitude of oscillations.

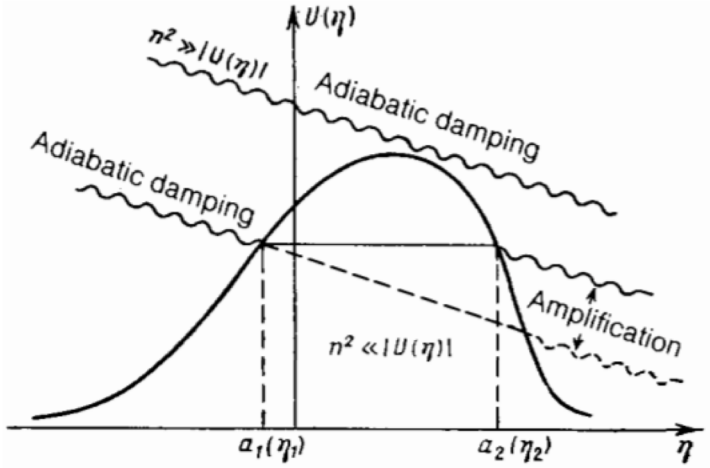


FIG. 3. Amplification of waves.

Grishchuk 1974

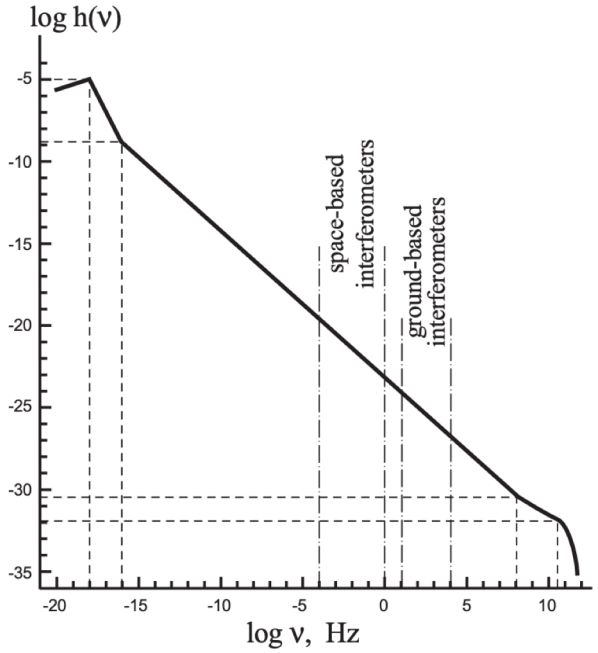


Fig. 7. Expected spectrum h(ν) for the case β = -1.9.

# PARAMETRIC RESONANCE IN MASSIVE GRAVITY

*Gumrukcuoglu et al. 2012*

$$\omega^2 = \frac{k^2}{a^2} + M_{GW}^2,$$

$$\omega^2(t_k) = H^2(t_k).$$

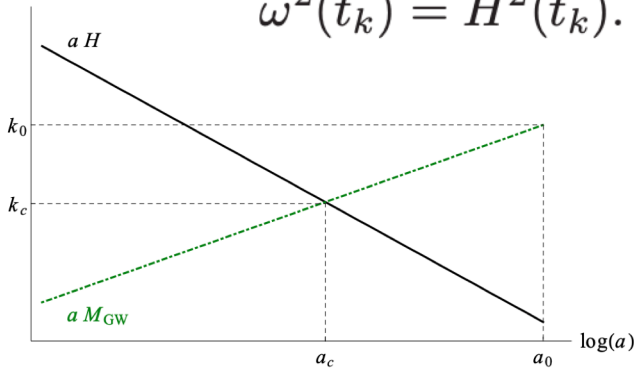


$$k^2 = \frac{H_{eq}^2\, a_{eq}^4}{2\,(a_k^{GR})^2}\left(1 + \frac{a_k^{GR}}{a_{eq}}\right).$$

$$H = \frac{H_{eq}}{\sqrt{2}}\left(\frac{a_{eq}}{a}\right)^2 \sqrt{1 + \frac{a}{a_{eq}}},$$

$$\bar{\gamma}_k'' + \left(c_g^2 k^2 + a^2 M_{GW}^2 - \frac{a''}{a} + 2K c_g^2\right)\bar{\gamma}_k = 0, \quad \bar{\gamma}_k \equiv a\gamma_k,$$

$\boldsymbol{k_c = a_c M_{GW}(t_c) = a_c H_c/\sqrt{2}}$ the horizon crossing occurs at time $t = t_c$, when both the momentum and the mass term contribute equally to the frequency, $\boldsymbol{k_0 \equiv a_0 M_{GW}(t_0)}$ The momentum of the mode for which, the mass term starts to dominate from today on,

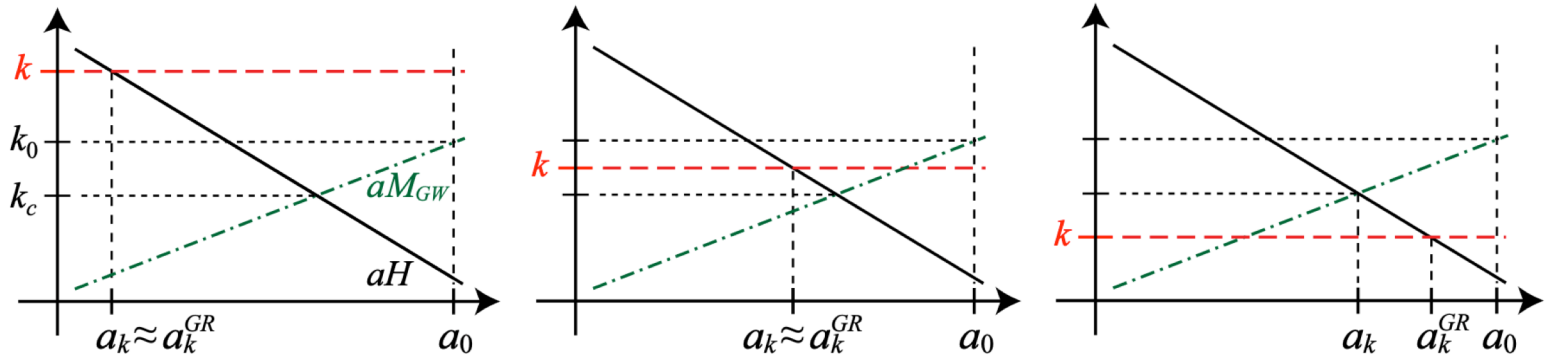


(a)Short wavelength: $k_0 < k$ (b)Intermediate wavelength: $k_c < k < k_0$ (c)Long wavelength: $k < k_c$

FIG. 2: Examples for each type of momenta based on the classification in the main text. For modes with short and intermediate wavelengths ($k_0 < k$ and $k_c < k < k_0$), the horizon entry time is the same as in GR, with $a_k \sim a_k^{GR}$. However, for modes with long wavelength ($k < k_c$), the momentum term never becomes dominant and the horizon entry in the massive theory occurs earlier than in GR, i.e. $a_k < a_k^{GR}$.

Gumrukcuoglu et al. 2012

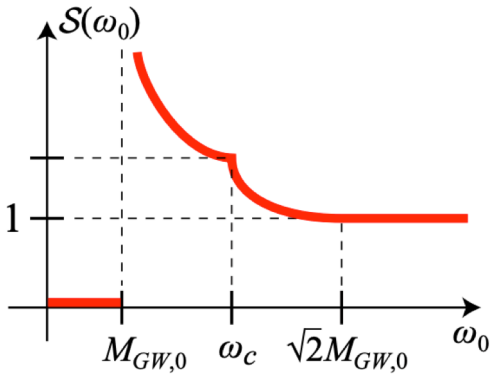


- Short wavelength ($k_0 < k$): modes for which the momentum is large enough to dominate the frequency after horizon re-entry. We thus have $t_k \simeq t_k^{GR}$, $a_k \simeq a_k^{GR}$ and $H_k \simeq H_k^{GR}$. Since the mass term never becomes important, the evolution is indistinguishable from its counterpart in GR.
- Intermediate wavelength ($k_c < k < k_0$): modes for which the mass term becomes dominant after horizon re-entry, but before today. We still have $t_k \simeq t_k^{GR}$, $a_k \simeq a_k^{GR}$ and $H_k \simeq H_k^{GR}$. We expect slight modifications with respect to GR signal.
- Long wavelength ($k < k_c$): modes for which the mass term is dominant at horizon re-entry. Since the momentum is negligible throughout the evolution after horizon exit, their evolution is the same, regardless of their momenta. In other words, $t_k$ for these modes is roughly independent of the momentum and all modes of this type re-enter the horizon simultaneously. We thus have $t_k \simeq t_c$, $a_k \simeq a_c$ and $H_k \simeq H_c$. The largest deviation from general relativity is expected in this category.

$$\mathcal{S}(\omega_0) = \frac{k' a_k}{c_g(t_0) k\, a_{k'}^{GR}} \sqrt{\frac{\omega_k a_k}{\omega_0 a_0}} \simeq \begin{cases} \frac{a_k}{a^{GR}_{c_g(t_0)k}} \sqrt{\frac{c_g(t_k)}{c_g(t_0)}} & (k_0 \ll k) \\ \frac{a_k}{a^{GR}_{c_g(t_0)k_0}} \sqrt{\frac{c_g(t_k)k_0}{c_g(t_0)k}} & (k_c \ll k \ll k_0) \\ \frac{a_c}{a^{GR}_{c_g(t_0)k}} \sqrt{\frac{c_g(t_c)k_0 k_c}{c_g(t_0)k^2}} & (k \ll k_c) \end{cases} .$$

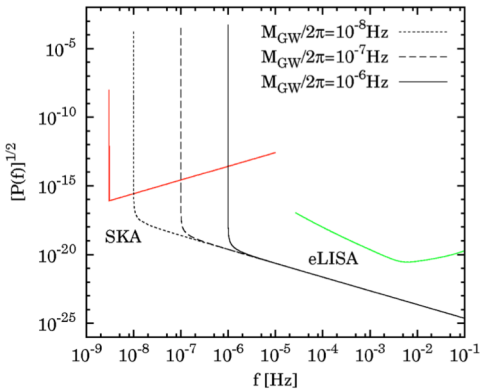


- Modest enhancement in the intermediate frequency range ($k_c < k < k_0 \Leftrightarrow \omega_c < \omega_0 < \sqrt{2}M_{GW,0}$):
- Sharp peak just above the cutoff ($0 < k < k_c \Leftrightarrow M_{GW,0} < \omega_0 < \omega_c$):
- No signal below the cutoff ($\omega_0 < M_{GW,0}$): $\mathcal{S}(\omega_0) = 0$.

$$\lim_{k \to +0} k^{-2} \mathcal{P}_{prim}(k) < \infty.$$

# TIME DEPENDENT GRAVITON MASS

Choi et al. 2023

$$\overline{h}_k'' + \left( c_g^2(\tau) k^2 + a^2 M_{\rm GW}^2 - \frac{a''}{a} + 2K c_g^2(\tau) \right) \overline{h}_k = 0 \,,$$

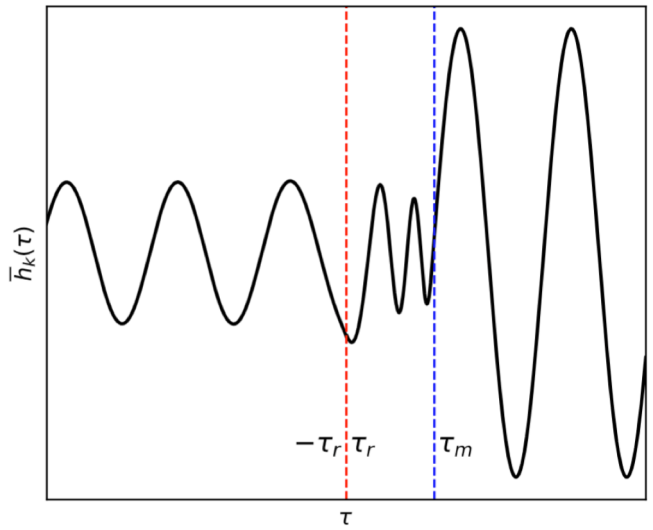


$$M_{\rm GW}(\tau) = \begin{cases} m & \tau < \tau_m \\ 0 & \tau > \tau_m \end{cases} \,,$$

Fujita et al. 2018

$$\Omega_{\rm GW,0}(f) = \frac{\pi^2}{3 a_0^2 H_0^2} f^2 \mathcal{P}_0(f) \,,$$

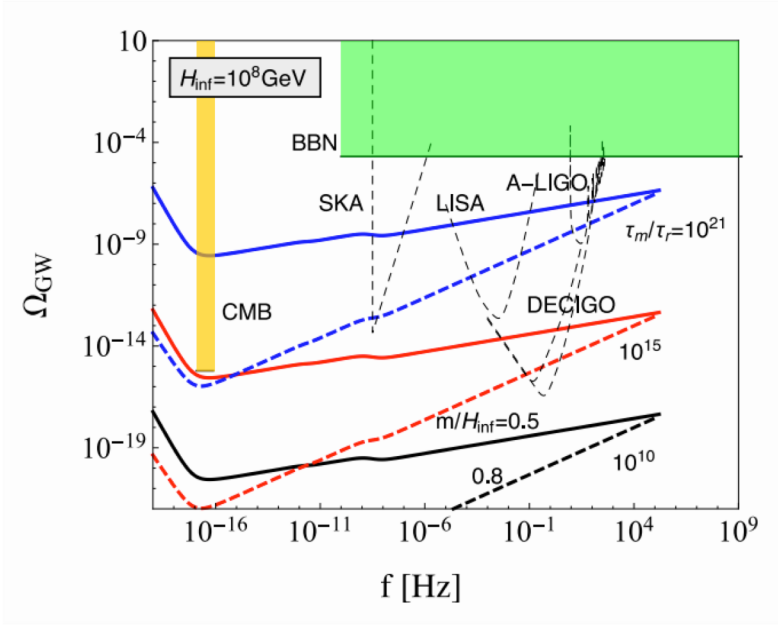


FIG. 1: We plot $\Omega_{\rm GW}$ for $H_{\rm inf} = 10^8$GeV and $\tau_m/\tau_r = 10^{10}$ (black), $10^{15}$ (red) and $10^{21}$ (blue) as thick lines. The graviton mass is $m = 0.5 H_{\rm inf}$ (solid) and $m = 0.8 H_{\rm inf}$ (dashed). The shaded regions are excluded by the BBN (green) and CMB (yellow) constraints. The sensitivity curves of SKA, LISA, A-LIGO and DECIGO (with the original and upgraded sensitivity curves [36]) are also shown as thin dashed lines.

$$\mathcal{P}_T^{\rm prim}(k) = A_T(k_{\rm ref})\left(\frac{k}{k_{\rm ref}}\right)^{n_T} \qquad \mathcal{P}_{\rm GR} = \mathcal{P}_T^{\rm prim} T_T^2(k)\ ,$$

$$\mathcal{P}_T^{\rm prim}(k) = A_T(k_{\rm ref})\left(\frac{k}{k_{\rm ref}}\right)^{n_T}$$

$$\Omega_{\rm GW}(f) \lesssim 1 \times 10^{-6},\ f > f_{\rm BBN}\ .$$

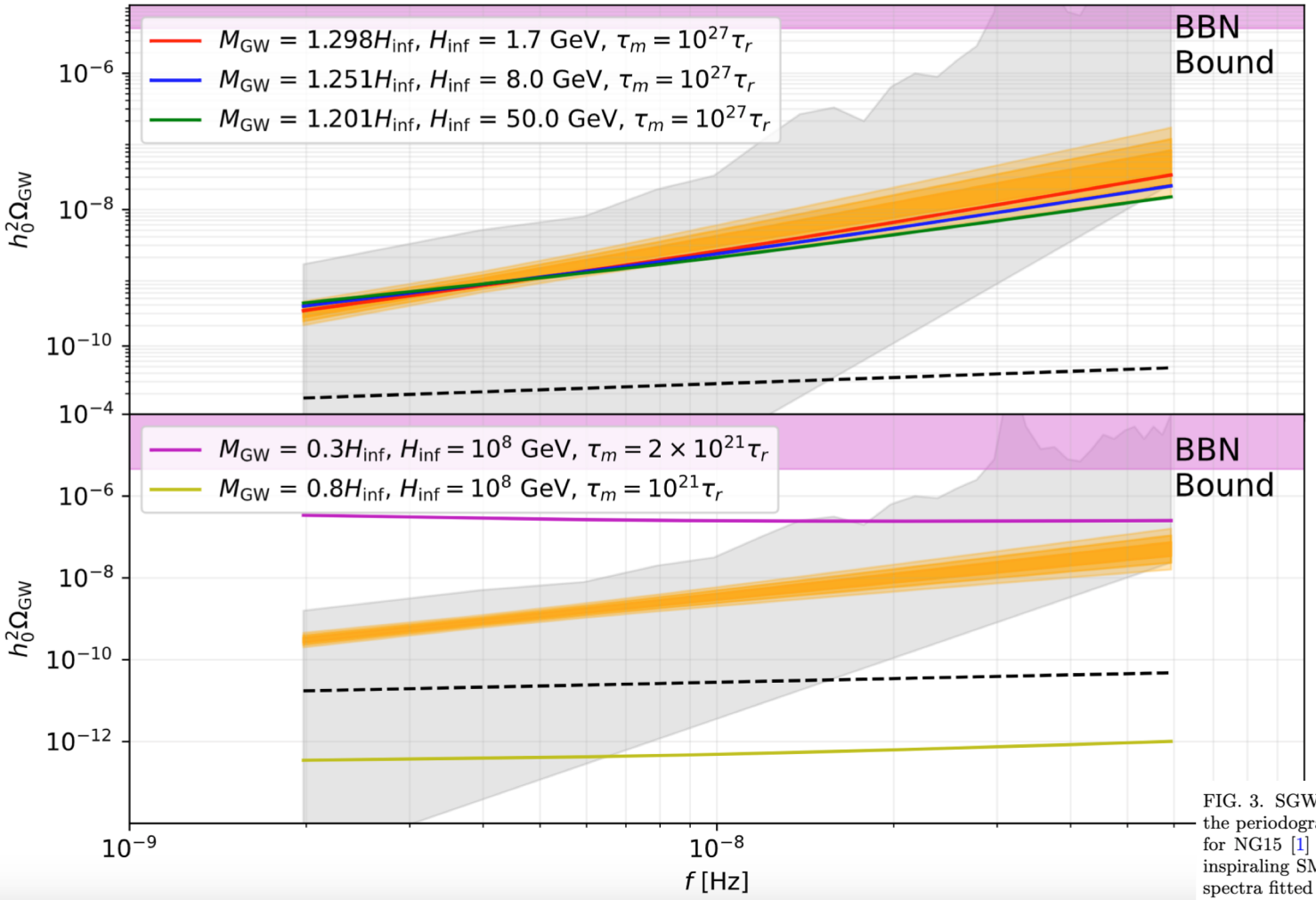


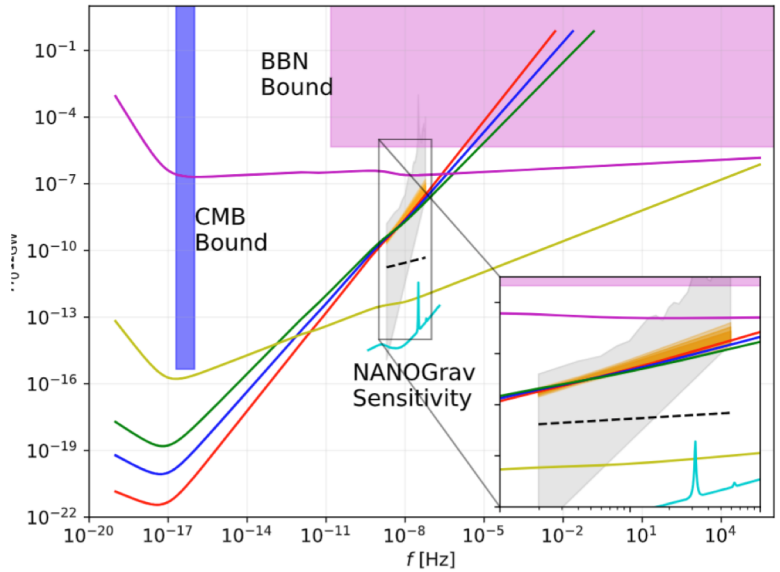


FIG. 3. SGWB produced by the SFM model. Both figures: we show the BBN excluded region shaded in purple at the top, the periodogram for a Hellings-Down-correlated free spectral process [1] in shaded grey, the $1\sigma$, $2\sigma$, and $3\sigma$ posterior medians for NG15 [1] in darker to lighter orange respectively, and the GWB spectrum produced by an astrophysical population of inspiraling SMBHBs with parameters detailed in Eq. A1 of Ref. [99] as a black dotted line. Top: The red curve is the GWB spectra fitted to the $1\sigma$ posterior, the blue curve is fitted to the $2\sigma$ posterior, and the green curve is fitted to the $3\sigma$ posterior. Bottom: the purple curve is the energy density that respects the BBN bound for high frequency and passes through the upper limit of the free spectral process of the data, and the golden curve is the energy density that respects the CMB bound for low frequency and passes through the lower limit of the free spectral process of the data.

Choi et al. 2023

# 15-YR DATA NANOGRAV

***Astrophysical:***

- ✓ Super massive black hole binary (SMBHB)

(Phinney 2001): γ=13/3

***Cosmological:***

- ✓ Bubbles collisions (Kosowsky et. al. 1993)
- ✓ Inflation (Vagnozzi 2020)
- ✓ Cosmic strings (Blanco-Pillado et al. 2020)
- ✓ Sound Waves (Hindmarsh et al. 2014)
- ✓ Seed magnetic fields (Neronov et. al. 2020)
- ✓ Hydrodynamic and MHD Turbulence (Brandenburg et al. 2021)

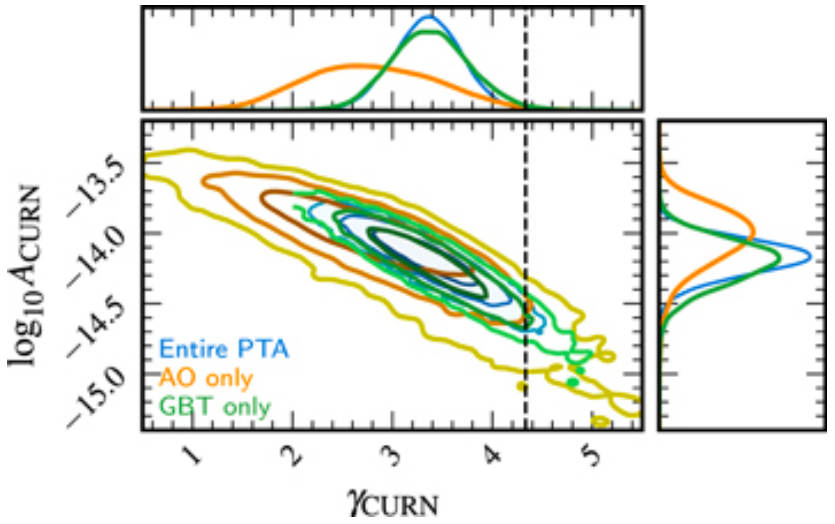


The NANOGrav 15 yr Data Set: Detection of a Gravitational-wave Background

$$h_c(f) = A_{\rm CP}\left(\frac{f}{f_{\rm yr}}\right)^{\alpha_{\rm CP}},$$

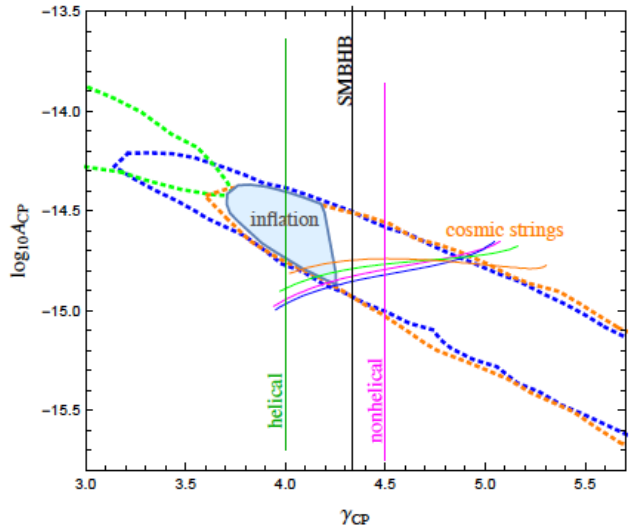


Credit: Emma Clarke

# COSMOLOGICAL PHASE TRANSITIONS: BUBBLES

Kosowsky, et al, 1992a,b & 1993, Kamionkowsky et al. 1994

VOLUME 69, NUMBER 14 PHYSICAL REVIEW LETTERS 5 OCTOBER 1992

**Gravitational Waves from First-Order Cosmological Phase Transitions**

Arthur Kosowsky,[1,2] Michael S. Turner,[1,2,3] and Richard Watkins[1,3]
[1]*NASA/Fermilab Astrophysics Center, Fermi National Accelerator Laboratory, Batavia, Illinois 60510-0500*
[2]*Department of Physics, Enrico Fermi Institute, The University of Chicago, Chicago, Illinois 60637-1433*
[3]*Department of Astronomy & Astrophysics, Enrico Fermi Institute, The University of Chicago, Chicago, Illinois 60637-1433*
(Received 6 December 1991; revised manuscript received 26 May 1992)

A first-order cosmological phase transition that proceeds through the nucleation and collision of true-vacuum bubbles is a potent source of gravitational radiation. Possibilities for such include first-order inflation, grand-unified-theory-symmetry breaking, and electroweak-symmetry breaking. We have calculated gravity-wave production from the collision of two scalar-field vacuum bubbles, and, using an approximation based upon these results, from the collision of 20 to 30 vacuum bubbles. We present estimates of the relic background of gravitational waves produced by a first-order phase transition; in general, $\Omega_{GW} \sim 10^{-8}$ and $f \sim (10^{-6}\ \mathrm{Hz})(T/1\ \mathrm{GeV})$.

PHYSICAL REVIEW D VOLUME 47, NUMBER 10 15 MAY 1993

**Gravitational radiation from colliding vacuum bubbles: Envelope approximation to many-bubble collisions**

Arthur Kosowsky
*Department of Physics, Enrico Fermi Institute, University of Chicago, Chicago, Illinois 60637-1433 and NASA/Fermilab Astrophysics Center, Fermi National Accelerator Laboratory, Batavia, Illinois 60510-0500*

Michael S. Turner
*Departments of Physics and Astronomy & Astrophysics, Enrico Fermi Institute, University of Chicago, Chicago, Illinois 60637-1433 and NASA/Fermilab Astrophysics Center, Fermi National Accelerator Laboratory, Batavia, Illinois 60510-0500*
(Received 9 November 1992)

We introduce an approximation to calculate the gravitational radiation produced by the collision of true-vacuum bubbles that is simple enough to allow the simulation of a phase transition by the collision of hundreds of bubbles. This "envelope approximation" neglects the complicated "overlap" regions of colliding bubbles and follows only the evolution of the bubble walls. The approximation accurately reproduces previous results for the gravitational radiation from the collision of two scalar-field vacuum bubbles. Using a bubble nucleation rate given by $\Gamma = \Gamma_0 e^{\beta t}$, we simulate a phase transition by colliding 20 to 200 bubbles; the fraction of vacuum energy released into gravity waves is $E_{GW}/E_{vac} = 0.06(H/\beta)^2$ and the peak of the spectrum occurs at $\omega_{max} = 1.6\beta$ ($H^2 = 8\pi G\rho/3$ is the Hubble constant associated with the false-vacuum phase). The spectrum is very similar to that in the two-bubble case, except that the efficiency of gravity-wave generation is about five times higher, presumably due to the fact that a given bubble collides with many others. Finally, we consider two further "statistical" approximations, where the gravitational radiation is computed as an incoherent sum over individual bubbles weighted by the distribution of bubble sizes. These approximations provide reasonable estimates of the gravitational-wave spectrum with far less computation.

- T∗ – the Universe temperature at which the PT takes place.
- a∗ – the strength of the phase transition, defined as the ratio of the vacuum and relativistic energy density at PT
- β/H∗ – the bubble nucleation rate in units of the Hubble rate at the time of the PT, H∗.
- v – the velocity of the bubble walls.

PHYSICAL REVIEW D VOLUME 45, NUMBER 12 15 JUNE 1992

**Gravitational radiation from colliding vacuum bubbles**

Arthur Kosowsky, Michael S. Turner, and Richard Watkins
*NASA/Fermilab Astrophysics Center, Fermi National Accelerator Laboratory, Batavia, Illinois 60510-0500 and Departments of Physics and Astronomy & Astrophysics, Enrico Fermi Institute, The University of Chicago, Chicago, Illinois 60637-1433*
(Received 20 December 1991)

In the linearized-gravity approximation we numerically compute the amount of gravitational radiation produced by the collision of two true-vacuum bubbles in Minkowski space. The bubbles are separated by distance $d$ and we calculate the amount of gravitational radiation that is produced in a time $\tau \sim d$ (in a cosmological phase transition $\tau$ corresponds to the duration of the transition, which is expected to be of the order of the mean bubble separation $d$). Our approximations are generally valid for $\tau \lesssim H^{-1}$. We find that the amount of gravitational radiation produced depends only upon the grossest features of the collision: the time $\tau$ and the energy density associated with the false-vacuum state, $\rho_{vac}$. In particular, the spectrum $dE_{GW}/d\omega \propto \rho_{vac}^2 \tau^8$ and peaks at a characteristic frequency $\omega_{max} \simeq 3.8/\tau$, and the fraction of the vacuum energy released into gravitational waves is about $1.3 \times 10^{-3} (\tau/H^{-1})^2$, where $H^2 = 8\pi G\rho_{vac}/3$ ($\tau/H^{-1}$ is expected to be of the order of a few percent). We address in some detail the important symmetry issues in the problem, and how the familiar "quadrupole approximation" breaks down in a most unusual way: it *overestimates* the amount of gravitational radiation produced in this highly relativistic situation by more than a factor of 50. Most of our results are for collisions of bubbles of equal size, though we briefly consider the collision of vacuum bubbles of unequal size. Our work implies that the vacuum-bubble collisions associated with a strongly first-order phase transition are a very potent cosmological source of gravitational radiation.

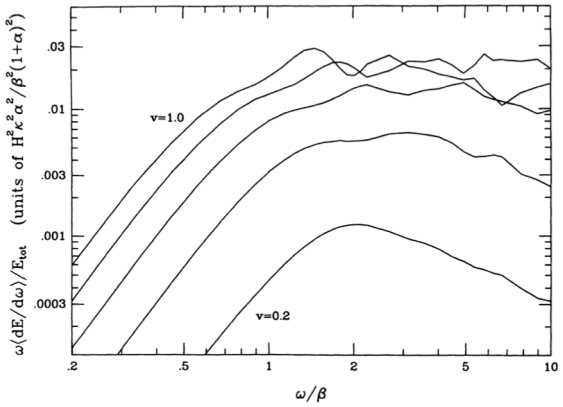


The energy per octave radiated in gravity waves for a phase transition with spherical bubbles expanding at velocity v, for v = 0.2, v = 0.4, v = 0.6, v = 0.8, and v = 1.0.

PHYSICAL REVIEW D VOLUME 49, NUMBER 6 15 MARCH 1994

**Gravitational radiation from first-order phase transitions**

Marc Kamionkowski*
*School of Natural Sciences, Institute for Advanced Study, Princeton, New Jersey 08540*

Arthur Kosowsky† and Michael S. Turner‡
*NASA/Fermilab Astrophysics Center, Fermi National Accelerator Laboratory, Batavia, Illinois 60510-0500 and Departments of Physics and of Astronomy and Astrophysics, Enrico Fermi Institute, The University of Chicago, Chicago, Illinois 60637-1433*
(Received 26 October 1993)

We consider the stochastic background of gravity waves produced by first-order cosmological phase transitions from two types of sources: colliding bubbles and hydrodynamic turbulence. First we discuss the fluid mechanics of relativistic spherical combustion. We then numerically collide many bubbles expanding at a velocity $v$ and calculate the resulting spectrum of gravitational radiation in the linearized gravity approximation. Our results are expressed as simple functions of the mean bubble separation, the bubble expansion velocity, the latent heat, and the efficiency of converting latent heat to kinetic energy of the bubble walls. A first-order phase transition is also likely to excite a Kolmogoroff spectrum of turbulence. We estimate the gravity waves produced by such a spectrum of turbulence and find that the characteristic amplitude of the gravity waves produced is comparable to that from bubble collisions. Finally, we apply these results to the electroweak transition. Using the one-loop effective potential for the minimal electroweak model, the characteristic amplitude of the gravity waves produced is $h \simeq 1.5 \times 10^{-27}$ at a characteristic frequency of $4.1 \times 10^{-3}$ Hz corresponding to $\Omega \sim 10^{-22}$ in gravity waves, far too small for detection. Gravity waves from more strongly first-order phase transitions, including the electroweak transition in nonminimal models, have better prospects for detection, though probably not by LIGO.

PACS number(s): 04.30.Db, 98.70.Vc, 98.80.Cq

$$\Omega_{GW} h^2 \approx 1.1 \times 10^{-6} \kappa^2 \left(\frac{H_*}{\beta}\right)^2 \left(\frac{\alpha}{1+\alpha}\right)^2 \left(\frac{v^3}{0.24+v^3}\right) \left(\frac{100}{g_*}\right)^{1/3},$$

$$f_{max} \approx 5.2 \times 10^{-8}\ \mathrm{Hz} \left(\frac{\beta}{H_*}\right) \left(\frac{T_*}{1\ \mathrm{GeV}}\right) \left(\frac{g_*}{100}\right)^{1/6},$$

$$h_c(f_{max}) \approx 1.8 \times 10^{-14} \kappa \left(\frac{\alpha}{1+\alpha}\right) \left(\frac{H_*}{\beta}\right)^2 \left(\frac{1\ \mathrm{GeV}}{T_*}\right) \left(\frac{v^3}{0.24+v^3}\right)^{1/2} \left(\frac{100}{g_*}\right)^{1/3}.$$

For follow papers see: Caprini and Figueroa 2018

# COSMOLOGICAL PHASE TRANSITIONS: HYDRO- AND MHD TURBULENCE

Kosowsky, et al, 2002, Caprini & Duurer, 2006, Gogoberidze et al. 2007

PHYSICAL REVIEW D **66**, 024030 (2002)

## Gravitational radiation from cosmological turbulence

Arthur Kosowsky*
*Department of Physics and Astronomy, Rutgers University, 136 Frelinghuysen Road, Piscataway, New Jersey 08854-8019 and School of Natural Sciences, Institute for Advanced Study, Olden Lane, Princeton, New Jersey 08540*

Andrew Mack†
*Department of Physics and Astronomy, Rutgers University, 136 Frelinghuysen Road, Piscataway, New Jersey 08854-8019*

Tinatin Kahniashvili‡
*Department of Physics and Astronomy, Rutgers University, 136 Frelinghuysen Road, Piscataway, New Jersey 08854-8019 and Center for Plasma Astrophysics, Abastumani Astrophysical Observatory, A. Kazbegi Ave. 2a, 380060 Tbilisi, Georgia*
(Received 6 April 2002; published 24 July 2002)

An injection of energy into the early Universe on a given characteristic length scale will result in turbulent motions of the primordial plasma. We calculate the stochastic background of gravitational radiation arising from a period of cosmological turbulence, using a simple model of isotropic Kolmogoroff turbulence produced in a cosmological phase transition. We also derive the gravitational radiation generated by magnetic fields arising from a dynamo operating during the period of turbulence. The resulting gravitational radiation background has a maximum amplitude comparable to the radiation background from the collision of bubbles in a first-order phase transition, but at a lower frequency, while the radiation from the induced magnetic fields is always subdominant to that from the turbulence itself. We briefly discuss the detectability of such a signal.

$$w = \frac{4\rho_*}{3} = \frac{2\pi^2}{45} g_* T_*^4, \qquad H_* = 1.66 g_*^{1/2} \frac{T_*^2}{m_{\rm Pl}},$$

$$\gamma H_*^{-1} = 2\pi/k_0, \qquad \zeta H_*^{-1} = \tau_T;$$

$$f = 1.55 \times 10^{-3}\ \text{Hz} \left(\frac{\omega_*}{k_0}\right)\left(\frac{g_*}{100}\right)^{1/6}\left(\frac{\gamma}{0.01}\right)^{-1}\left(\frac{T_*}{100\ \text{GeV}}\right),$$

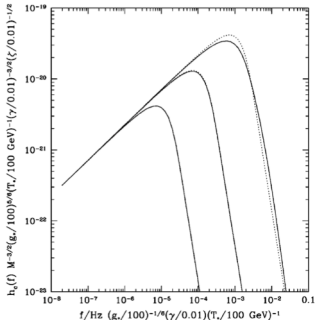

PHYSICAL REVIEW D **74,** 063521 (2006)

## Gravitational waves from stochastic relativistic sources: Primordial turbulence and magnetic fields

Chiara Caprini* and Ruth Durrer†
*Département de Physique Théorique, Université de Genève, 24 quai Ernest Ansermet, CH-1211 Genève 4, Switzerland*
(Received 17 March 2006; published 22 September 2006)

The power spectrum of a homogeneous and isotropic stochastic variable, characterized by a finite correlation length, does not, in general, vanish on scales larger than the correlation scale. If the variable is a divergence-free vector field, we demonstrate that its power spectrum is blue on large scales. Accounting for this fact, we compute the gravitational waves induced by an incompressible turbulent fluid and by a causal magnetic field present in the early universe. The gravitational wave power spectra show common features: they are both blue on large scales, and they both peak at the correlation scale. However, the magnetic field can be treated as a coherent source and it is active for a long time. This results in a very effective conversion of magnetic energy in gravitational wave energy at horizon crossing. Turbulence instead acts as a source for gravitational waves over a time interval much shorter than a Hubble time, and the conversion into gravitational wave energy is much less effective. We also derive a strong constraint on the amplitude of a primordial magnetic field when the correlation length is much smaller than the horizon.

PHYSICAL REVIEW D **76,** 083002 (2007)

## Spectrum of gravitational radiation from primordial turbulence

Grigol Gogoberidze,[1,2,*] Tina Kahniashvili,[3,2,†] and Arthur Kosowsky[4,‡]
[1]*Centre for Plasma Astrophysics, K.U. Leuven, Celestijnenlaan 200B, 3001 Leuven, Belgium*
[2]*National Abastumani Astrophysical Observatory, 2A Kazbegi Ave, GE-0160 Tbilisi, Georgia*
[3]*Center for Cosmology and Particle Physics, New York University, 4 Washington Plaza, New York, New York 10003, USA*
[4]*Department of Physics and Astronomy, University of Pittsburgh, 3941 O'Hara Street, Pittsburgh, Pennsylvania 15260, USA*
(Received 4 May 2007; published 5 October 2007)

Energy injection into the early universe can induce turbulent motions of the primordial plasma, which in turn act as a source for gravitational radiation. Earlier work computed the amplitude and characteristic frequency of the relic gravitational wave background, as a function of the total energy injected and the stirring scale of the turbulence. This paper computes the frequency spectrum of relic gravitational radiation from a turbulent source of the stationary Kolmogoroff form which acts for a given duration, making no other approximations. We also show that the limit of long source wavelengths, commonly employed in aeroacoustic problems, is an excellent approximation. The gravitational waves from cosmological turbulence around the electroweak energy scale will be detectable by future space-based laser interferometers for a substantial range of turbulence parameters.

For follow papers see: Caprini and Figueroa 2018

# COSMOLOGICAL PHASE TRANSITIONS: SOUND WAVES

Hindmarsh et al. 2014, 2015

PRL 112, 041301 (2014) PHYSICAL REVIEW LETTERS week ending 31 JANUARY 2014

## Gravitational Waves from the Sound of a First Order Phase Transition

Mark Hindmarsh,[1,2,*] Stephan J. Huber,[1,†] Kari Rummukainen,[2,‡] and David J. Weir[2,§]
[1]*Department of Physics and Astronomy, University of Sussex, Falmer, Brighton BN1 9QH, United Kingdom*
[2]*Department of Physics and Helsinki Institute of Physics, University of Helsinki, PL 64, FI-00014, Helsinki, Finland*
(Received 16 April 2013; revised manuscript received 12 October 2013; published 27 January 2014)

We report on the first three-dimensional numerical simulations of first-order phase transitions in the early Universe to include the cosmic fluid as well as the scalar field order parameter. We calculate the gravitational wave (GW) spectrum resulting from the nucleation, expansion, and collision of bubbles of the low-temperature phase, for phase transition strengths and bubble wall velocities covering many cases of interest. We find that the compression waves in the fluid continue to be a source of GWs long after the bubbles have merged, a new effect not taken properly into account in previous modeling of the GW source. For a wide range of models, the main source of the GWs produced by a phase transition is, therefore, the sound the bubbles make.

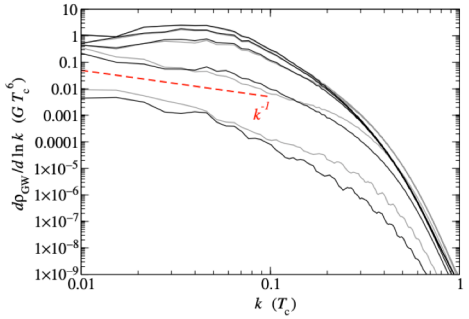


FIG. 3 (color online). Gravitational wave power spectra during the phase transition, for the intermediate strength transition, from fluid only (black lines) and both fluid and field (gray lines). From bottom to top, the times are $t = 600$, 800, 1000, 1200, and $1400T_c^{-1}$. The red dashed line indicates the expected $k^{-1}$ behavior.



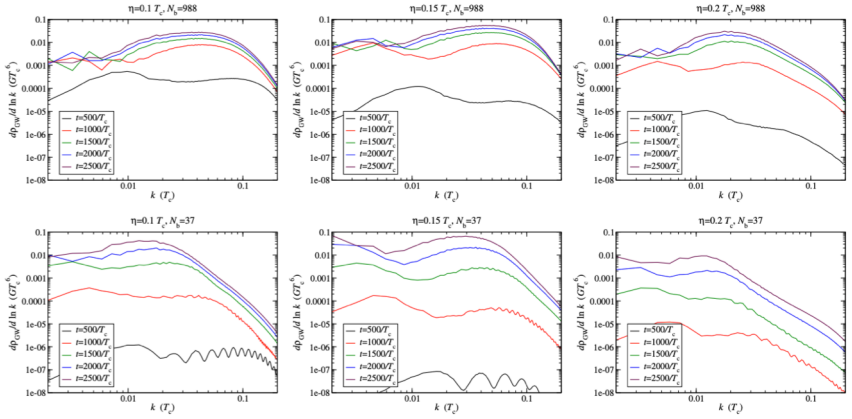


FIG. 8 (color online). Gravitational wave power spectra, for weak transitions, at $\eta/T_c = 0.1$, 0.15 and 0.2 ($v_w = 0.83$, 0.54 and 0.44) for $N_b = 988$ (top row) and $N_b = 37$ (bottom row). Note that the axes and time intervals are the same for all plots, which means that in some cases the latest $(2500/T_c)$ curve is from before the completion of the phase transition.



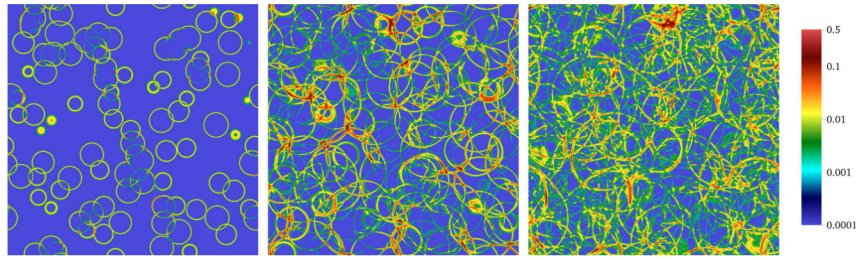


FIG. 4 (color online). Slices of fluid kinetic energy density $E/T_c^4$ at $t = 500T_c^{-1}$, $t = 1000T_c^{-1}$ and $t = 1500T_c^{-1}$ respectively, for the $\eta/T_c = 0.15$, $N_b = 988$ simulation.

PHYSICAL REVIEW D 92, 123009 (2015)

## Numerical simulations of acoustically generated gravitational waves at a first order phase transition

Mark Hindmarsh,[1,2,*] Stephan J. Huber,[1,†] Kari Rummukainen,[2,‡] and David J. Weir[3,§]
[1]*Department of Physics and Astronomy, University of Sussex, Falmer, Brighton BN1 9QH, United Kingdom*
[2]*Department of Physics and Helsinki Institute of Physics, P.O. Box 64, FI-00014 University of Helsinki, Finland*
[3]*Institute of Mathematics and Natural Sciences, University of Stavanger, 4036 Stavanger, Norway*
(Received 5 May 2015; published 22 December 2015)

We present details of numerical simulations of the gravitational radiation produced by a first order thermal phase transition in the early Universe. We confirm that the dominant source of gravitational waves is sound waves generated by the expanding bubbles of the low-temperature phase. We demonstrate that the sound waves have a power spectrum with a power-law form between the scales set by the average bubble separation (which sets the length scale of the fluid flow $L_f$) and the bubble wall width. The sound waves generate gravitational waves whose power spectrum also has a power-law form, at a rate proportional to $L_f$ and the square of the fluid kinetic energy density. We identify a dimensionless parameter $\tilde{\Omega}_{GW}$ characterizing the efficiency of this "acoustic" gravitational wave production whose value is $8\pi\tilde{\Omega}_{GW} \simeq 0.8 \pm 0.1$ across all our simulations. We compare the acoustic gravitational waves with the standard prediction from the envelope approximation. Not only is the power spectrum steeper (apart from an initial transient) but the gravitational wave energy density is generically larger by the ratio of the Hubble time to the phase transition duration, which can be 2 orders of magnitude or more in a typical first order electroweak phase transition.

For follow papers see: Caprini and Figueroa 2018

# PULSAR TIMING ARRAYS: COSMOLOGICAL PHASE TRANSITIONS

PHYSICAL REVIEW LETTERS **127,** 251302 (2021)

Editors' Suggestion | Featured in Physics

## Searching for Gravitational Waves from Cosmological Phase Transitions with the NANOGrav 12.5-Year Dataset

Zaven Arzoumanian,[1] Paul T. Baker,[2] Harsha Blumer,[3,4] Bence Bécsy,[5] Adam Brazier,[6,7] Paul R. Brook,[3,4] Sarah Burke-Spolaor,[3,4,8] Maria Charisi,[9] Shami Chatterjee,[6] Siyuan Chen,[10,11,12] James M. Cordes,[6] Neil J. Cornish,[5] Fronefield Crawford,[13] H. Thankful Cromartie,[6] Megan E. DeCesar,[14,15*] Paul B. Demorest,[16] Timothy Dolch,[17,18] Justin A. Ellis,[19] Elizabeth C. Ferrara,[20,21,22] William Fiore,[3,4] Emmanuel Fonseca,[23] Nathan Garver-Daniels,[3,4] Peter A. Gentile,[3,4] Deborah C. Good,[24] Jeffrey S. Hazboun,[25] A. Miguel Holgado,[26,27] Kristina Islo,[28] Ross J. Jennings,[6] Megan L. Jones,[28] Andrew R. Kaiser,[3,4] David L. Kaplan,[28] Luke Zoltan Kelley,[29] Joey Shapiro Key,[25] Nima Laal,[30] Michael T. Lam,[31,32] T. Joseph W. Lazio,[33] Vincent S. H. Lee,[34] Duncan R. Lorimer,[3,4] Jing Luo,[35] Ryan S. Lynch,[36] Dustin R. Madison,[3,4] Maura A. McLaughlin,[3,4] Chiara M. F. Mingarelli,[37,38] Andrea Mitridate,[34] Cherry Ng,[39] David J. Nice,[14] Timothy T. Pennucci,[40,41] Nihan S. Pol,[3,4,9] Scott M. Ransom,[40] Paul S. Ray,[42] Brent J. Shapiro-Albert,[3,4] Xavier Siemens,[30,28] Joseph Simon,[33,43] Renée Spiewak,[44] Ingrid H. Stairs,[24] Daniel R. Stinebring,[45] Kevin Stovall,[16] Jerry P. Sun,[30] Joseph K. Swiggum,[14] Stephen R. Taylor,[9] Jacob E. Turner,[3,4] Michele Vallisneri,[33] Sarah J. Vigeland,[28] Caitlin A. Witt,[3,4] and Kathryn M. Zurek[34]

(NANOGrav Collaboration)

We search for a first-order phase transition gravitational wave signal in 45 pulsars from the NANOGrav 12.5-year dataset. We find that the data can be modeled in terms of a strong first order phase transition taking place at temperatures below the electroweak scale. However, we do not observe any strong preference for a phase-transition interpretation of the signal over the standard astrophysical interpretation in terms of supermassive black hole mergers; but we expect to gain additional discriminating power with future datasets, improving the signal to noise ratio and extending the sensitivity window to lower frequencies. An interesting open question is how well gravitational wave observatories could separate such signals.



TABLE III. Prior distributions for the parameters used in all the analyses in this work. The prior for the bubble wall velocity reported in this table is the one used for the SWO analysis, for the BO analyses we use $v_w = 1$ as explained in the text.

| Parameter | Description | Prior | Comments |
|---|---|---|---|
| | White noise | | |
| $E_k$ | EFAC per backend-receiver system | Uniform [0, 10] | Single-pulsar analysis only |
| $Q_k$ [s] | EQUAD per backend-receiver system | Log-uniform $[-8.5, -5]$ | Single-pulsar analysis only |
| $J_k$ [s] | ECORR per backend-receiver system | Log-uniform $[-8.5, -5]$ | Single-pulsar analysis only |
| | Red noise | | |
| $A_{\rm red}$ | Red-noise power-law amplitude | Log-uniform $[-20, -11]$ | One parameter per pulsar |
| $\gamma_{\rm red}$ | Red-noise power-law spectral index | Uniform [0, 7] | One parameter per pulsar |
| | Phase transition | | |
| $T_*$ [GeV] | Phase transition temperature | Log-uniform $[-4, 3]$ | One parameter for PTA |
| $\alpha_*$ | Phase transition strength | Log-uniform $[-1.3, 1]$ | One parameter for PTA |
| $H_*/\beta$ | Bubble nucleation rate | Log-uniform $[-2, 0]$ | One parameter for PTA |
| $v_w$ | Bubble wall velocity | Log-uniform $[-2, 1]$ | One parameter for PTA |
| | Supermassive black bole binaries (SMBHBs) | | |
| $A_{\rm GWB}$ | Common process strain amplitude | Log-uniform $[-18, -14]$ | One parameter for PTA |
| $\gamma_{\rm GWB}$ | Common process power-law spectral index | Delta function ($\gamma_{\rm GWB} = 13/3$) | Fixed |

TABLE I. Parameters for the gravitational wave spectrum of Eq. (4). The values of the parameters $(a, b, c)$ in the spectral shape of the bubble contribution are reported in Table II.

| | Bubbles [58] | Sound waves [59] |
|---|---|---|
| $\Delta(v_w)$ | $[0.48 v_w^3/(1 + 5.3 v_w^2 + 5 v_w^4)]$ | $0.513 v_w$ |
| $\kappa$ | $\kappa_\phi$ | $\kappa_{\rm SW}$ |
| $p$ | 2 | 2 |
| $q$ | 2 | 1 |
| $\mathcal{S}(x)$ | $\{(a+b)^c/[b x^{-a/c} + a x^{b/c}]^c\}$ | $x^3[7/(4+3x^2)]^{7/2}$ |
| $f_*/\beta$ | $[0.35/(1 + 0.07 v_w + 0.69 v_w^4)]$ | $(0.536/v_w)$ |

$$h^2\Omega(f) = \mathcal{R}\Delta(v_w)\left(\frac{\kappa\alpha_*}{1+\alpha_*}\right)^p\left(\frac{H_*}{\beta}\right)^q\mathcal{S}(f/f_*^0),$$

$$f_*^0 \simeq 1.13\times10^{-10}\ \text{Hz}\left(\frac{f_*}{\beta}\right)\left(\frac{\beta}{H_*}\right)\left(\frac{T_*}{\text{MeV}}\right)\left(\frac{g_*}{10}\right)^{1/6},$$

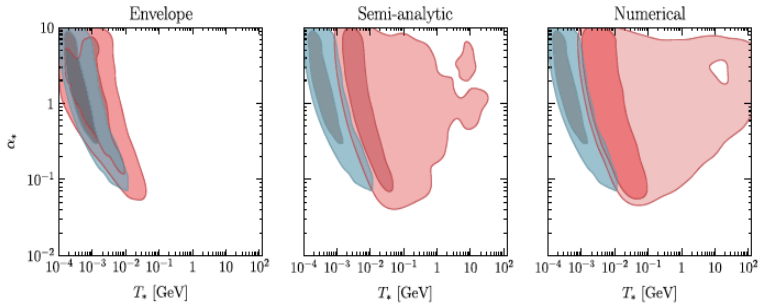


FIG. 1. In red (blue) the 1-$\sigma$ (68% posterior credible level), and 2-$\sigma$ (95% posterior credible level) contours for the two-dimensional posterior distributions in the $(T_*, \alpha_*)$ plane obtained in the BO (SWO). The BO analysis has been performed with the spectral shape computed by using the envelope approximation (left panel), semianalytic results (central panel), and numerical results (right panel). Specifically, we use $(a, b, c) = (1, 2.61, 1.5)$ for the semianalytic results, and $(a, b, c) = (0.7, 2.3, 1)$ for the numerical results.

TABLE II. Comparison of the bubble spectral shape parameters derived using the envelope and thin wall approximation [58] (left column), the semianalytic approach of reference [64] (middle column), and lattice simulations [62] (right column). For numerical and semianalytic results the values of the parameters depend on the choice of the scalar field potential; we report the range of values obtained for the different scalar field potentials considered in the above mentioned works.

| | Envelope | Semianalytic | Numerical |
|---|---|---|---|
| $a$ | 3 | 1–2.2 | 1.6–0.7 |
| $b$ | 1 | 2.6–2.9 | 1.4–2.3 |
| $c$ | 1.5 | 1.5–3.5 | 1 |
| $f_*/\beta$ | $[0.35/(1 + 0.07 v_w + 0.69 v_w^2)]$ | 0.1 | 0.2 |

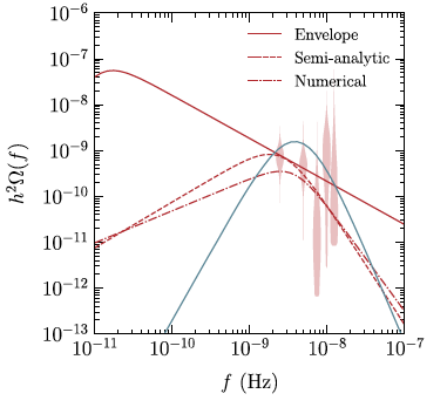


FIG. 2. Maximum likelihood GWB fractional energy-density spectrum for the BO (red) and SWO (blue) analyses compared with the marginalized posterior for the free power spectrum (independent per-frequency characterization; red violin plot) derived in NG12gwb For the BO analysis we show the results derived by using the envelope (solid line), semianalytic (dashed), and numerical (dot-dashed) spectral shapes. For the BO analyses the values of $(\alpha_*, T_*)$ for these maximum likelihood spectra are (0.28,0.7 MeV) for the envelope results, (1.2,3.4 MeV) for the semianalytic results, and (0.13,14.1 MeV) for the numerical results. While for the SO analysis we get (6.0,0.32 MeV).

# PULSAR TIMING ARRAYS AND NEW PHYSICS

NANOGrav 2023

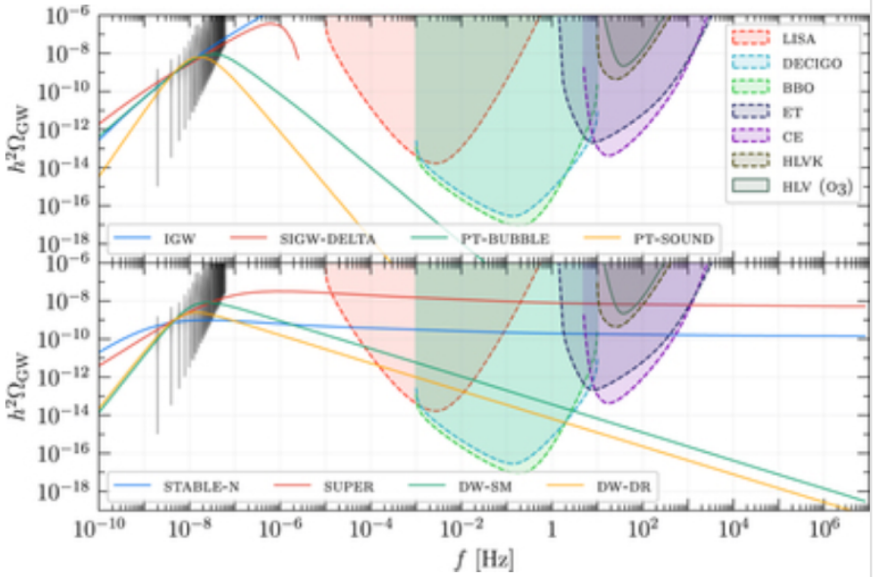


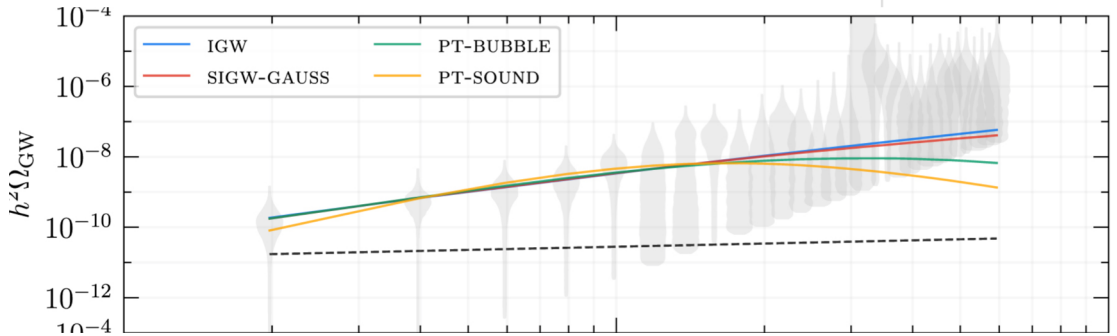


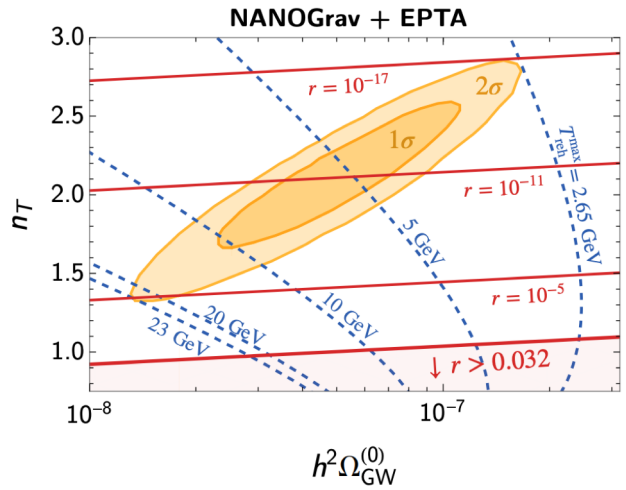


FIG. S.1. The CMB observations tightly constrain the PTA-signal interpretation as the inflationary GWB (blue contours). The bound on the tensor-to-scalar ratio (in red) excludes the region with $r > 0.032$. The BBN-$N_{\rm eff}$ bound requires a low-scale reheating: $T_{\rm reh} < 10.6$ GeV, at 68% CL.

Figueroa et al. 2024

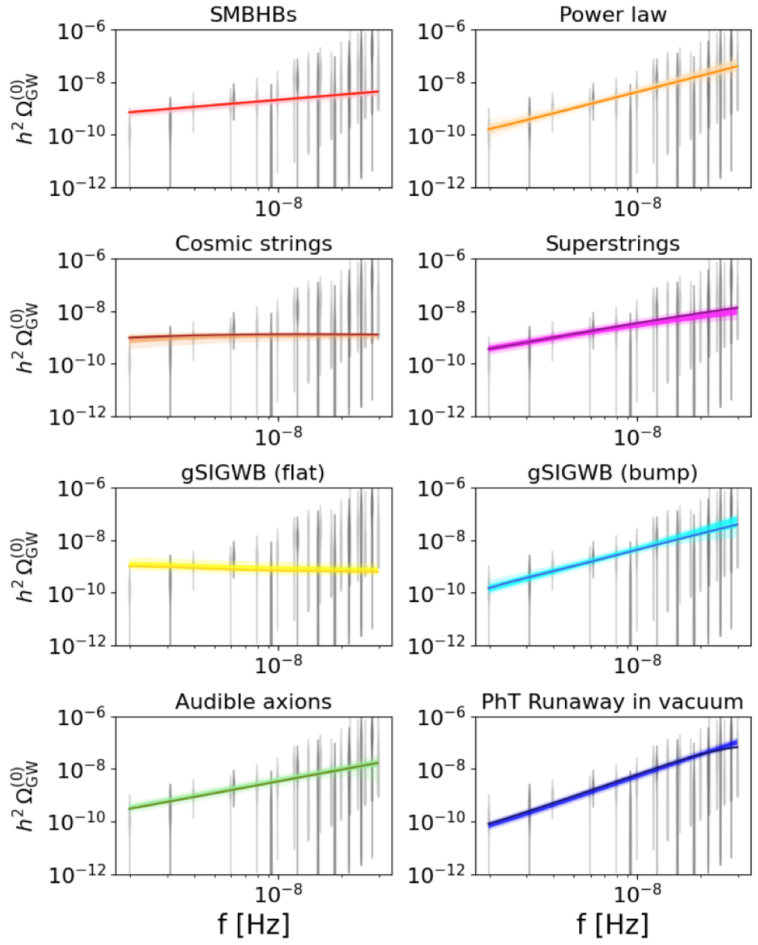


FIG. 2. $h^2\Omega_{\rm GW}^{(0)}(f)$ for various cases. Solid-colored lines represent central values, while lighter (lightest) regions the 68% (95%) CL intervals. Dark and light gray violins are the EPTA and NANOGrav free spectrum data, respectively.

# ANISOTROPIC PHASES AND GRAVITATIONAL WAVES

Modern Physics Letters A | Vol. 01, No. 11, pp. 593-600 (1986) | Cosmology and Elementa...



## POSSIBLE ANISOTROPIC PHASES IN THE EARLY UNIVERSE AND GRAVITATIONAL WAVE BACKGROUND

D.V. DERYAGIN, D. YU. GRIGORIEV, V.A. RUBAKOV, and M.V. SAZHIN

**Abstract**

We discuss possible anisotropic and inhomogeneous phases in the early Universe at relatively late epochs corresponding to the temperatures 1 GeV–10 TeV. The anisotropy and inhomogeneity of the energy-momentum tensor at the horizon scale gives rise to the generation of a stochastic gravitational wave background. It is shown that the present amplitudes and frequencies of this background may be well within the access of planned gravitational wave detectors.

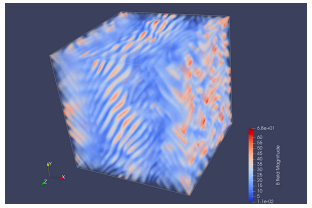

*Mon. Not. R. astr. Soc.* (1987) **229**, 357–370

**Generation of gravitational waves by the anisotropic phases in the early Universe**

D. V. Deryagin, D. Yu. Grigoriev and V. A. Rubakov *Institute for Nuclear Research, USSR Academy of Sciences, Moscow 117312, USSR*

M. V. Sazhin *P. K. Sternberg Astronomical Institute, Universitetskii pr. 13, Moscow 119899, USSR*

Accepted 1987 June 1. Received 1987 April 30

**Summary.** We discuss possible anisotropic and inhomogeneous phases in the early Universe at relatively late epochs corresponding to the temperatures 300 MeV–1 TeV. The anisotropy and inhomogeneity of the stress-energy tensor at the horizon scale gives rise to the generation of a stochastic gravitational wave background. Both the amplitude and spectral energy density of this background are estimated. We also discuss the possibility of the detection this background on working and planned gravitational wave detectors.

The frequency decreases because of the cosmological redshift and at the present moment its value is

$$\nu_0 = 3.7\times10^{-8}\left(\frac{T_g}{1\,\mathrm{GeV}}\right)\mathrm{Hz},$$

while the amplitude of the wave is

$$h_0 = 3\times10^{-13}h_g\left(\frac{1\,\mathrm{GeV}}{T_g}\right).$$

The order of magnitude estimate of the energy density of these background waves is

$$\varepsilon_g = 2\varepsilon_\gamma h_g^2.$$

Let us estimate the values of amplitudes and frequencies corresponding to two moments of the generation. Both of them can be relevant for the anisotropic phases connected with cold baryogenesis: $T_g = 1$ TeV and $T_g = 100$ GeV. For the temperature $T_g = 1$ TeV, the amplitude and frequency are

$$h_0 = 3\times10^{-20}, \qquad \nu_0 = 4\times10^{-5}\,\mathrm{Hz},$$

where we assume that $h_g = 10^{-4}$. For the temperature $T_g = 100$ GeV one has

$$h_0 = 3\times10^{-19}, \qquad \nu_0 = 4\times10^{-6}\,\mathrm{Hz}.$$

Smaller anisotropic domains may appear during the QCD phase at temperatures above

$$\nabla^2 h_{ij}(\boldsymbol{x},t) - \frac{\partial^2}{\partial t^2}h_{ij}(\boldsymbol{x},t) = -16\pi G\, S_{ij}(\boldsymbol{x},t)$$



$T_g = 300$ MeV. The amplitude of the anisotropic pressure is hard to calculate although dimensional estimates (Shaposhnikov 1987) give $\Delta \sim 10^{-2}$–$10^{-3}$. In this case the gravitational wave background is also generated, and the present amplitude and the frequency is of order of

$$h_0 = 3\times10^{-15}, \qquad \nu_0 = 4\times10^{-8}\,\mathrm{Hz}.$$

It is worth emphasizing that the anisotropy of the early Universe discussed in this paper is one of the most strong possible sources of the gravitational radiation in this frequency band. Indeed, the gravitational radiation from binary stars in our Galaxy in this frequency band is expected to have the amplitudes as high as

$$h \sim (10\text{–}3)\times10^{-20}.$$

The amplitudes of gravitational waves created during the inflation period are

$$h \sim (10^{-20}\text{–}10^{-21}) \quad \text{at} \quad \nu \sim 10^{-5}\,\mathrm{Hz}$$

and

$$h \sim 10^{-18} \quad \text{at} \quad \nu \sim 10^{-8}\,\mathrm{Hz}.$$

The most intense gravitational wave background in the frequency range $\sim 10^{-4}$ Hz cannot have the amplitudes exceeding $h \sim 10^{-16}$ in order not to contradict the nucleosynthesis data (Shvarstman 1969). According to Grishchuk (1987), the gravitational wave background can also be created from the zero-point fluctuations at rather late epoch ($T \sim 1$ TeV–1 GeV). But in this case the equation of state in the Universe has to be

$$p = -\varepsilon/3.$$

To conclude this section we mention that the electroweak and QCD phase transitions could also have produced the gravitational waves (Witten 1984; Hogan 1986). The full sketch of the generation mechanisms and the possibilities of the detection can be found in the review by Thorne (1987).

# WHY PRIMORDIAL TURBULENCE?

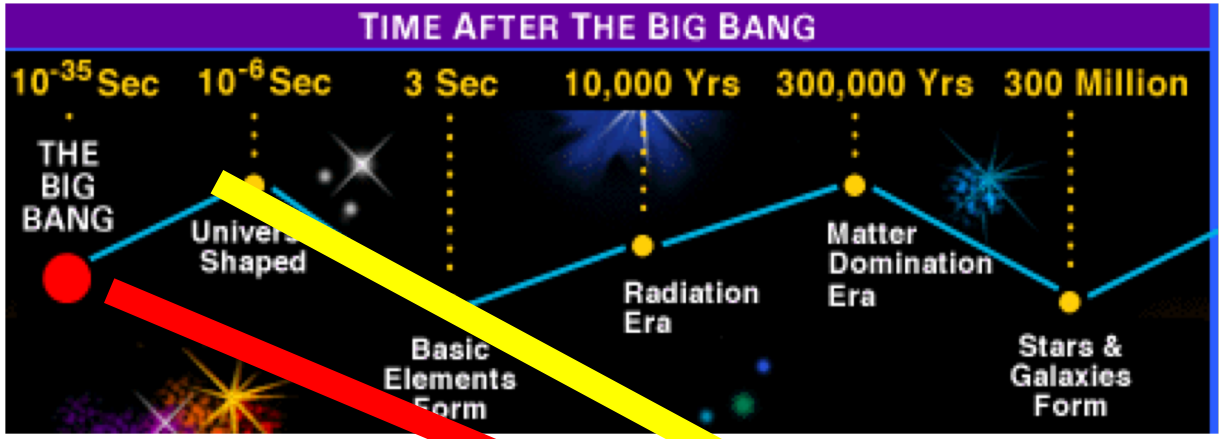


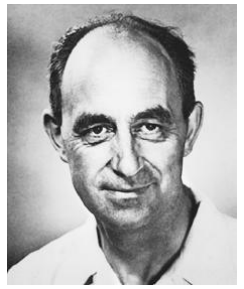

F. Hoyle
in Proc. "*La structure et l'evolution de l'Universe*" (1958)

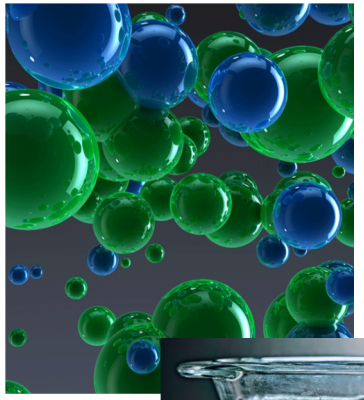

magnetic field origin

- red-inflation
- yellow- phase transitions

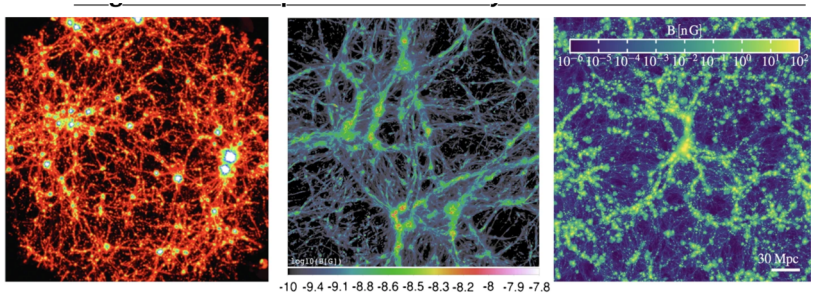


Projection of magnetic field strength in three cosmological simulations using different MHD approaches and solvers. Left: non-radiative GADGET SPH simulations with galactic seeding by Donnert et al. (2009), based on the MHD method by Dolag and Stasyszyn (2009). Middle: non-radiative ENZO MHD simulation on a fixed grid by Vazza et al. (2014) using the Dender cleaning (Dedner et al. 2002); Right: Simulation with full "Illustris TNG" galaxy formation model using a Lagrangian finite volume method (Marinacci et al. 2018b)

Donnert et al. 2018

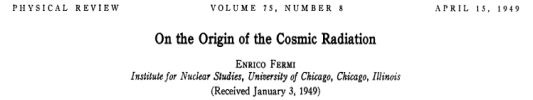

PHYSICAL REVIEW VOLUME 75, NUMBER 8 APRIL 15, 1949

**On the Origin of the Cosmic Radiation**

ENRICO FERMI
*Institute for Nuclear Studies, University of Chicago, Chicago, Illinois*
(Received January 3, 1949)

A theory of the origin of cosmic radiation is proposed according to which cosmic rays are originated and accelerated primarily in the interstellar space of the galaxy by collisions against moving magnetic fields. One of the features of the theory is that it yields naturally an inverse power law for the spectral distribution of the cosmic rays. The chief difficulty is that it fails to explain in a straightforward way the heavy nuclei observed in the primary radiation.

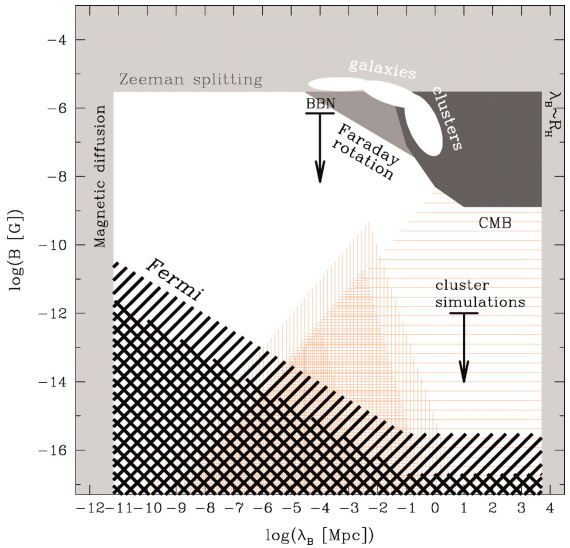


**A. Neronov & E. Vovk**," *Evidence for Strong Extra-galactic Magnetic Fields from Fermi Observations of TeV Blazars*", Science 328, 5974 (2010)

# HYDRO – AND MHD TURBULENCE : GRAVITATIONAL WAVES

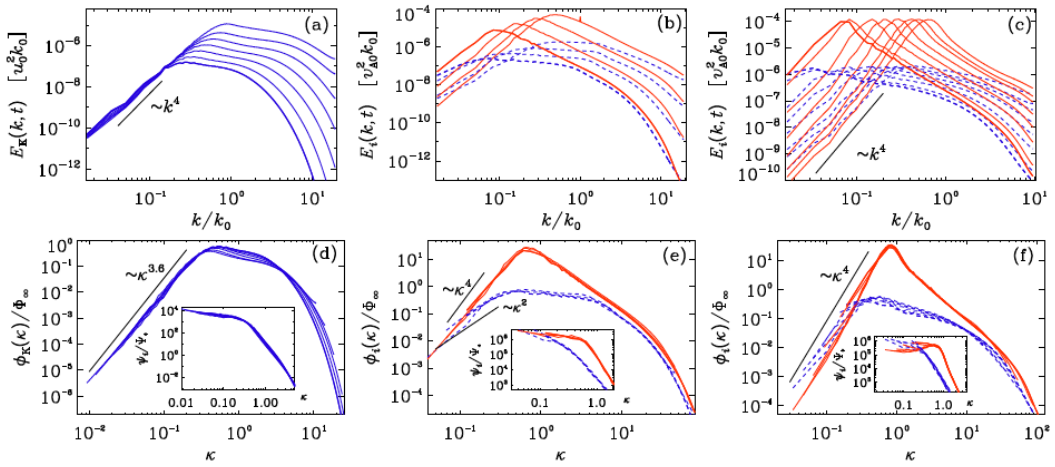


Brandenburg and Kahniashvili 2017

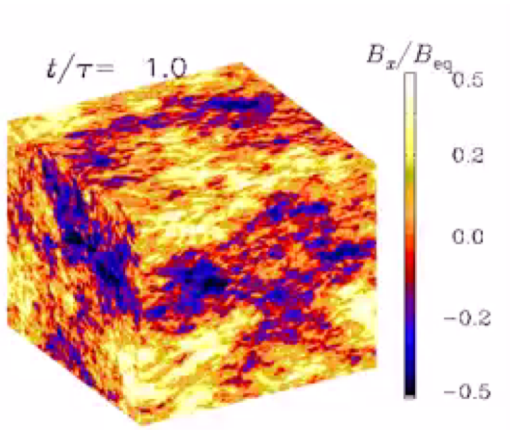


$$\frac{\partial \ln\rho}{\partial t} = -\frac{4}{3}(\boldsymbol{\nabla}\cdot\boldsymbol{u} + \boldsymbol{u}\cdot\boldsymbol{\nabla}\ln\rho) + \frac{1}{\rho}[\boldsymbol{u}\cdot(\boldsymbol{J}\times\boldsymbol{B}) + \eta\boldsymbol{J}^2],$$

$$\frac{\partial \boldsymbol{u}}{\partial t} = -\boldsymbol{u}\cdot\boldsymbol{\nabla}\boldsymbol{u} + \frac{\boldsymbol{u}}{3}(\boldsymbol{\nabla}\cdot\boldsymbol{u} + \boldsymbol{u}\cdot\boldsymbol{\nabla}\ln\rho) - \frac{\boldsymbol{u}}{\rho}[\boldsymbol{u}\cdot(\boldsymbol{J}\times\boldsymbol{B}) + \eta\boldsymbol{J}^2] - \frac{1}{4}\boldsymbol{\nabla}\ln\rho + \frac{3}{4\rho}\boldsymbol{J}\times\boldsymbol{B} + \frac{2}{\rho}\boldsymbol{\nabla}\cdot(\rho\nu\boldsymbol{S}) + \boldsymbol{\mathcal{F}},$$

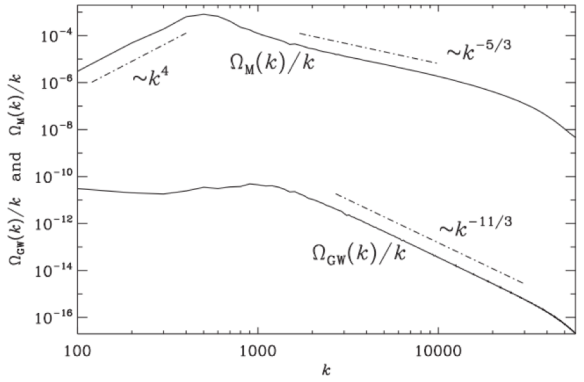


FIG. 1. Magnetic and GW energy spectra for run ini2 averaged over late times ($t > 1.1$), after the GW spectrum has started to fluctuate around a steady state.

$$(\partial_t^2 - c^2\boldsymbol{\nabla}^2)h_{ij}(\boldsymbol{x},t) = \frac{16\pi G}{ac^2}T_{ij}^{\rm TT}(\boldsymbol{x},t)$$

$$T_{ij} = \frac{4}{3}\frac{\rho u_i u_j}{1-\boldsymbol{u}^2} - B_i B_j + (\rho/3 + \boldsymbol{B}^2/2)\delta_{ij},$$

TABLE II. Correspondence between the slopes expected from Ref. [12] for the subinertial range ("ana") and what is obtained in our run ini2 ("sim"), and the results for spectra with the Kolmogorov slope ("Kol") and the Golitsyn slope ("Gol"), which agrees with Ref. [12].

| Slope of | ana | sim | Kol | Gol |
|---|---|---|---|---|
| $\Omega_M$ | 5 | 5 | −2/3 | −8/3 |
| $\Omega_{GW}$ | 3 | 1 | −8/3 | −14/3 |
| $h_c$ | 1/2 | −1/2 | −7/3 | −10/3 |

Roper Pol et al.. 2019

PHYSICAL REVIEW D **102,** 083512 (2020)

**Numerical simulations of gravitational waves from early-universe turbulence**

Alberto Roper Pol,[1,2,3,*] Sayan Mandal,[4,3,†] Axel Brandenburg,[5,2,3,4,6,7,‡] Tina Kahniashvili,[4,3,8,9,§] and Arthur Kosowsky[10,‖]

[1]Department of Aerospace Engineering Sciences, University of Colorado, Boulder, Colorado 80303, USA
[2]Laboratory for Atmospheric and Space Physics, University of Colorado, Boulder, Colorado 80303, USA
[3]Faculty of Natural Sciences and Medicine, Ilia State University, 3-5 Cholokashvili Street, 0194 Tbilisi, Georgia
[4]McWilliams Center for Cosmology and Department of Physics, Carnegie Mellon University, 5000 Forbes Avenue, Pittsburgh, Pennsylvania 15213, USA
[5]Nordita, KTH Royal Institute of Technology and Stockholm University, Roslagstullsbacken 23, 10691 Stockholm, Sweden
[6]Department of Astronomy, AlbaNova University Center, Stockholm University, 10691 Stockholm, Sweden
[7]JILA, University of Colorado, Boulder, Colorado 80303, USA
[8]Abastumani Astrophysical Observatory, M. Kostava Street 47/57, Tbilisi GE-0179, Georgia
[9]Department of Physics, Laurentian University, Ramsey Lake Road, Sudbury, Ontario P3E 2C, Canada
[10]Department of Physics and Astronomy, University of Pittsburgh, and Pittsburgh Particle Physics, Astrophysics, and Cosmology Center (PITT PACC), Pittsburgh, Pennsylvania 15260, USA

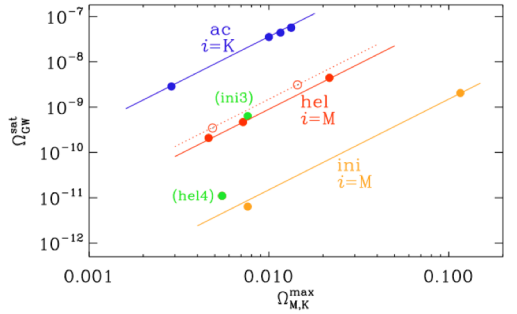


FIG. 7. $\Omega_{GW}^{sat}$ versus $\Omega_{M,K}^{max}$. The quadratic dependence inferred from the +2 slope of the lines holds within runs of the same type. Note that runs ini3 ($N = 10$) and hel4 ($N = 1000$) in green have different stirring scales than the rest of the runs ($N = 100$).

See

- Alberto Roper Pol Colloquium
- Axel Brandenburg talk

# HYDRO – AND MHD TURBULENCE : GRAVITATIONAL WAVES

Credit: Axel Brandenburg

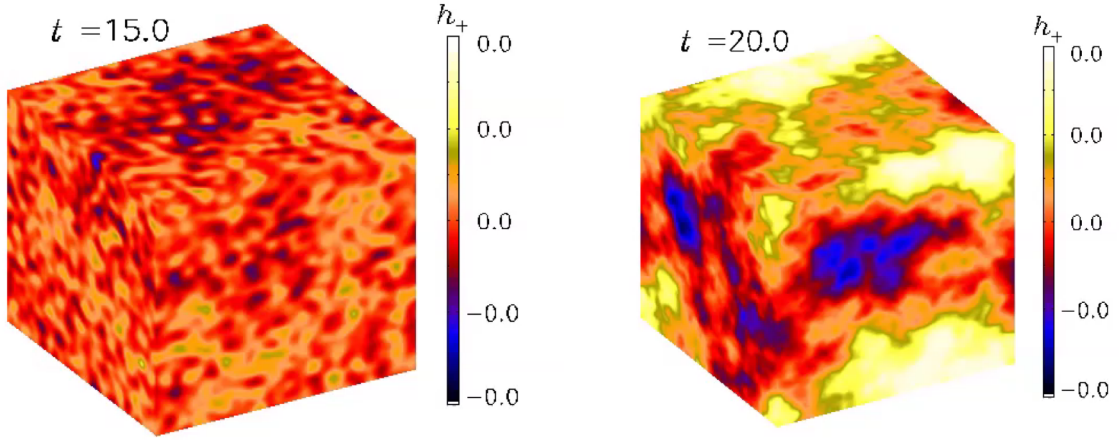


$$\mathcal{E}_M(t) \simeq \mathrm{w} b_1^2 \left(1+\frac{t}{\tau_1}\right)^{-2/3},$$

$$\mathcal{E}_v(t) \simeq \mathrm{w} v_1^2 \left(1+\frac{t}{\tau_1}\right)^{-2/3},$$

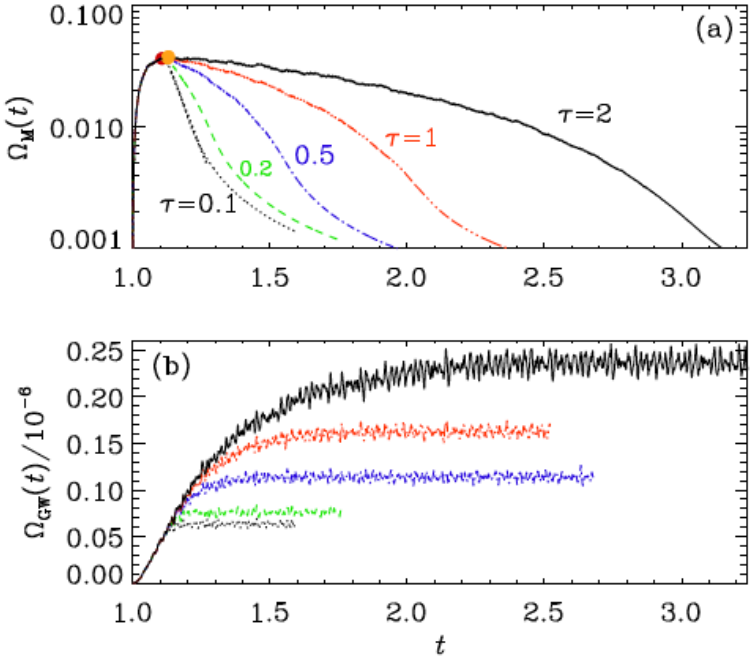


FIG. 1: Evolution of magnetic energy (top) and growth of GW energy density (bottom) for simulations where the driving is turned off at $t = 1.1$ (black dotted line), or the strength of the driving is reduced linearly in time over the duration $\tau = 0.2$ (green), 0.5 (blue), 1 (red), or 2 (black). Time is in units of the Hubble time at the moment of source activation.



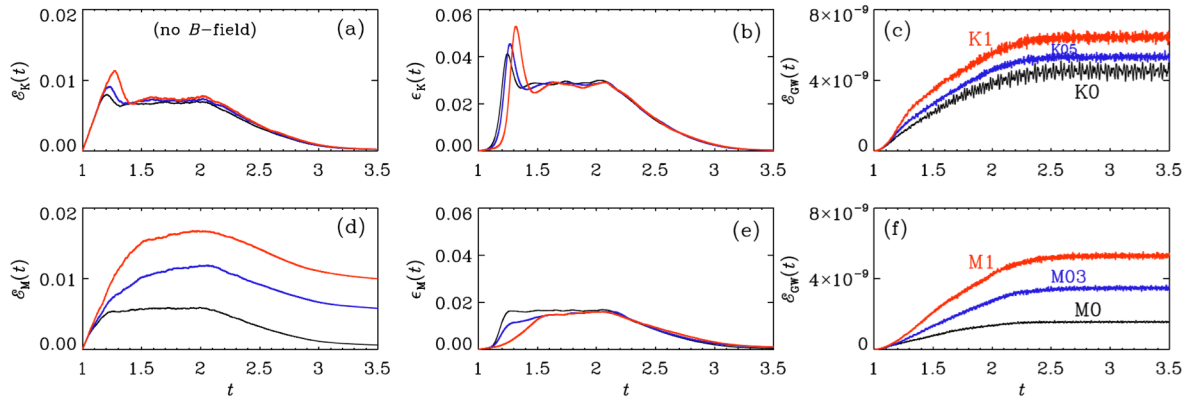


FIG. 2. Evolution of (a) $\mathcal{E}_K$, (b) $\epsilon_K$, and (c) $\mathcal{E}_{GW}$ for kinetically driven cases with $\sigma = 0$ (run K0, black), 0.5 (run K05, blue), and 1 (run K1, red), and of (d) $\mathcal{E}_M$, (e) $\epsilon_M$, and (f) $\mathcal{E}_{GW}$ for magnetically driven cases with $\sigma = 0$ (run M0, black), 0.3 (run M03, blue), and 1 (run M1, red).

Kahniashvili et al. 2022

# PRIMORDIAL MAGNETIC FIELDS LIMITS FROM BBN

Kaahniashvili, et al. 2022

- EXTRA RADIATION LIKE ENERGY DENSITY LESS THAN ~3% OF THE RADIATION ENERGY DENSITY AT BBN

$$\frac{\rho_{\rm add}}{\rho_{\rm rad}} = 0.277\left(\frac{\Delta N_{\rm eff}}{0.122}\right); \qquad \Delta N_{eff} = N_{\rm eff} - N^{\nu}_{\rm eff}$$

- THE UPPER BOUND ON THE MAGNETIC (EFFECTIVE) AMPLITUDE ORDER OF MICROGAUSS AT BBN
- ACCOUNTING FOR THE MAGNETIC FIELD DECAY:
  - THE MAGNETIC ENERGY DENSITY DOES NOT EXCEED THE RADIATION ENERGY DENSITY AT THE MOMENT OF GENERATION
  - BBN BOUNDS ARE SATISFIED

Possible turbulent evolution of the comoving MF strength B (and correlation length $\xi_M$ from generation at the EW and QCD scales in the cases of fully helical (β = 0 ), nonhelical (β = 1, 2, 4), and partially helical MHD turbulence. Upper limits on $\xi_M$ are determined by the size of the horizon and number of domains (bubbles) at generation, ranging from 1 to 6 (at QCD) or 100 (at EW), depending on the PT modeling. Lines terminate (on the right) at recombination (T = 0.25 eV). The upper limit of the comoving MF strength at BBN (T = 0.1 MeV) is indicated by the black dot-dashed line. Regimes excluded by observations of blazar spectra are marked in gray. The hatched regions are bounded by an (upper) limit from BBN and a (lower) limit from the blazar spectra.,

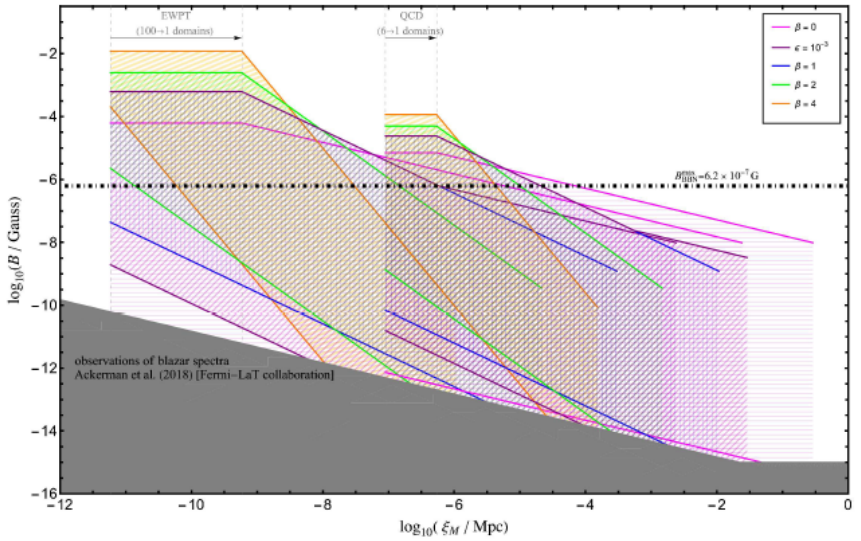

# GRAVITATIONAL WAVES FROM PRIMORDIAL HD & MHD TURBULENCE

Kaahniashvili, et al. 2022

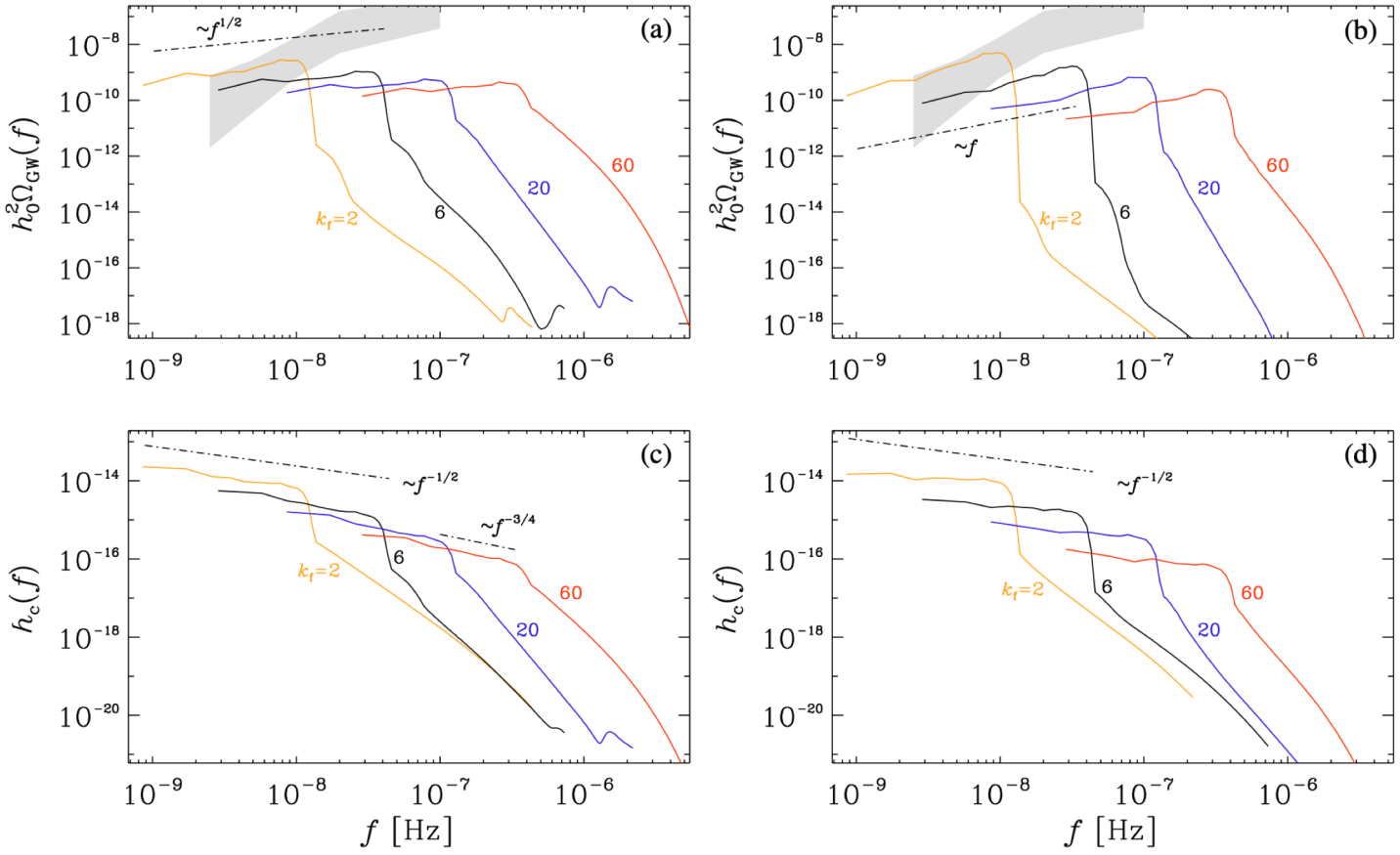


$$\mathcal{E}_{GW} = \left( q \frac{\mathcal{E}_M}{k_f} \right)^n$$

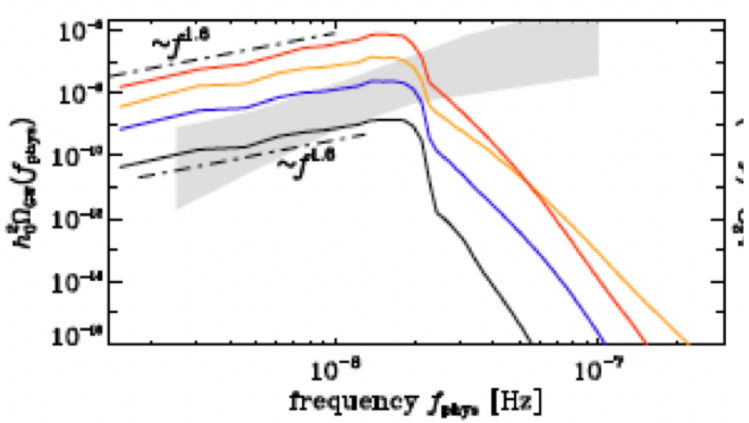


FIG. 2: Frequency spectra, $h_0^2\Omega_{GW}(f)$, for both the QCDPT R
orange, blue, and black, respectively.

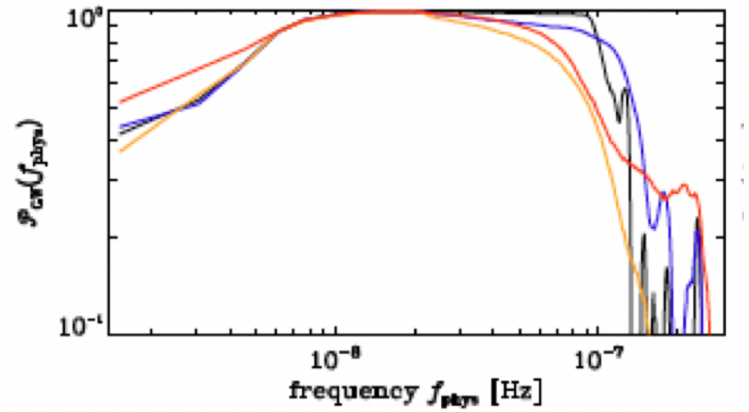


FIG. 3: Polarization spectra, $\mathcal{P}_{GW}(f)$, for the QCDPT Runs a
orange, blue, and black, respectively.

# PULSAR TIMING ARRAYS AND EARLY UNIVERSE TURBULENCE

A&A, 685, A94 (2024)
https://doi.org/10.1051/0004-6361/202347433


Astronomy & Astrophysics

## The second data release from the European Pulsar Timing Array

### IV. Implications for massive black holes, dark matter, and the early Universe★

EPTA Collaboration and InPTA Collaboration: J. Antoniadis (Ιωάννης Αντωνιάδης)[1,2], P. Arumugam[3], S. Arumugam[4], S. Babak[6], M. Bagchi[7,8], A.-S. Bak Nielsen[2,9], C. G. Bassa[11], A. Bathula[12], A. Berthereau[13,14], M. Bonetti[15,16,17], E. Bortolas[15,16,17], P. R. Brook[18], M. Burgay[19], R. N. Caballero[20], A. Chalumeau[15], D. J. Champion[2], S. Chanlaridis[1], S. Chen[23], I. Cognard[13,14], S. Dandapat[24], D. Deb[7], S. Desai[25], G. Desvignes[2], N. Dhanda-Batra[26], C. Dwivedi[27], M. Falxa[6,13], R. D. Ferdman[29], A. Franchini[15,16], J. R. Gair[31], B. Goncharov[32,33], A. Gopakumar[24], E. Graikou[2], J.-M. Grießmeier[13,14], A. Gualandris[28], L. Guillemot[13,14], Y. J. Guo[2], Y. Gupta[34], S. Hisano[35], H. Hu[2], F. Iraci[36,19], D. Izquierdo-Villalba[15,16], J. Jang[2], J. Jawor[2], G. H. Janssen[11,37], A. Jessner[2], B. C. Joshi[34,3], F. Kareem[38,39], R. Karuppusamy[2], E. F. Keane[40], M. J. Keith[41], D. Kharbanda[25], T. Kikunaga[35], N. Kolhe[42], M. Kramer[2,41], M. A. Krishnakumar[2,9], K. Lackeos[2], K. J. Lee[43,64], K. Liu[2], Y. Liu[43,9], A. G. Lyne[41], J. W. McKee[44,45], Y. Maan[34], R. A. Main[2], M. B. Mickaliger[41], I. C. Niţu[41], K. Nobleson[47], A. K. Paladi[48], A. Parthasarathy[2], B. B. P. Perera[49], D. Perrodin[19], A. Petiteau[50,6], N. K. Porayko[15,2,★★], A. Possenti[19], T. Prabu[51], H. Quelquejay Leclere[6,★★], P. Rana[24], A. Samajdar[52], S. A. Sanidas[41], A. Sesana[15,16,17,★★], G. Shaifullah[15,16,19], J. Singha[3], L. Speri[31], R. Spiewak[41], A. Srivastava[25], B. W. Stappers[41], M. Surnis[54], S. C. Susarla[55], A. Susobhanan[56], K. Takahashi[57,58], P. Tarafdar[7], G. Theureau[13,14,59], C. Tiburzi[19], E. van der Wateren[11,37], A. Vecchio[18], V. Venkatraman Krishnan[2], J. P. W. Verbiest[61,9,2], J. Wang[9,62,63], L. Wang[41], Z. Wu[43,9], and P. Auclair[5], E. Barausse[10], C. Caprini[21,22], M. Crisostomi[10], F. Fastidio[28,15], T. Khizriev[30], H. Middleton[18], A. Neronov[6,46], K. Postnov[30,53], A. Roper Pol[21], D. Semikoz[6], C. Smarra[10], D. A. Steer[6], R. J. Truant[15], and S. Valtolina[60]

$$\Omega_{\rm GW}(f) = 3\,\mathcal{A}\,\Omega_*^2\,(\lambda_*\mathcal{H}_*)^2 F_{\rm GW,0}\,S_{\rm turb}(\lambda_* f), \tag{21}$$

where $\Omega_*$ is the ratio of the (M)HD turbulent energy density to the radiation one, and $\lambda_*\mathcal{H}_*$ is the ratio of the characteristic length scale of the turbulence, $\lambda_*$, to the comoving Hubble horizon $\mathcal{H}_*^{-1}$ at the QCD epoch. The parameter $\mathcal{A} \simeq 1.75 \times 10^{-3}$ is the efficiency of GW production[8], estimated in Roper Pol et al. (2022a). The function $F_{\rm GW,0}$ is the fractional radiation energy density at the epoch of GW generation to its value at the present time. It depends on the temperature scale $T_*$ via the number of degrees of freedom $g_*$,

$$F_{\rm GW,0} \simeq 8 \times 10^{-5} \left(\frac{10}{g_*}\right)^{1/3}. \tag{22}$$

The spectral shape of the GWB signal, $S_{\rm turb}(f)$, is

$$S_{\rm turb}(\lambda_* f) = \mathcal{B}\,(\lambda_* f)^3\, p_\Pi(\lambda_* f) \times \begin{cases} \ln^2[1 + \mathcal{H}_*\,\delta t_{\rm fin}/(2\pi)], & \text{if } f < 1/\delta t_{\rm fin}, \\ \ln^2[1 + \lambda_*\mathcal{H}_*/(2\pi\lambda_* f)], & \text{if } f \geq 1/\delta t_{\rm fin}, \end{cases} \tag{23}$$

[8] This estimate is conservative since it only considers the decaying stage of turbulence. Numerical simulations find larger values when including a stage of turbulence production (Roper Pol et al. 2020b, 2022b; Kahniashvili et al. 2021).

$$\mathcal{H}_* \simeq 10^{-8}\,\frac{T_*}{100\,\text{MeV}}\left(\frac{g_*}{10}\right)^{\frac{1}{6}}\ \text{Hz},$$

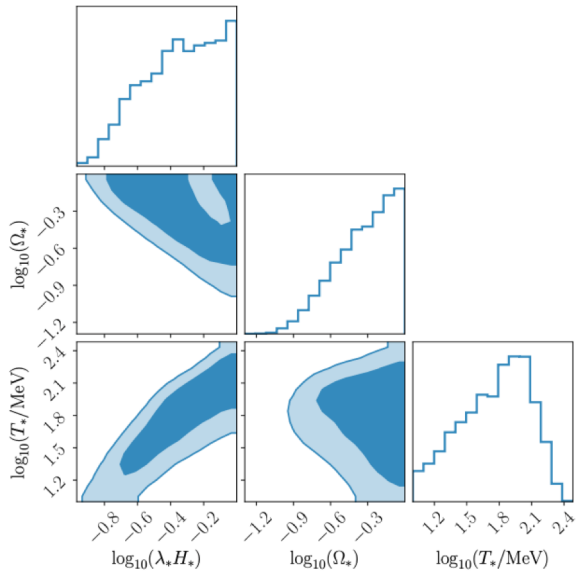


**Fig. 18.** 2D posteriors for the parameters of the background from turbulence around the QCD energy scale obtained using a free spectrum fit on DR2new data. The 68% and 95% credible regions are displayed.

The GWB produced from vortical (M)HD turbulence is therefore determined by three parameters: the temperature scale T∗, the turbulence strength Ω∗, and the turbulence characteristic length scale λ∗H∗.

# GRAVITATIONAL WAVES POLARIZATION

$$\mathcal{P}(k) = \frac{\langle h_+^\star(\mathbf{k})h_+(\mathbf{k}') - h_-^\star(\mathbf{k})h_-(\mathbf{k}')\rangle}{\langle h_+^\star(\mathbf{k})h_+(\mathbf{k}') + h_-^\star(\mathbf{k})h_-(\mathbf{k}')\rangle} = \frac{\mathcal{H}(k)}{H(k)}.$$

- Matter-Antimatter Asymmetry – Baryongenesis and Leptogenesis
- CP Symmetry Breaking/Chern Simons
- Chiral Magnetic Fields…

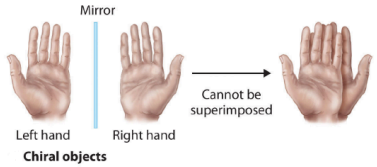


$$H_B(t) = \int d^3x \mathbf{A} \cdot \nabla \times \mathbf{A},$$

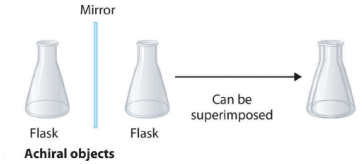


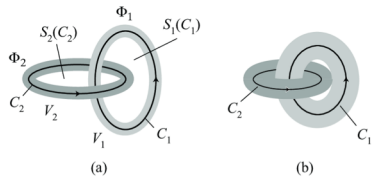


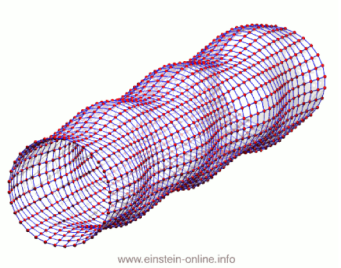


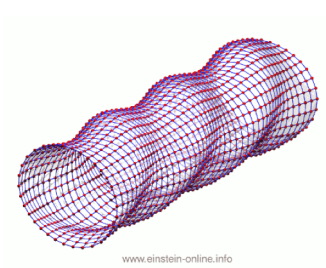


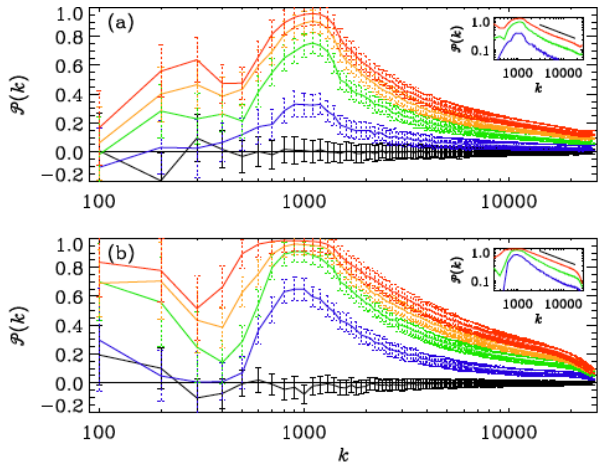


FIG. 3: Degree of circular polarization for (a) kinetically and (b) magnetically forced cases with $\sigma = 0$ (black) 0.1 (blue), 0.3 (green), 0.5 (orange), and 1 (red). Approximate error bars based on the temporal fluctuations and statistical spread for different random seeds of the forcing are shown as solid black lines for $\sigma = 0$ and as dotted lines otherwise.


Journal of Cosmology and Astroparticle Physics
An IOP and SISSA journal


**Measuring the net circular polarization of the stochastic gravitational wave background with interferometers**


Valerie Domcke,[a] Juan García-Bellido,[b] Marco Peloso,[c,d] Mauro Pieroni,[b,e] Angelo Ricciardone,[c] Lorenzo Sorbo[f] and Gianmassimo Tasinato[g]



PHYSICAL REVIEW RESEARCH 3, 013193 (2021)


**Circular polarization of gravitational waves from early-Universe helical turbulence**


Tina Kahniashvili,[1,2,3,4,*] Axel Brandenburg,[5,6,2,1,†] Grigol Gogoberidze,[2,‡] Sayan Mandal,[7,2,§] and Alberto Roper Pol[8,2,‖]

[1]McWilliams Center for Cosmology and Department of Physics, Carnegie Mellon University, Pittsburgh, Pennsylvania 15213, USA
[2]Faculty of Natural Sciences and Medicine, Ilia State University, 0194 Tbilisi, Georgia
[3]Abastumani Astrophysical Observatory, Tbilisi, GE-0179, Georgia
[4]Department of Physics, Laurentian University, Sudbury, Ontario, Canada P3E 2C
[5]Nordita, KTH Royal Institute of Technology and Stockholm University, 10691 Stockholm, Sweden
[6]Department of Astronomy, AlbaNova University Center, Stockholm University, 10691 Stockholm, Sweden
[7]Physics and Astronomy Department, Stony Brook University, Stony Brook, New York 11794, USA
[8]Université de Paris, CNRS, Astrophysique et Cosmologie, Paris, F-75013, France



(Received 17 November 2020; accepted 19 January 2021; published 26 February 2021)



We perform direct numerical simulations to compute the net circular polarization of gravitational waves from helical (chiral) turbulent sources in the early Universe for a variety of initial conditions, including driven (stationary) and decaying turbulence. We investigate the resulting gravitational wave signal assuming different turbulent geneses such as magnetically or kinetically driven cases. Under realistic physical conditions in the early Universe we compute numerically the wave number-dependent polarization degree of the gravitational waves. We find that the spectral polarization degree strongly depends on the initial conditions. The peak of the spectral polarization degree occurs at twice the typical wave number of the source, as expected, and for fully helical decaying turbulence, it reaches its maximum of nearly 100% *only* at the peak. We determine the temporal evolution of the turbulent sources as well as the resulting gravitational waves, showing that the dominant contribution to their spectral energy density happens shortly after the activation of the source. Only through an artificially prolonged decay of the turbulence can further increase of the gravitational wave amplitude be achieved. We estimate the detection prospects for the net polarization, arguing that its detection contains *clean* information (including the generation mechanisms, time, and strength) about the sources of possible parity violations in the early Universe.


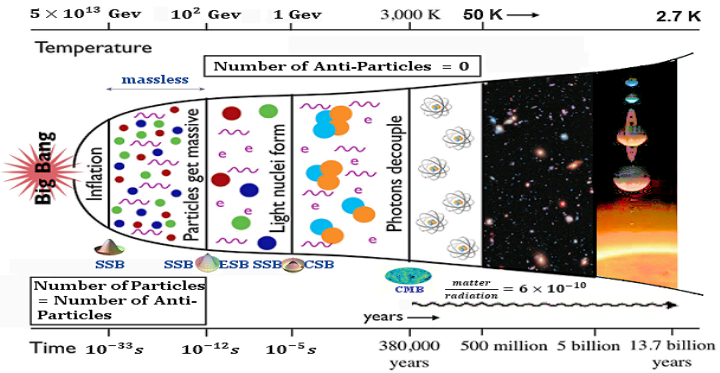


See
- Axel Brandenburg talk
- Igor Rogachevski talk
- Jennifer Schober talk

# ACKNOWLEDGEMENTS

**Workshop Organizers** (especially Alberto Roper Pol) and **NORDITA** Hospitality

**Collaborators:** Axel Brandenburg, Giga Gogoberidze, Arthur Kosowsky, Sayan Mandal, Alberto Roper Pol

**Students:** Chris Choi, Emma Clarke, Murman Gurgenidze Ved Kenjale, Jacob Magallanes, Jonathan Stepp

**Partial support from**

- Shota Rustaveli National Science Foundation of Georgia FR24-2606
- NASA Astrophysics Theory Program: ATP80NSSC22K0825
- NSF Astrophysics and Astronomy Research Grant Program: AST2307698 & AST2408411